[Frontiers in Bioscience 16, 3072-3132, June 1, 2011]

Light-induced water oxidation in photosystem II

Frank Muh[1,2], Athina Zouni[2]

[1]Institut fur Chemie und Biochemie/Kristallographie, Freie Universitat Berlin, Fabeckstrasse 36a, D-14195 Berlin, Germany, [2]Max-Volmer-Laboratorium fur Biophysikalische Chemie, Technische Universitat Berlin, Strasse des 17. Juni 135, D-10623 Berlin, Germany

TABLE OF CONTENTS

1. ABSTRACT

The photosystem II core complex (PSIIcc) is the key enzyme of oxygenic photosynthesis, as it catalyzes the light-induced oxidation of water to form dioxgyen and protons. It is located in the thylakoid membrane of cyanobacteria, algae, and plants and consists of 20 protein subunits binding about 100 cofactors. In this review, we discuss what is presently known about the "donor side" of PSIIcc, covering the photosynthetic reaction center and the water oxidase part. The focus is on the catalytic Mn_4Ca cluster and its protein environment. An attempt is made to connect recent crystallographic data (up to 2.9 Å resolution) with the wealth of information about Nature´s water oxidation device from spectroscopic, biochemical and theoretical work.

2. INTRODUCTION

In times of global warming and forseeable shortage of fossil fuels, the need for an efficient usage of solar energy becomes more and more evident (1). Learning from nature in this respect means to understand the molecular mechanisms of photosynthesis (2). During the last decade, the spatial structures of the relevant photosynthetic membrane proteins have been elucidated (3-17). Yet, unraveling the many functional implications of the structural information is both a fascinating and challenging enterprise. This is particularly true for the site of water cleavage in oxygenic photosynthesis, photosystem II, where many molecular details could be reliably determined only very recently (14, 15, 18).

Light-induced water oxidation is catalyzed by the photosystem II core complex (PSIIcc), a multi-subunit water:plastoquinone oxidoreductase spanning the thylakoid membrane of cyanobacteria, algae and higher plants (19-21). The light energy is harvested by specialized chlorophyll (Chl) cofactors and transferred to the reaction center (RC), where a charge separation process creates a strong oxidant that is able to extract electrons (under release of protons) from water. These electrons serve to reduce plastoquinone (PQ) to plastoquinol (PQH_2) in the Q_B-site. PQH_2 diffuses into the thylakoid membrane and is replaced by fresh PQ (Figure 1A). A byproduct of the water oxidation reactions is molecular oxygen (O_2), which became essential for life on earth. The actual catalytic site of water oxidation is a metal center containing four manganese and one calcium ion (18, 22-26), the water oxidizing complex (WOC). Making this catalyst work requires the whole machinery of PSIIcc including mechanisms for efficient excitation energy transfer, charge separation, proton-coupled electron transfer and the protection against unwanted side reactions.

Cyanobacterial PSIIcc occurs in both, a dimeric and a monomeric form, which both could be crystallized (10-15, 27, 28) and the X-ray structures refined to 2.9 Å (15) and 3.6 Å resolution (28), respectively. As reviewed recently (18), each PSIIcc-monomer consists of 20 different polypeptide chains that could be identified in the crystal structures (Figures 1B, C). The central part of the core complex is build up by the two large membrane-intrinsic, symmetry-related subunits PsbA (D1) and PsbD (D2), which bind the RC cofactors and the WOC. They are flanked by the other two large membrane-intrinsic subunits PsbB (CP47) and PsbC (CP43) containing light-harvesting pigments (for reviews, see (29, 30)) and contributing significantly to the large membrane-extrinsic part of PSIIcc protruding into the lumen. The remaining membrane-intrinsic subunits of PSIIcc are small and have only one or two (PsbZ) transmembrane helices (TMH). Their function still needs clarification (18, 30-32). The lumenal extension of PSIIcc further consists of three extrinsic subunits PsbO, PsbU and PsbV visible in the crystal structure (Figures 1B, C). All three extrinsic subunits are in contact with intrinsic polypeptides and influence water oxidation with PsbO being indispensable. There is a strong variation between organism types with respect to the nature of the other two (or more) extrinsic subunits (33-35). Altogether, the peptides of PSIIcc bind 96 cofactors including 35 Chl *a*, two pheophytin (Pheo) *a*, three PQ (Q_A, Q_B, Q_C), a non-heme iron, bicarbonate, two heme groups (cyt *b*559 shown in Figure 2 as well as cyt *c*550 not shown and absent in green algae and plants), 12 carotenoids (β-carotene), 25 integral lipids, seven detergent molecules (n-dodecyl β-D-maltoside) probably occupying lipid binding niches, one calcium (Ca^{2+}), four manganese and (at least) one chloride ion of the WOC as well as two additional Ca^{2+} ions (Ca^{2+}-PsbK and Ca^{2+}-PsbO, see Figures 1B, C). This abundance of non-proteinogenous molecules is suggestive of the diversity of functions that PSIIcc has to fulfil. The present review describes aspects of our current knowledge of PSIIcc taking the crystal structure at 2.9 Å resolution as a starting point (15) and focussing on the water oxidase part and its structure elucidation with different methods.

3. EXCITATION ENERGY TRANSFER, CHARGE SEPARATION, AND QUINONE REDUCTION

3.1. Excitation energy transfer and charge separation

Our current knowledge of the core antenna system of PSIIcc as well as the charge separation (CS) in the RC have been reviewed recently (21, 36-38), so that we can limit the following description to a short summary. To enhance the aborption cross section of the photochemical processes, the RC is coupled to a large number of pigments that serve to collect the light energy and to transfer it to the crucial pigments in the RC that are able to initiate CS. Besides separate antenna proteins that vary in size, shape, pigment composition and location between different organism types (39, 40), PSIIcc is equipped with a core antenna system provided by the Chl *a* bound to CP43 and CP47 (29, 30). One of the key questions presently debated is, whether excitation energy transfer (EET) from the core antennae to the RC pigments is significantly slower than the initial CS step as suggested by structure-based calculations (41) or significantly faster than or on a similar time scale as CS (42-44).

The RC of PSIIcc (PSII-RC) is structurally homologous to the photosynthetic RC of purple bacteria (bRC (45-48)) with two branches related by a pseudo C_2-symmetry as shown in Figure 2. The excited state formed in the RC is traditionally denoted P^*_{680} because of a bleaching observed at 680 nm in optical spectra upon formation of a radical pair (49). This led to the identification of a "pigment P_{680}" with the "primary electron donor" in the RC (50). However, the excited state structure of PSII-RC is complex and can not be related in a simple manner to just one pigment (21, 37, 51). According to the simulations of Raszewski *et al.* (51), the lowest excited state of the RC is essentially localized on Chl_{D1}. At physiological temperatures, higher excited states are populated as well, so that the excitation energy is found to only about 30 % on Chl_{D1} and to 10 – 20 % on each of the other five pigments. This situation is quite different from that in bRC, where the lowest excited state is localized on the "special pair" P_L-P_M (52), which is the counterpart of

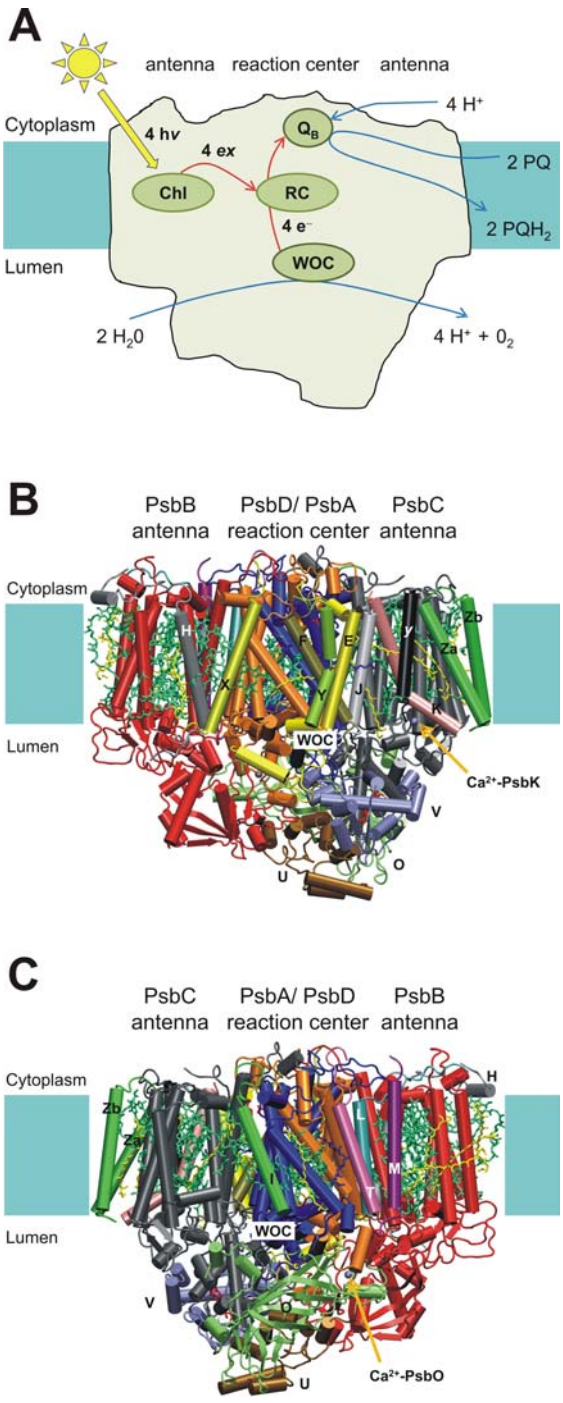

Figure 1. (A) Schematic representation of photochemical reactions taking place in PSIIcc embedded in the thylakoid membrane. For details, see text and Figure 2A. (B) Structure of one PSIIcc monomer at 2.9 Å resolution (15) viewed along the membrane plane in the same orientation as the scheme in A. Different polypeptide chains are shown as backbone cartoons in distinct colors, and small subunits are labeled according to their one-letter code. Small membrane-intrinsic subunits visible from this side are PsbE and F (cyt *b*559) as well as PsbH, J, K, X, Y and Z. Za and Zb refer to the two trans-membrane α-helices of PsbZ. Also shown are chlorophyll *a* (green) and β-carotene (yellow) pigments as stick models. The positions of the WOC and an additional Ca^{2+} ion bound to PsbK are indicated. (C) Same as in B, but viewed from the opposite side. The visible small membrane-intrinsic subunits are PsbI, L, M, T, and Z. In addition, the N-terminus of PsbH shows up at the cytoplasmic side (right). The positions of the WOC and an additional Ca^{2+} ion bound to PsbO are indicated. Figures 1B and C made with VMD (492).

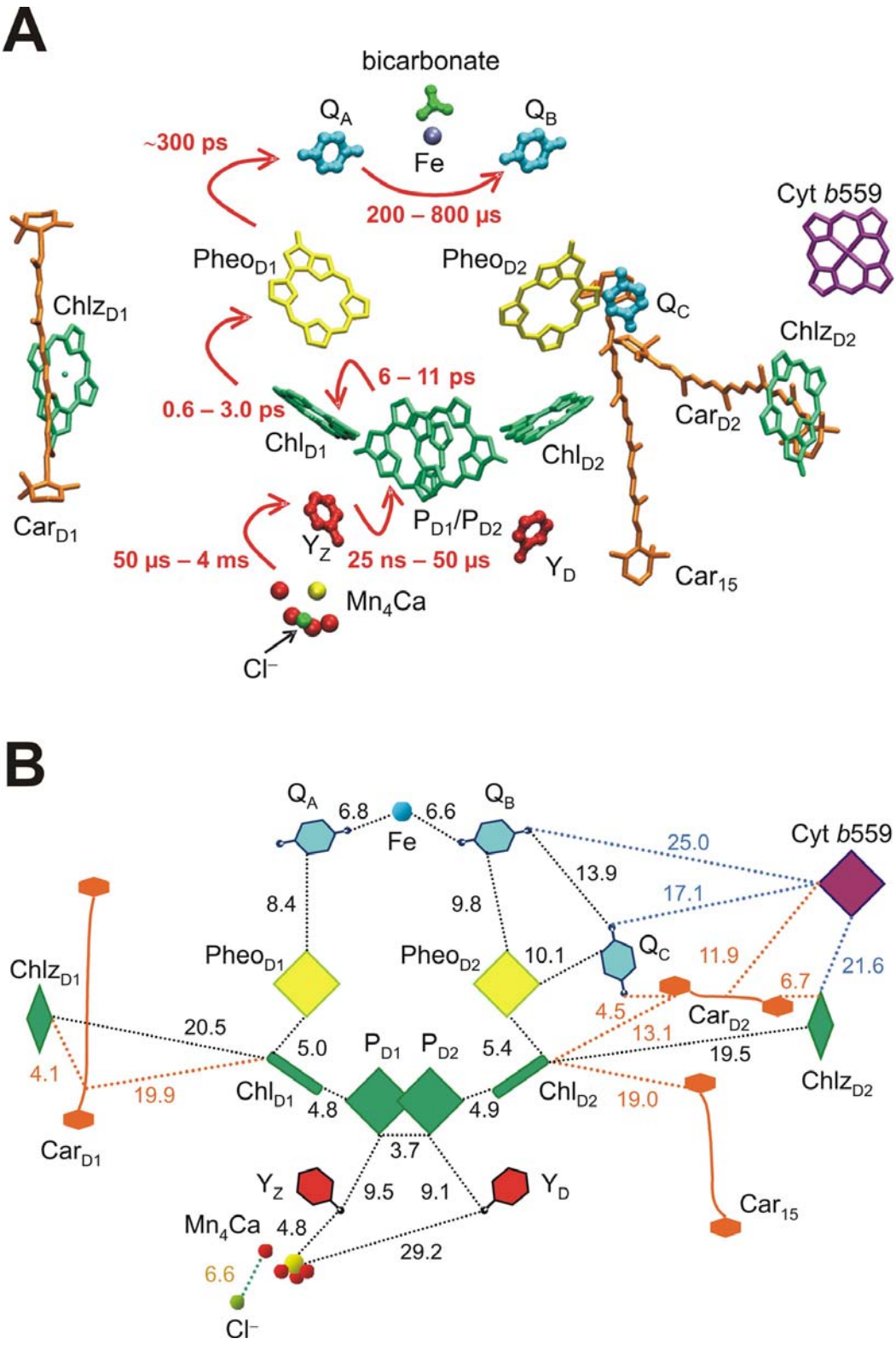

Figure 2. (A) Arrangement of cofactors in and around the reaction center of PSIIcc according to the 2.9 Å resolution structure (15). The red arrows indicate electron transfer steps along with their time scale, detailing the rough scheme in Figure 1A. Figure made with VMD (492). (B) Schematic representation of the cofactor arrangement in A along with edge-to-edge distances given in Å.

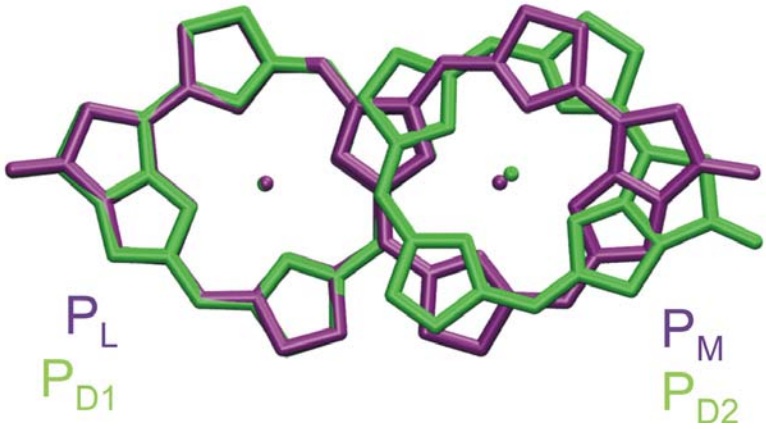

Figure 3. Superposition of the tetrapyrrole sceletons of the P_{D1}-P_{D2}-dimer (Chl *a*) of the PSII-RC of *Thermosynechococcus elongatus* (15) and the P_L-P_M-"special pair" (bacteriochlorophyll *a*) of the bRC of *Rhodobacter sphaeroides* (46). The superposition was obtained from a minimization of the mean-square deviation in positions of equivalent atoms of one dimer half of the two molecule pairs using VMD (492).

the P_{D1}-P_{D2}-dimer (Figure 3). The two bacteriochlorophylls P_L and P_M in bRC have a strong overlap of their electronic wavefunctions allowing for a significant delocalization of electrons (53, 54). As a consequence, the excited states of the P_L-P_M-dimer are coupled to charge-transfer states with a concomitant red-shift of the lowest excited state, so that an energy sink is formed at the "special pair" (55, 56), where the excitation energy is trapped also at ambient temperatures. In contrast, the two Chl of the P_{D1}-P_{D2}-dimer have a larger separation of their tetrapyrrole ring systems (Figure 3), so that the coupling of excited states to charge-transfer states is small. This decoupling avoids formation of a deep energy sink at the P_{D1}-P_{D2}-pair (which is therefore not so "special") and allows for a wider excitation energy distribution in equilibrium. The underlying (local) excited state energies are probably determined primarily by electrostatic pigment-protein interactions as found in other systems (57, 58), but the detailed mechanisms of excited-state tuning in PSII-RC remain to be uncovered.

In accordance with the preferential localization of the excited state of the RC on Chl_{D1}, CS is assumed to start from this cofactor with the primary radical pair, $Chl_{D1}^{\bullet+}\,Pheo_{D1}^{\bullet-}$, being created in 0.6 – 3.0 ps. The second radical pair, $P_{D1}^{\bullet+}\,Pheo_{D1}^{\bullet-}$, is formed in 6 – 11 ps. $P_{D1}^{\bullet+}$ is the strong oxidant needed for water splitting. The first real stabilization of CS occurs in the third step yielding $P_{D1}^{\bullet+}\,Q_A^{\bullet-}$ in about 300 ps (59) (Figure 2A). This primary CS is formally a one-electron process that has to take place four times to allow for the formation of one O_2 (Figure 1A). As with the excited state structure, there are fundamental differences between PSII-RC and bRC concerning the mechanism of primary CS. In bRC, the P_L-P_M-dimer is the primary electron donor and B_A, the counterpart of Chl_{D1}, is the primary electron acceptor (52). However, also in bRC, CS can be started at B_A in certain site-directed mutants that raise the energy level of the $(P_L\text{-}P_M)^{\bullet+}\,B_A^{\bullet-}$ state (60). This finding indicates that the protein environment can alter the photochemical properties of the RC profoundly without changing the overall pigment arrangement, a fact that should be kept in mind when comparing structures. Furthermore, the crystal structures only show a kind of averaged structure, but structural variations due to protein motions cause disorder. As a result, the electronic states of protein-bound chromophores show a distribution of energy levels, so that multiple pathways of EET or CS can be operative (61, 62). Indeed, it has been proposed that there are actually two different CS mechanisms possible in PSII-RC (63, 64): One follows the path $Chl_{D1}^{\bullet+}\,Pheo_{D1}^{\bullet-} \rightarrow P_{D1}^{\bullet+}\,Pheo_{D1}^{\bullet-}$ and the other the path $P_{D1}^{\bullet+}\,Chl_{D1}^{\bullet-} \rightarrow P_{D1}^{\bullet+}\,Pheo_{D1}^{\bullet-}$, so that P_{D1} and $Pheo_{D1}$ are always electron donor and acceptor, respectively, but Chl_{D1} can act as both.

A further complication arises from the observation that CS and ET leading to water oxidation can be induced with photons of wavelengths as long as 780 – 800 nm (65-71). This finding has been explained with a low-lying excited state of PSIIcc similar to the so-called long-wavelength Chl of photosystem I (62, 72). A possible candidate for such a state is a charge-transfer state of the P_{D1}-P_{D2}-dimer coupled to exciton states (37). It could be formed in a sub-population of PSII-RC as a consequence of structural variations resulting in an increased coupling between P_{D1} and P_{D2}, so that these two Chl would after all form a "special pair". This state could then allow for CS initiated by far-red light via the path $P_{D1}^{\bullet+}\,Chl_{D1}^{\bullet-} \rightarrow P_{D1}^{\bullet+}\,Pheo_{D1}^{\bullet-}$. We note that also in bRC, there are different conformations of the P_L-P_M-dimer that presumably differ in the coupling between the dimer halves (73). Another possible "red state" is suggested by the CS mechanism involving $Chl_{D1}^{\bullet+}\,Pheo_{D1}^{\bullet-}$ as the first charge-separated state: Clearly, this state has to be coupled to excited states (e.g., Chl_{D1}^{*}) to allow for light-induced CS. If this coupling is

strong enough, the state $Chl_{D1}^{\bullet+}Pheo_{D1}^{\bullet-}$ could borrow some oscillator strength. This idea is supported by electric field effects on the optical spectra (Stark effect) of isolated PSII-RC (74). However, this study suggests the state $Chl_{D1}^{\bullet+}Pheo_{D1}^{\bullet-}$ to be close in energy to the lowest excited state of the RC implying a small driving force for the first ET step. Also, the spectrum of such a state should be significantly broadened by coupling to vibrations. At present, the nature of the "red Chl" in PSIIcc is unclear, and there is more to be learned about primary CS in the future.

3.2. Non-heme iron and quinones

The formation of PQH_2 from PQ requires two electrons and two protons and thus needs two turnovers of the RC (Figure 1A). The first step is the creation in 200 – 400 µs of a semiquinone anion radical $Q_B^{\bullet-}$, which is likely stabilized by protonation of a nearby amino acid side chain (21). It could be shown for the analogous bRC of purple bacteria that a glutamate residue (Glu L212) has to take up a proton from the cytoplasm prior to ET (75-77). This residue is part of a network of electrostatically coupled titratable groups that influence the proton uptake of the RC after quinone reduction (78, 79), but it is not conserved in PSIIcc. Presently, it is unknown, which group(s) take(s) over the role of the glutamate or are responsible for proton uptake from the cytoplasm. Studies on mutant bRC suggest that water molecules may functionally replace protonatable amino acid side chains (78, 80). Thus, water molecules near the Q_B-site in PSIIcc may also play an important role in quinone reduction, but could not yet be assigned in the crystal structure. The second ET step in PSIIcc occurs in 500 – 800 µs and is followed by protonation of the formed Q_B^{2-} (21). In bRC, the Glu L212 is likely one proton donor, while the second proton probably takes the route via a serine (Ser L223), which is in hydrogen bonding distance to Q_B and takes up a proton from Asp L213 (75-77, 81, 82). The latter serine is present in PSIIcc as well (Ser A264), and the role of the aspartate is taken over by His A252 as suggested by the crystal stucture and electrostatic calculations (83).

In recent years, the non-heme iron located equidistantly from both Q_A and Q_B has been in the spotlight again because of renewed interest in its possible participation in the ET reactions between the quinones in bRC (84-87). A mechanism is discussed, in which arrival of an electron on Q_A triggers ET from the non-heme iron complex to Q_B followed by rereduction of the non-heme iron complex by $Q_A^{\bullet-}$. Remarkably, a similar reaction sequence has been considered two decades ago for PSII (88). An important difference is that the non-heme iron is ligated besides the four histidines by bicarbonate in PSIIcc instead of a glutamate residue (Glu M234) in bRC. Bidentate ligation of bicarbonate to the non-heme iron in PSIIcc was detected by Fourier transform infrared (FTIR) difference spectroscopy using ^{13}C-labeled bicarbonate (89) and later confirmed by X-ray crystallography. Since bicarbonate emanates from the substrate of the dark reactions, CO_2, it is tempting to assign to it a role as activator of PSIIcc and hence the light reactions. Indeed, it is well known that bicarbonate is required for efficient reoxidation of $Q_A^{\bullet-}$ and protonation of Q_B^{2-} (90, 91). The analogous Glu M234 in bRC has been shown very recently to have a direct influence on proton uptake (79). A recent study on PSIIcc applied electron paramagnetic resonance (EPR) spectroscopy and quantum chemical modeling to the $Q_A^{\bullet-}$-Fe^{2+} complex and concluded that the ligand is actually carbonate, i.e., deprotonated (92). Indeed, the three putative hydrogen bond donors to this carbonate identified in the crystal structure together with the Fe^{2+} ion could significantly lower the pK_a value of HCO_3^- from ~10.3 in aqueous solution to below 6.0, which would be necessary for such an observation (92). In this situation, the carbonate ligand could act as a protonatable group relevant for proton transfer to Q_B^{2-} in agreement with a proposal based on FTIR studies of a hydrogen bond network from the non-heme iron toward the Q_B pocket involving (bi)carbonate and His A215 (93). These findings point to a possible role of the non-heme iron in the regulation of the quinone reductase activity of PSIIcc by CO_2. However, the precise function of this important metal center remains to be elucidated.

3.3. Creation of a strong oxidant

A key issue in PSII research is the question of how the oxidative power for water splitting is created. In the pH interval of 5.7 – 7.8 (the likely pH of the lumen under physiological conditions (94, 95)), the midpoint potential for the formal conversion of two water molecules into one O_2 molecule, four protons and four electrons is 770 – 890 mV (verus normal hydrogen electrode (1)). Notably, the potential for oxidation of Chl *a* is in a similar range depending on the solvent (96). The midpoint potential of the $P_{D1}/P_{D1}^{\bullet+}$ couple, $E_m(P_{D1}^{\bullet+}/P_{D1})$, has been estimated from experimental data to be about 1.25 V (36), so that there is just enough driving force for water splitting in PSIIcc. Theoretical calculations based on the 3.0 Å structure (14) yield $E_m(P_{D1})$ = 1.21 V (97) and suggest that the potential increase of P_{D1} compared to Chl *a* in solution is caused by the charge distribution of the protein environment with important contributions from the polypeptide backbone (i.e., helix dipoles of TMH **d** of PsbA and PsbD), the Mn_4Ca cluster and the peripheral protein subunits. It should be noted that the "decoupling" of P_{D1} and P_{D2} discussed in subsection 3.1 also contributes to the oxidative power of $P_{D1}^{\bullet+}$. A strong orbital overlap between P_{D1} and P_{D2} as in the "special pair" of bRC (Figure 3) would probably decrease the potential by up to 150 mV (53).

4. REDOX STATES OF THE Mn_4Ca CLUSTER

4.1. Kok-cycle and S-states

The oxidation of two water molecules to one molecule of O_2 is a four-electron process that has to be linked to the one-electron process of oxidizing P_{D1} in the RC (Figure 1A). This linkage is provided by the ability of

the WOC to store four oxidation equivalents during its reaction cycle, for which there is direct experimental evidence: If dark-adapted PSII is excited by saturating single-turnover light flashes, the oxygen evolution exhibits a damped period-four oscillation as a function of flash number (98-102) with maxima after the third, seventh, eleventh flash etc. (Figure 4A). This pattern has been interpreted by Kok *et al.* (99) in terms of five states of the WOC, S_i (i = 0, 1, 2, 3, 4), where i is the number of stored oxidation equivalents. A one-step advancement in this so-called "Kok-cycle", i.e., $S_i \rightarrow S_{i+1}$ for i = 0, 1, 2, 3, corresponds to the one-electron oxidation of the WOC by $P_{D1}^{\bullet+}$ triggered by light-induced CS in the RC (Figure 4B). The ET from the WOC to $P_{D1}^{\bullet+}$ actually involves an intermediate redox active tyrosine, Y_Z (see section 8), which was discovered later (103). The state S_4 is not stable, but circumstantial evidence for an intermediate between S_3 and S_0 has been reported (to be discussed in subsection 10.3). Dioxygen is believed to be formed in the $[S_4] \rightarrow S_0$ transition (Figure 4C), so that it is the $S_3 \rightarrow [S_4] \rightarrow S_0$ sequence, in which O_2 is released and the WOC is reset to its original redox state. This scheme implies that the stable state in the dark is S_1.

Flash excitation can cause a double turnover of the RC, resulting in a "double-hit", i.e, a two-step advance $S_i \rightarrow S_{i+2}$ of the WOC. In fact, double-hits are necessary to explain, why the oxygen evolution after the second flash is not strictly zero. In addition, some photosystems may not be able to turn over, e.g., due to competing charge recombination processes, which results in what is called a "miss" ("zero-step advance" $S_i \rightarrow S_i$ after flash excitation). Double-hits and misses have been invoked by Kok *et al.* (99, 100) to explain the observed oxygen evolution pattern. More recent analyses suggest that additional factors such as inactivation or backward-transitions may have to be considered (104). Processes of this kind cause a dephasing of the S-state cycling in a sample and hence a damping of the period-four oscillation until the steady-state oxygen evolution rate is reached (dashed line in Figure 4A). We note that Kok *et al.* (99) had to assume that besides S_1 a certain amount of S_0 is present in dark-adapted samples to satisfactorily fit the observed O_2 evolution pattern. They proposed to illuminate samples with one saturating flash prior to the dark adaptation period to reduce the amount of S_0. The initial presence of S_0 in the dark was explained by a redox equilibrium between S_0 and S_1 (105, 106). In an alternative explanation, which is preferred nowadays (104), there is no real S_0 population in the dark, but merely an apparent population being an artifact of the modeling (107, 108). Electron donation to S_2 and S_3 by an unknown donor has been invoked as explanation for these complications (108). For further details concerning the analysis of O_2 evolution patterns, see (104, 109).

Since the publication of the original model of Kok *et al.* (99), several extensions have been proposed that introduced additional states. Models with additional redox states, i.e., overreduced states of the WOC, are the topic of subsection 4.5. In contrast, Dau and Haumann (25, 110, 111) supplemented the cycle with protonation states. Initially, a second "S_4" state was introduced to account for time-resolved X-ray absorption data (110). However, if we take the index "i" of "S_i" as representing the redox state of the WOC in the spirit of Kok *et al.* (99), this new "S_4" is actually a deprotonated S_3 state (see further discussion in subsection 10.3). Later, a nine-state model (i.e., eight states + $[S_4]$) was proposed, in which there is a strict alternation of oxidation and deprotonation of the WOC (25, 111). Albeit intriguing, this model remains largely hypothetical; see (25) for an in-depth discussion. In the following, we shall base the description of the WOC on the traditional five-state model.

Flash-excitation of PSIIcc causes oxidation of the WOC at the "donor side" and reduction of the iron-quinone complex at the "acceptor side" (Figure 1A). While the WOC requires four turnovers of the RC to complete one cycle (period-four oscillation), the acceptor side needs two turnovers (binary oscillation). Thus, one may ask how the two reaction cycles, that are driven by the same trigger, are synchronized and whether the state of the acceptor side has any influence on the donor side. This problem was tackled by Shinkarev and Wraight (112). They distinguished between two reaction cycles of the WOC referred to as V- and W-cycle representing two different states of the iron-quinone complex and demonstrated that the details of the O_2 evolution pattern depend on these states. For example, a RC with Q_A reduced at the instant of light-excitation will not be able to perform stable charge separation allowing for a one-step advance of the WOC. Consequently, it will produce a miss. In this way, it can be rationalized that the miss probability depends on the redox state of the acceptor side and consequently also on the flash number. We refer the reader to the work of Shinkarev (104, 113, 114) for further details.

Before discussing the structure of the Mn_4Ca-cluster and the identification of its proteinogeneous ligands (see subsection 5.5), it is reasonable to look at the available information about its electronic structure, i.e., the redox states of the Mn ions in the different S-states (the Ca^{2+} ion is supposed not to change its redox state). Suitable methods for probing the redox states of metal centers are X-ray absorption (XAS) and emission (XES) (115-117) spectrosopy as well as electron paramagnetic resonance (EPR) and electron-nuclear double resonance (ENDOR) spectroscopy (118-120).

4.2. X-ray spectroscopy

In XAS, the energy from an X-ray beam is absorbed by the core electrons of an atom, and electrons are either promoted to a higher vacant orbital or ejected as a photoelectron. X-ray absorption spectra feature sharp increases in absorption at specific energies, which are characteristic for the absorbing element and referred to as "edges". The edge is due to an allowed transition according to the selection rule for dipole transitions, which states that the transition probability is high for $\Delta l = 1$, where l is the orbital momentum quantum number. For example, electrons from the 1s orbital (K-shell, l = 0) of Mn have a high probability for a transition into a p-orbital (l = 1). Since the lowest vacant p-orbital is 4p, it is the $1s \rightarrow 4p$ transition that gives rise to the "K-edge" (Figure 5A).

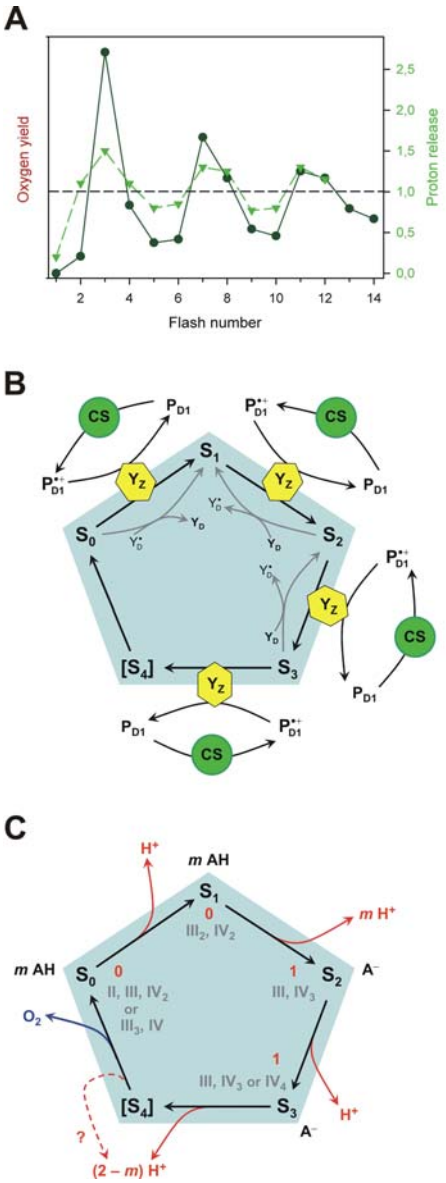

Figure 4.(A) Oxygen yield per flash in dark-adapted spinach thylakoids (red, arb. units, data from Messinger *et al.* (101)) and proton release per flash in dark-adapted PSIIcc from *Thermosynechococcus elongatus* (green, right scale, data from Suzuki *et al.* (431)) as a function of flash number. The dashed line marks the normalized steady-state oxygen yield per flash (see also (21)). (B) S-state model according to Kok *et al.* (99) describing the catalytic cycle of the water oxidizing complex (WOC). The number "*i*" in "S_i" indicates the number of oxidation equivalents stored in the WOC. The state "$[S_4]$" is kinetically elusive and still hypothetical as discussed in subsection 10.3. Excitation of PSIIcc with a saturating light flash effectuates S-state progression ($S_i \rightarrow S_{i+1}$) by initiating charge separation (CS) in the reaction center (cf. Figures 1A and 2A) producing the strong oxidant $P^{\bullet+}_{D1}$. $P^{\bullet+}_{D1}$ oxidizes the redox active tyrosine Y_Z that in turn oxidizes the WOC (103). The remote tyrosine Y_D (cf. Figure 2A) is in redox equilibrium with the WOC as indicated by the grey arrows. (C) S-state model according to Kok *et al.* (99) describing the catalytic cycle of the WOC as in B, but depicting a different set of details: The red arabic numerals refer to the accumulated positive surplus charge of the WOC according to Saygin and Witt (197, 198). The grey roman numerals indicate the presumed Mn redox states as explained in the text. AH/A^- is a hypothetical, deprotonatable amino acid side chain with protonation probability *m* coupled to the WOC and influencing the proton release pattern according to Schlodder and Witt (438). The proton release pattern (red arrows) is compatible with the data of Suzuki *et al.* (431) shown in A. The blue arrow indicates, where O_2 is released in the cycle. The dashed red arrow and question mark point to our lack of knowledge about the order of events between S_3 and S_0 and the actual mechanism of O_2 formation. However, there is circumstantial evidence that proton release precedes any redox reaction during $S_3 \rightarrow S_0$ as discussed in subsection 10.3.

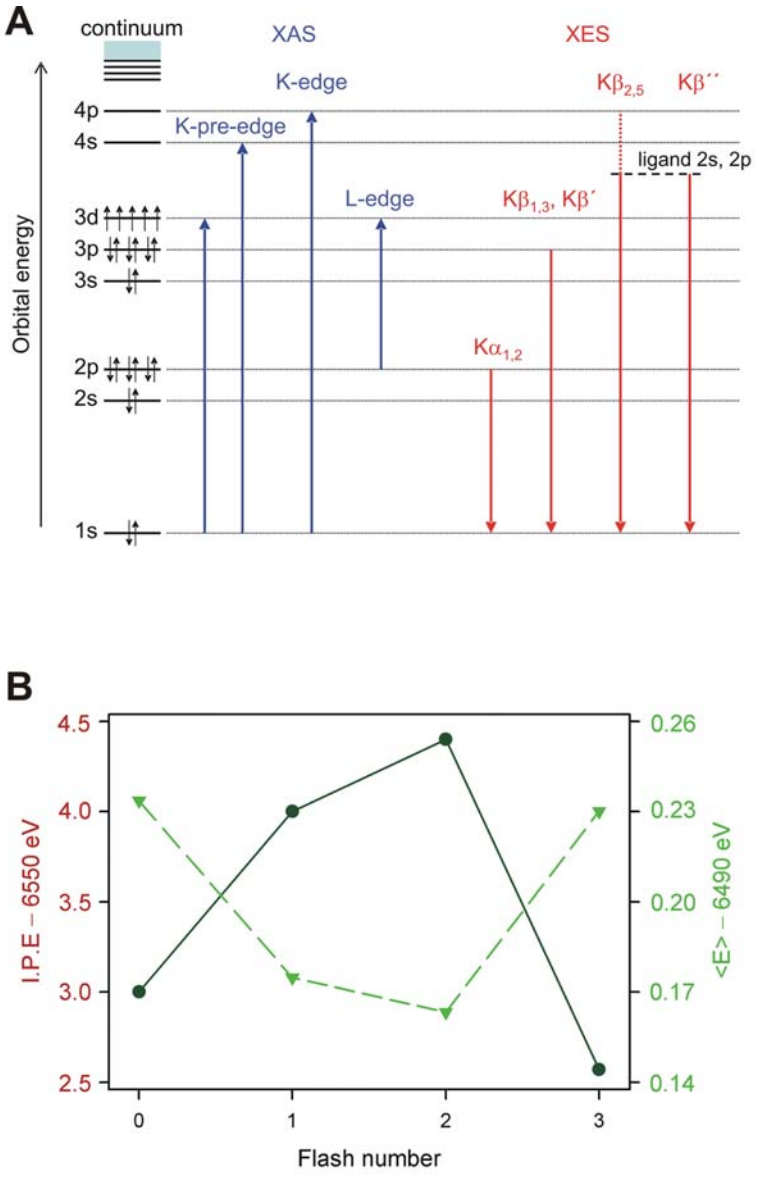

Figure 5. (A) Orbital energy scheme illustrating relevant XAS and XES transitions for a Mn complex. The shown electron configuration is that of Mn^{2+}. (B) Change of the Mn K-edge (inflection point energy, I.P.E., red, left scale) and the $K\beta_{1,3}$ emission (first moment <E> of emission peak, green, right scale) in PSII membranes from spinach as a function of flash number. Data from Messinger *et al.* (124).

Similarly, the lowest, not doubly occupied orbital to be reached from 2s or 2p (L-shell) is one of the 3d orbitals (l = 2) and, consequently, the L-edge is dominated by a 2p → 3d transition. Note that the L-edge is at significantly lower X-ray energies (soft X-rays) than the K-edge (hard X-rays). In addition, there are "weakly allowed" transitions that do not obey the selection rule (e.g., quadrupole transitions) and result in weak absorption bands in the pre-edge region (121). If the incident energy is high enough to eject the electron into the continuum, it is back-scattered from the surrounding atoms, which creates an extended X-ray absorption fine structure (EXAFS) containing important information about atom-atom distances (to be discussed in subsection 5.2).

As L-edge spectroscopy on biological samples is associated with some experimental difficulties (116), the focus in applying XAS to PSII has been on the K-edge. Goodin *et al.* (122), in their pioneering work, observed a shift of the K-edge to higher energies upon going from the S_1 to the S_2 state. Later experiments with improved technology confirmed this shift and furthermore revealed a

smaller shift to higher energies for the $S_2 \rightarrow S_3$ transition together with a back-shift to lower energies upon going to S_0 (Figure 5B) and an oscillatory behavior as a function of flash number (123, 124). These data were interpreted to indicate a Mn-centered oxidation during the $S_0 \rightarrow S_1$ and $S_1 \rightarrow S_2$ transitions, but the absence of Mn oxidation during $S_2 \rightarrow S_3$. However, other authors came to a different conclusion and assigned a Mn oxidation to each of the three S-state transitions (125-127). As discussed in detail in the literature (124, 127-130), there are some difficulties associated with the interpretation of the K-edge data including the precise quantitation of S-states as a function of flash number, the different methods to extract edge energies from the raw data and the explanation of the K-edge shift, making the determination of the metal oxidation state on the basis of the K-edge position difficult.

In XES, a core hole is created by excitation of the metal ion with X-rays of sufficient energy. The hole has a lifetime of only about 10^{-15} s, because it is rapidly filled by an electron from a higher shell with the excess energy being emitted as an X-ray photon (116, 117). For example, K fluorescence originates from electrons falling into the 1s orbital (red arrows in Figure 5A). In the context of redox states, the $K\beta_{1,3}$ fluorescence, which is due to a $3p \rightarrow 1s$ transition, was found to be a good probe for the oxidation state of Mn, since its energy is sensitive to the number of 3d electrons presumably because of exchange interaction between 3p and 3d electrons (131). In contrast to the K-edge, the $K\beta_{1,3}$ fluorescence shifts to lower energies upon removal of 3d electrons and, on the basis of XES studies of model complexes, was suggested to be less sensitive to the ligand environment (132). The $K\beta_{1,3}$ fluorescence energy of the Mn_4Ca cluster of PSII shows the same flash-dependent pattern as the K-edge position, i.e., a strong change after the first, a weaker shift after the second and a strong back-shift after the third flash (Figure 5B). Accordingly, these data were interpreted to confirm Mn-centered oxidation during the $S_1 \rightarrow S_2$ transition and its absence during $S_2 \rightarrow S_3$ (124). However, this interpretation is still not generally accepted, and the question was raised as to whether significant rearrangments in the ligand sphere of Mn could affect the $K\beta_{1,3}$ fluorescence (127).

Another complication arises from studies using resonant XES (RXES), also called resonant inelastic X-ray scattering (RIXS). In this type of experiment, the metal center is excited in the pre-edge region and X-ray emission originating from, e.g., electron relaxation from 2p orbitals into the 1s hole is monitored (116, 117). The data were analysed in terms of an effective number of 3d electrons, and it was conlcuded that the electron that is removed from the WOC during the S1 $\rightarrow$ S2 transition occupies a strongly delocalized orbital in the Mn4Ca-cluster (133). Under these circumstances, any assignment of oxidation states to individual Mn ions within the WOC appears to be merely a formality. Nonetheless, the formal oxidation states remain a useful framework for the analysis of the redox chemistry of the WOC.

4.3. Electron paramagnetic resonance spectroscopy

So far, we have only discussed redox state changes. But what about absolute oxidation numbers? To get this information, we have to resort to EPR and ENDOR spectroscopy. EPR spectra arise from the absorption of microwave radiation by a system carrying one or more unpaired electrons ($S \geq ½$) causing spin-state transitions (134). The transition energies depend on the strength of the applied magnetic field, which is usually expressed in terms of the microwave frequency and characterized by waveguide frequency bands. The more important bands for EPR of biological samples are S (2.60 – 3.95 GHz), X (8.2 – 12.4 GHz), K_u (12.4 – 18.0 GHz, also referred to as P-band), K_a (26.5 – 40.0 GHz), Q (33 – 50 GHz) and W (75 – 110 GHz). For a single unpaired electron with $S = ½$, the energy splitting between the two spin levels (electron Zeeman interaction) is proportional to the applied field with proportionality constant $g\beta_e$, where the Bohr magneton β_e is a universal constant and the "g-factor" g is characteristic of the spin system. Since in a molecule or cluster, the unpaired electron experiences local magnetic fields (e.g, due to orbital angular momentum), its g-factor can differ markedly from the value $g_e = 2.0023$ of the free electron, which is particularly true for transition metal compounds. Atomic nuclei may also carry a spin (e.g., $I = {}^5/_2$ for ^{55}Mn with the nuclear g-factor $g_n = 1.3819$), but the nuclear Zeeman splitting characterized by $g_n\beta_n$ (with β_n the nuclear magneton) is much smaller ($g_n\beta_n/g_e\beta_e = 37.587 \times 10^{-5}$ for ^{55}Mn). Of importance for EPR is rather the magnetic interaction between electron and nucleus, the hyperfine interaction characterized by the hyperfine coupling (hfc) constant a, giving rise to signal splitting. Both, g-factor and hfc constant, can show anisotropy that is characteristic of the symmetry of the molecular environment. In contrast to the Zeeman interaction, the hfc is independent of the applied field, so that studies of a system in different frequency bands can help to disentangle spectral features (135-137). If there is more than one unpaired electron ($S > ½$), additional line splittings occur due to electron-exchange and magnetic dipole-dipole interaction (134). Thus, in a system such as the WOC with four coupled Mn ions cycling through different oxidation states with possibly up to five unpaired 3d electrons per ion, a rich variety of EPR signals can be expected; and this is indeed found.

To date, EPR signals have been obtained from all (meta)-stable S-states (i.e., S_0, S_1, S_2, S_3). A recent overview is given by Haddy (119). Here, we focus on those states, in which Y_Z is not oxidized. So-called metalloradical signals with an additional $S = ½$ radical on Y_Z are discussed in subsection 8.2. The EPR signals known for the longest time are those associated with the S_2 state, comprising a multiline signal centered at $g = 2.0$ and a broad signal at $g = 4.1$ in X-band (119). The amplitude of the multiline signal exhibits a damped period-four oscillation with maxima after the first and fifth flash indicating its connection to S_2 (Figure 6A) (138, 139). The g-factor of the multiline signal was determined to $g = 1.98$ in Q-band (140). To reveal its g-anisotropy, W-band experiments were conducted on single crystals of PSII from *T. vulcanus* (141) and *T. elongatus* (142). There is consensus that the S_2

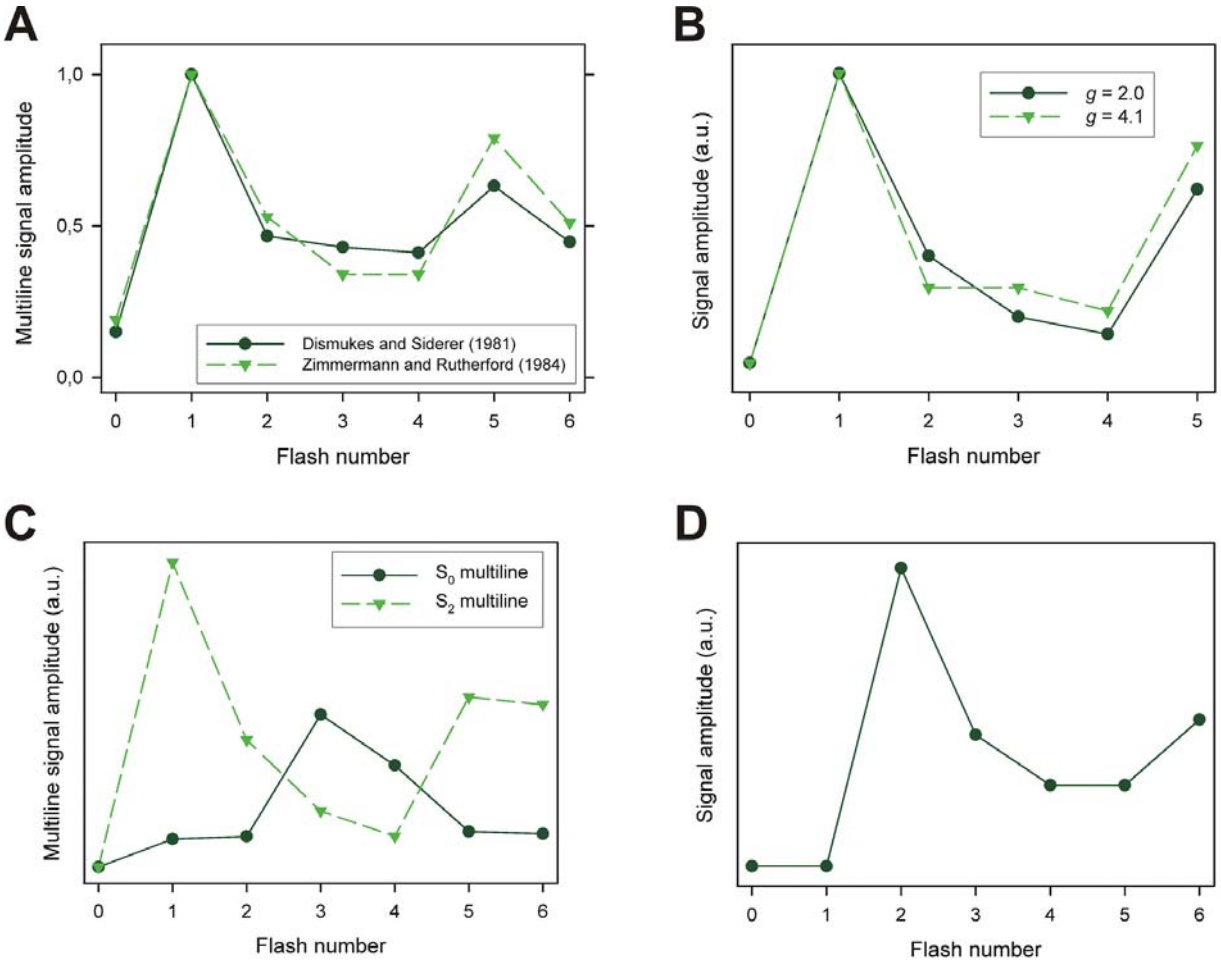

Figure 6. (A) Intensity of the S_2-state multiline signal at g = 2.0 in spinach samples as a function of flash number. Data from Dismukes and Siderer (138) as well as from Zimmermann and Rutherford (139) normalized to the signal amplitude after the first flash. (B) Intensity of the S_2-state multiline signal at g = 2.0 and the g = 4.1 signal in PSII membranes as a function of flash number. Data from Zimmermann and Rutherford (150) normalized to the signal amplitude after the first flash. (C) Intensity of the S_0- and S_2-state multiline signals in PSII membranes from spinach as a function of flash number. Data from Åhrling *et al.* (158). (D) Intensity of the S_3-state signal at g = 12.0 in PSII membranes from spinach as a function of flash number. Data from Matsukawa *et al.* (168).

multiline signal arises from the S = ½ ground state of the Mn_4Ca cluster. The many lines giving the signal its name (about 40 – 50 in S-band (136, 143)) are due to hfc between this spin and the ^{55}Mn nuclei. A number of different sets of hfc constants have been derived from EPR studies in various frequency bands (136, 144-146). The hyperfine data are consistent with Mn^{III} and Mn^{IV} oxidation states, but not Mn^{II} (138). The S = ½ ground state arises from antiferromagnetic exchange coupling between Mn ions and leaves only two possibilities for the formal oxidation states: Either there are one Mn^{III} and three Mn^{IV} (abbreviated in the following with (III, IV_3) as indicated in Figure 4C) or three Mn^{III} and one Mn^{IV}, i.e., (III_3, IV) (144). To decide on these possibilities, EPR experiments were conducted (145) on oxygen-evolving, PSII-enriched membranes from spinach (147) that were oriented by a partial-dehydration procedure (148, 149). Both, g- and hfc-anisotropy were exploited in simulations of the S_2-multiline signal (145) to conclude that the formal oxidation state is (III, IV_3) and to propose an arrangement of the Mn_4 moiety relative to the membrane normal (see subsection 5.4). The (III, IV_3) oxidation state was later confirmed by further simulations (146) and is also in agreement with interpretations of the K-edge in XAS (129, 130).

The broad g = 4.1 signal exhibits the same damped period-four oscillation as the g = 2 multiline signal (Figure 6B) and is thus also attributed to the S_2 state (150). Resolution of the hyperfine structure of the g = 4.1 signal, also exhibiting some "multiline" character, confirmed its tetranuclear Mn origin and suggested an $S = {}^3/_2$ or ${}^5/_2$ spin state associated with the same redox state of the Mn_4Ca-cluster as the g = 2.0 signal (151, 152). Later studies favored the $S = {}^5/_2$ variant (135, 146, 153-155). The relative

intensity of the two S_2-state signals depends on experimental conditions such as the temperature of illumination or the presence of small alcohols and cryoprotectants (119) as well as the binding of extrinsic protein subunits (156). Of particular interest is that both S_2-state signals are influenced by the presence of the chloride ion (119), which is required for oxygen evolution activity (157). We return to this aspect in section 7.

By applying three flashes to a dark-adapted PSII-sample, another multiline signal at $g = 2$ can be produced (Figure 6C), which is associated with the S_0-state (158-160). On the basis of EPR, this signal is interpreted as an $S = ½$ ground state of the WOC (161) being likely in the formal oxidation state (III_3, IV) or (II, III, IV_2). Assigning a spin ground state of $S = ½$ to S_0 and S_2 and a Mn-centered oxidation to the $S_0 \rightarrow S_1$ and $S_1 \rightarrow S_2$ transitions implies that the S_1 state should have an integral spin. Indeed, an EPR signal at $g = 4.8$ in the S_1-state consistent with $S = 1$ was detected (162). In coventional EPR, the microwave field is polarized perpendicular to the applied magnetic field. However, states with integer spin are better studied with parallel polarization (163), since in this case other selection rules apply. In this way, the existence of an EPR signal of dark-adapted PSII-samples from plants was demonstrated that vanishes upon illumination as expected for the $S_1 \rightarrow S_2$ transition (162, 164). However, the signal is weak, difficult to detect and absent after chloride or calcium depletion (164). Later attempts to find an EPR signal of the S_1-state in parallel mode revealed yet another multiline signal at $g = 12$ (165). This signal only appears in cyanobacterial PSIIcc or in plant PSIIcc with extrinsic subunits other than PsbO removed (166). The hyperfine structure of the $g = 12$ signal confirmed its manganese origin and suggests that all four Mn ions are exchange-coupled. On the basis of a comparison with a tetranuclear Mn model complex, this state was proposed to be compatible with a (III_2, IV_2) redox state (167).

The S_3-state can be generated by two flashes or by continuous illumination at 235 K. Matsukawa *et al.* (168) were the first to detect EPR signals of this state in both parallel and perpendicular mode. In particular, the parallel polarization EPR signal at $g = 12$ shows the expected flash number dependence (Figure 6D). Later, Ioannidis and Petrouleas (169) optimized the trapping protocol of the S_3-state and confirmed the results. Very recently, Boussac *et al.* (170) detected additional signals and found a satisfying fit for an $S = 3$ spin state. So far, the EPR spectra do not allow to decide, whether a Mn-centered oxidation occurs in the $S_2 \rightarrow S_3$ transition. They suggest, however, that if a ligand is oxidized in S_3, it is strongly magnetically coupled to Mn and thus from the first ligand sphere (170).

4.4. Electron nuclear double resonance spectroscopy

The multiline signals discussed in subsection 4.3 are suitable to demonstrate the limits of EPR spectroscopy as applied to the WOC: The many possible transitions arising from the hfc with ^{55}Mn can not be resolved. For example, the up to 50 lines of the $g = 2$ multiline signal of the S_2-state seen in S-band EPR (136, 143) represent only a small fraction of the possible $6^4 = 1296$ EPR transitions (171). Moreover, the spectra are dominated by ^{55}Mn hfc and weaker hfc from ligand nuclei are suppressed. Therefore, alternative methods have been applied to gain complementary information about hfc. The pulsed EPR method known as electron spin-echo envelope modulation (ESEEM) spectroscopy is sensitive to the weaker couplings arising from nuclei of putative ligands to the Mn_4Ca-cluster (172, 173). Results from this type of experiment are discussed in subsection 5.5. Here, we focus on the ^{55}Mn hfc studied with ENDOR.

In an ENDOR experiment, a radiofrequency (rf) field or pulse as used in nuclear magnetic resonance (NMR) is applied to drive nuclear spin transitions, which by virtue of the hfc act back on the electron spin system to produce a change in a specific EPR signal or the electron spin echo (ESE) intensity (for details, see (120) and references therein). The number of nuclear spin transitions observed in this way increases additively with the number of inequivalent classes of coupled nuclei (= 4 in the Mn_4Ca-cluster), so that there are "only" 40 distinct allowed ^{55}Mn nuclear spin transitions in the S_2-state with $S = ½$ and $I = {}^5/_2$ (174). Due to the dependence of the ENDOR spectrum on the probed EPR transition (field position), a further selection is possible. The advantage of a simultaneous simulation of EPR and ENDOR spectra to obtain reliable hfc parameters was clearly demonstrated by Peloquin *et al.* (174), who investigated the S_2-state in X-band. Later, Kulik *et al.* (175, 176) extended these studies to Q-band and also examined the S_0-state. They performed a simultaneous simulation of EPR and ENDOR spectra in X- and Q-band and also considered the g-anisotropy of the $g = 2$ multiline signal of the S_2-state apparent from W-band EPR studies on single crystals (142) to arrive at a final assignment of redox states (III_3, IV), (III_2, IV_2) and (III, IV_3) to S_0, S_1 and S_2, respectively. However, the experiments were performed in the presence of 3% methanol to enhance the multline signals, so that the variant (II, III, IV_2) for S_0, albeit unlikely, cannot be completely ruled out for methanol-free samples. We thus have at present the assignment of redox states to S-states as depicted in Figure 4C, with the two variants for the S_3-state arising from the uncertainty concerning Mn-centered oxidation in the $S_2 \rightarrow S_3$ transition. Further implications of EPR/ENDOR data for the structure of the inorganic core of the WOC (including more recent data on single crystals (177)) will be discussed in subsections 5.4 and 5.5.

4.5. Chemical reduction of the Mn_4Ca-cluster

It has been noticed quite early that treatment of PSII with chemical reductants such as hydroxylamine (NH_2OH) results in a delay in oxygen evolution from the third to the fifth flash (178). These results were interpreted in terms of the formation of an S_{-1}-state, i.e., a state of the WOC with one electron in excess of the S_0-state (179-181). Further studies, in which hydrazine (N_2H_4) was used besides NH_2OH, revealed the possibility to reversibly reduce the WOC to states S_{-2} and S_{-3} with concomitant shifts of the oxygen evolution pattern (101, 182-184). It was even possible to create states S_{-4} and S_{-5}, but these states appear to be less stable (185). Nonetheless, these

studies support the redox state assigment given in Figure 4C. In addition, hydroquinone was used to create the S_{-1}-state (186, 187), and chemical reduction was applied to create an analog of the S_0-state from S_1 in the dark (188). This analog was shown to have the same EPR properties as the S_0-state accumulated by "flashing through the Kok-cycle" (159).

Interaction of nitric oxide (NO) with dark-adapted PSIIcc was demonstrated to produce, among other products (189-191), an S_1-derived state exhibiting an EPR multiline signal centered at g = 2 (192). This signal was later attributed to a Mn^{II}-Mn^{III} interaction (193, 194) and, on the basis of the retarded oxygen evolution pattern, assigned to S_{-2} (195). NO also reacts with the S_2 and S_3-states produced by pre-flashes. The exceptionally fast reaction of NO with S_3 was interpreted as the possible presence of an organic radical in the S_3-state, which would be in line with the absence of a Mn-centered oxidation in the $S_2 \rightarrow S_3$ transition (196).

4.6. Net charge changes of the Mn_4Ca-cluster

The fact that the Mn_4Ca-cluster is oxidized at least in each of the steps leading from S_0 to S_3 raises the question of whether positive charges are accumulated in the WOC-site. In their seminal work, Saygin and Witt used electrochromic band shifts of carotenoids (197) as well as chlorophylls (198) to demonstrate that a positive surplus charge (i.e., the net charge change relative to S_1) is accumulated in S_2 compared to S_1, but not in S_3 compared to S_2 or in S_1 compared to S_0. Since one electron is released in each step of the sequence $S_0 \rightarrow S_1 \rightarrow S_2 \rightarrow S_3$, the found surplus charge pattern of 0:0:1:1 in S_0: S_1:S_2:S_3 (Figure 4C) can only be explained by processes leading to a compensation of one positive charge accompanying the formation of S_1 and S_3. These processes are likely related to proton release as discussed in section 9. The interpretation of the electrochromic shifts is supported by the S-state dependence of the re-reduction kinetics of $P_{D1}^{\bullet+}$ (199). Electrochromic shifts were also studied in PSIIcc-samples treated with NH_2OH indicating the presence of a negative surplus charge in the S_{-1}-state (180).

5. STRUCTURE OF THE Mn_4Ca CLUSTER

5.1. X-ray crystallography

The progress in structure elucidation of PSIIcc by X-ray crystallography can be assessed from two quantities. The indicated resolution of, e.g., 2.9 Å, implies that the crystallographic model takes into account diffraction from sets of equivalent, parallel planes of atoms with a minimum lattice plane distance of 2.9 Å. As a rule of thumb, two objects in the electron density map at 2.9 Å resolution can be resolved, if they are 2.9 Å apart. Notwithstanding, the precision of atom positions is higher, since structural constraints such as known bond lengths and angles of amino acid residues are considered in the modeling. The estimated coordinate error of PSIIcc at 2.9 Å resolution is 0.26 Å (200) as calculated by using the programm SFCHECK (201). Another measure of data quality is the number of unique reflections, which counts the number of measured reflections in a crystallographic data set after neglect of all repeated measurements of the same reflection or symmetry-related reflections. This number increased considerably from the first to the most recent 3D-structure of dimeric PSIIcc, and even the last step, albeit seemingly small as regards the resolution enhancement, implies a significant increase in the reliability of the model. We note that this latter progress is due to an improved data processing (15), whereas the earlier steps imply an improvement of crystal quality (14).

The quality of the structure of the Mn_4Ca-cluster as derived from X-ray diffraction is a more complicated issue (24). Here, we face four main problems: (i) unavoidable radiation damage, (ii) high electron density in the Mn_4Ca-cluster, (iii) structural heterogeneity, and (iv) lack of stringent structural constraints. As discussed in subsection 4.2., X-rays are not only scattered by atoms, but also absorbed depending on the electronic energy levels and the X-ray wavelength. Exposure of any material to X-rays thus will lead to some production of photoelectrons (202) that eventually are trapped by redox-active centers (203-207). As shown by applying XAS and EXAFS, the X-radiation indeed causes a reduction of the Mn-ions in the WOC under conditions of X-ray diffraction studies (208-210). This reduction may result in structural alterations, thereby causing a larger distribution of metal-metal distances, or even result in a destruction of the active center. The concomitant loss of phase relationship ultimately limits the quality of the electron density in this region. Even without this damage, the high electron density originating from the Ca and the four Mn ions makes it impossible even at 2.9 Å resolution to clearly resolve individual metal sites and also overshadows the electron density of proteinogeneous ligands. In addition, about 10 % of the catalytic centers can be inactive or damaged per se or only partly assembled (24). Even fully active centers in the S_1-state can principally occur in different conformers and/or tautomers as suggested by quantum chemical model calculations (211, 212). Finally, there are no stringent constraints concerning bond lengths, binding topology etc. as in the case of amino acids or other cofactors except for some information from EXAFS (see subsection 5.2; in fact, some constraints have been applied in the modeling, see below). All these factors increase the coordinate error of the WOC-region considerably compared to other parts of PSIIcc.

In normal X-ray crystallography, most X-ray photons can be considered to a good approximation as being elastically scattered without any phase delay (Thomson scattering). In general, the ability of the atoms to absorb X-ray photons at specific wavelengths (see subsection 4.2) influences the scattering behavior. If the X-ray energy is close to an absorption edge, anomalous dispersion occurs, resulting in a change of amplitude and phase of the scattered radiation (213, 214). Since like the absorption edges, the anomalous scattering is element-specific, tuning of the X-ray wavelength can be used as a means of contrast variation to distinguish certain atom types and to locate their positions in the unit cell (215). In this way, Zouni *et al.* (10), by using a wavelength close to the Mn-edge, were able, for the first time, to locate the

Mn_4-cluster (at that time without the Ca). The four metal ions showed up as a pear-shaped electron density, which was interpreted tentatively in terms of an "Y"-like arrangement (Figure 7). This interpretation was essentially confirmed by Kamiya and Shen (11) at a slightly better resolution. Ferreira *et al.* (12), still in a similar resolution range, extended the anomalous diffraction studies to a wavelength that allowed, for the first time, to locate the Ca-ion. It is located on top of the triangle formed by three of the Mn-ions and points towards the redox-active tyrosine A161 (Figure 7A). The fourth Mn-ion appears to be somewhat segregated and has been baptized the "dangling" manganese (174). This basic arrangement was confirmed by Loll *et al.* (14) with some changes of ion positions within the error limits of X-ray crystallography at this site (for a comparison, see (18, 24, 26)), and no further changes were identified in the refinement made by Guskov *et al.* (15).

It is important to understand that structural details such as μ-oxo bridges can not be inferred from the X-ray diffraction data at the presently available resolutions for reasons described above. To have at least some constraints at hand to cope with the unresolved electron density at 3.0 Å resolution, Loll *et al.* (14) used information from EXFAS about metal-metal distances in the Mn_4Ca-cluster (Figure 7B), but the positioning of metal ions and their ligands necessarily remains tentative. Ferreira *et al.* (12) used a rather detailed working model for the Mn_4Ca-cluster to interpret the electron density at 3.5 Å resolution, which is, in our view, an overinterpretation of the crystallographic data. Not surprisingly, some of these details will have to be revised, while other aspects are worth a further consideration (see below). In the following, we descibe the less detailed (that is, "μ-oxo-free") model by Guskov *et al.* (15).

In Figures 7A, C we show the (tentative) arrangement of metal ions in the Mn_4Ca-cluster according to the 2.9 Å resolution structure in relation to α-helical segments of the peptide backbone and some amino acid residues of interest including putative metal ligands (Figure 7B). Also shown in Figures 7C, D is the position of the chloride ion as inferred from the electron density at 2.9 Å resolution and work on bromide-substituted PSIIcc to be further discussed in section 7. Despite the uncertainties alluded to above, some points can be made: (i) The redox active Tyr A161 (Y_Z) is in hydrogen bonding distance to His A190, but both residues do not belong to the first ligand sphere of the Mn_4Ca-cluster (the Tyr-Ca distance is about 5 Å, see Figure 2B). (ii) The Mn_4Ca-cluster is located together with the Cl^--ion close to three α-helices of PsbA (**A-cd**, **A-et**) and PsbD (**D-et**; Figure 7C), which are rather stiff structural elements. (iii) Mn1 is likely coordinated by two residues (Glu A189 and His A332), which are located at the ends of different α-helices from PsbA. In this position, Mn1 seems to form a bridge between the α-helices (Figure 7A). (iv) Likewise, the Cl^--ion is coordinated by residues Asn A181, Glu A333 and Lys D317 from three different helices (Figure 7C, D) and thus may serve to stabilize the mutual arrangement of these helices, which likely contributes to the overall stability of the WOC. Also, the orientation of the putative ligand Glu A333, which is located next to His A332, but already in a loop-region, might be stabilized by the interaction of its backbone NH-group with the Cl^--ion. (v) All other putative ligands from PsbA (shown with yellow carbon atoms in Figures 7A, C) are located in loop regions and thus are likely more flexible and prone to structural perturbations, which is particularly true for Asp A342 and Ala A344 in the C-terminal loop of PsbA. (vi) All carboxylate ligands are modeled as bidentate ligands bridging two metal ions (Figure 7B). Albeit tentative at the present resolution, such a bidentate ligation could stabilize the inorganic core of the WOC and also assist in structural rearrangements that might occur during the catalytic cycle. (vii) The position of the "dangling" Mn4 appears to be the least certain among the metal ion positions. This is further substantiated by anomalous scattering studies at different temperatures, suggesting that Mn4 is most prone to radiation damage (14, 24). (viii) The Mn4-Cl^- distance is 6.6 Å (Figure 2B). Taking into account the uncertainty of the Mn4-position (point vii), this result is in accordance with EXAFS-studies on bromide-substituted PSIIcc, suggesting a metal-bromide distance of about 5 Å (216). (ix) Electron density between Mn4 and Cl^- could be due to a water molecule, which at this position would be ligated by the side chains of Asn A181 and Glu A333 (Figure 7D). (x) There is only one putative ligand from PsbC (Glu C354) located in a small helical loop segment (not shown, but see (30) for a topological map of PsbC). A protonatable residue of potential interest, Arg C357 (not shown, but see section 9), is located close to Glu C354 on the same helical segment with its side chain pointing towards the Mn_4Ca-cluster (Ca-$N_{\eta 1}$ distance ~ 5 Å).

5.2. Extended X-ray absorption fine structure (EXAFS)

A suitable method to study the structure of multinuclear metal complexes is EXAFS (115). As discussed in subsection 4.2, an X-ray photon with sufficient energy (i.e., above an element´s absorption edge) can create a photoelectron. In a simple picture, this quasi-free electron can be envisaged as a wave that goes out from one center (the absorber, e.g., a Mn-ion) and is scattered by another center (the backscatterer, e.g., a Mn or Ca ion or a μ-oxo bridge). The interference of outgoing and backscattered waves characterizes the final state of the electron after absorption of the X-ray photon and hence influences the absorption coefficient. As the interference pattern depends not only on the distance between absorber and backscatterers, but also on the wavelength of the electron, which in turn depends on the excess energy (that is, X-ray photon energy minus ionization energy), an oscillatory component of the absorption coefficient ("fine structure") results, extending to about 1 keV above the edge and containing information about the backscatterer positions. Extracting this information requires subtraction of the pre-edge background and normalization. A Fourier-transformation (FT) of the obtained oscillatory pattern then yields an FT-amplitude spectrum with peaks at the apparent absorber-backscatterer distances (115, 208). Advantages of this method are that it is element-specific as are the absorption edges, that principally each metal in any state (e.g., spin state) can be probed and that radiation damage is

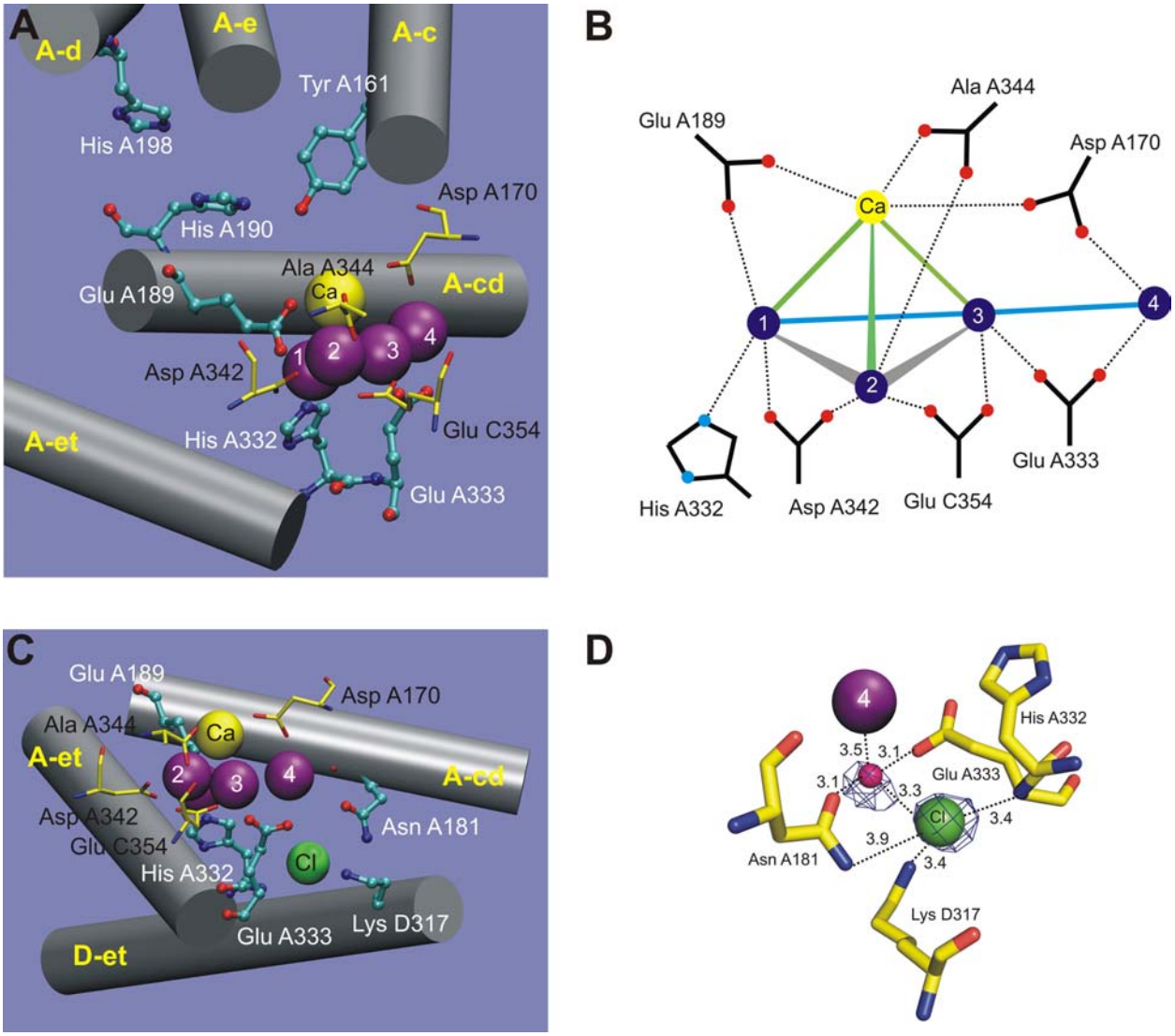

Figure 7. (A) Metal ion arrangement of the Mn_4Ca cluster (Mn ions labeled 1–4) relative to key amino acid residues and α-helices as inferred from the 2.9 Å resolution structure (15). Residues located in helical regions are shown as ball-and-stick model with carbon in cyan, those in loop regions as stick model with carbon in yellow. Transmembrane α-helices (TMH) of PsbA are labeled **A-c**, **A-d**, and **A-e**. Non-transmembrane helices **A-cd** and **A-et** are located between TMH **A-c** and **A-d** as well as between TMH **A-e** and the C-terminus of PsbA, respectively. Glu A333 is already outside the helical region, but stabilized by interaction of its backbone with the chloride ion (see C, D). Tyr A161 is the redox active tyrosine Y_Z. His A198 is the axial ligand to P_{D1}. (B) Tentative first ligand sphere of the Mn_4Ca cluster (Mn ions labeled 1–4 as in A) as inferred from the 2.9 Å resolution structure (15). The lines connecting Mn ions do not represent chemical bonds, but merely indicate distances (grey, 2.7 Å; blue, 3.3 Å; green, 3.4 Å). (C) Same as in A, but viewed from a different perspective (Mn1 covered) and showing the chloride ion (Cl_1 site) identified in the native data set at 2.9 Å resolution (15) as well as non-transmembrane helices **A-cd** and **A-et** of PsbA and **D-et** of PsbD and a different set of selected amino acid residues. (D) Environment of the Cl_1 site including Mn4 of the WOC and a putative water molecule between Mn4 and the chloride ion (adapted from Guskov *et al.* (15)). The numbers are distances in units of Å.

reduced due to the use of lower X-ray doses compared to X-ray crystallography. Problems arise from the facts that backscatterers with similar atomic numbers (e.g., C, N, O) can not be distinguished, that there is some structural disorder in the absorber-backscatterer arrangement and that a quantification of the spectra, e.g., in terms of coordination numbers is not easy. Therefore, spectra are interpreted with reference to experiments on model complexes of known structure.

As is well documented in the literature (25, 117, 217), FT-amplitude spectra derived from EXAFS at

the Mn K-edge of isotropic PSII-samples exhibit three major peaks that are interpreted as Mn-O/N distances at 1.8 – 2.2 Å (peak I), Mn-Mn-distances at 2.7 – 2.8 Å (peak II) and Mn-Mn/Ca distances at 3.3 – 3.4 Å (peak III). In particular, the discovery of peak II was a significant breakthrough, as it stimulated the interpretation of the EXAFS-data of the WOC in terms of a μ-oxo bridged Mn complex (218). A bridge is called μ_2, μ_3 or μ_4 depending on whether it connects two, three or four metal ions (examples of each type can be seen in Figure 8). Numerous studies on synthetic multinuclear Mn complexes revealed that bridging Mn-O distances in these cases are typically about 1.8 Å, and that of Mn-O/N distances pertaining to terminal ligands are between 1.9 and 2.2 Å. The Mn-Mn distances depend on the number and type of bridges: They range between 2.6 and 2.8 Å for complexes with at least two μ_2-oxo or two μ_3-oxo bridges, but complexes containing μ_3-oxo bridges also feature Mn-Mn distance > 3 Å, and the distance can be as short as 2.3 Å for tri-μ_2-oxo bridging; for reviews, see (217, 219-222). Another interesting aspect is that protonation of one bridging oxygen in a di-μ_2-oxo-bridged unit causes a lengthening of the Mn-Mn distance by ~ 0.1 Å (223, 224). There seems to be a consensus that peak II of the WOC is heterogeneous with contributions from ~ 2.7 Å and ~ 2.8 Å Mn-Mn-distances (25, 117, 225). Small, but distinct changes of Mn-Mn distances occur during all S-state transitions, but these are least pronounced in $S_1 \rightarrow S_2$ (117). Haumann *et al.* (127) interpreted their data in terms of a shortening of a Mn-Mn distance during $S_0 \rightarrow S_1$ as well as $S_2 \rightarrow S_3$ and proposed *inter alia* deprotonation events (e.g., deprotonation of a μ_2-hydroxo bridge in $S_0 \rightarrow S_1$) as a possible explanation.

A plethora of topology models of the inorganic core of the WOC is compatible with the EXAFS data of isotropic samples (217, 226). A possibility to reduce the ambiguity is the use of oriented samples, as the EXAFS FT-amplitude is orientation dependent and proportional to $\sim\cos^2\theta$, where θ is the angle between the electric field vector of the polarized X-ray beam and the absorber-backscatterer vector. There are two types of oriented samples, on which EXAFS-experiments have been performed: (i) oriented membranes from spinach chloroplasts (227-230) and (ii) single crystals of dimeric PSIIcc from *T. elongatus* (22).

Already the pioneering work of George *et al.* (227) on oriented chloroplast membranes revealed a pronounced dichroism of peaks II and III, the latter suggesting the orientation of a 3.3 Å absorber-backscatterer vector (interpreted as Mn-Mn distance at that time) close to the membrane normal in the S_1-state. Later work confirmed the dichroism of peak II with average angles of 2.7 Å vectors relative to the membrane normal of ~60°, but arrived at a different conclusion about peak III with a 3.38 Å vector at an angle of ~43° relative to the membrane normal (228). Another study reported 80 ± 10° for the 2.7 Å vectors (229). More recently, improved technology (115, 117) allowed for a better resolution of absorber-backscatterer vectors, and its was concluded that there are three di-μ_2-oxo-bridged Mn-Mn distances of ~2.7 and ~2.8 Å in a 2:1 ratio aligned at an average orientation of ~60° relative to the membrane normal (230). Furthermore, the puzzle about peak III could be solved by separating it into a ~3.2 Å Mn-Mn vector lying nearly in the membrane plane and ~3.4 Å Mn-Ca vectors with their average aligned along the membrane normal (230). A problem arises from the fact that the membranes in these experiments are only partially oriented, i.e., the various membrane sheets in the sample have a different orientation with respect to the substrate plane as illustrated in (115, 231). This mosaicity causes uncertainties in the angle θ of up to ~20°.

Polarized EXAFS was applied to single crystals of dimeric PSIIcc to obtain further constraints for the modeling of the WOC-structure (22). Although the mosaicity is significantly smaller in this type of sample, the arrangement of PSIIcc-units is more complicated as each PSIIcc-dimer contains two Mn_4Ca-clusters related by a non-crystallographic C_2 symmetry, and four dimers are arranged in different orientations in the unit cell. By measuring EXAFS polarized along the three different crystal axes and controlling the crystal orientation *in situ* by X-ray diffraction, Yano *et al.* (22) were able to select essentially three out of the many proposed topology models of the inorganic core of the WOC that are consistent with the EXAFS dichroism. In agreement with the later modeling based on oriented membranes (230), the remaining models obtained from the crystal study contain Mn-Mn distances of ~2.7 and ~2.8 Å in a 2:1 ratio, a ~3.2 Å Mn-Mn vector and two ~3.4 Å Mn-Ca vectors. The models were placed into the crystal structure by using information concerning the relative position of Ca and Mn ions from anomalous X-ray diffraction and the overall shape of the electron density. As an example, we show in Figure 8A the model IIa of Yano *et al.* (22) and a possible ligation pattern that follows from placing this model into the more recent crystal structure of Guskov *et al.* (15). A problem of the model is the mismatch of the inorganic core with some of the proteinogeneous ligands (e.g., Ala A344 experiences a steric clash with Mn1 with an unrealistic Mn-O distance of 0.9 Å). This type of discrepancy could result from the uncertainty of placing the Mn_4CaO_5-core correctly into the crystal structure, but likewise could be due to the larger coordinate error of the crystal structure in the WOC region (see subsection 5.1). Therefore, the ligand topology shown in Figure 8A remains necessarily tentative.

The filtering of models performed by Yano *et al.* (22) based on polarized EXAFS does not exclude the possibility that further models may be constructed that satisfy the EXAFS constraints. Sproviero *et al.* found such a model (232-234). They performed hybrid quantum mechanics/molecular mechanics (QM/MM) computations using density functional theory (DFT) in the QM part (for reviews, see (234-236)) based on the 3.5 Å resolution model of Ferreira *et al.* (12). The resulting QM/MM model of the WOC was subjected to a fitting routine to make it compatible with the polarized EXAFS data of Yano *et al.* (22), resulting in a so-called R-QM/MM model (233). This model features a heterocubane Mn_4CaO_4 core with three μ_3-oxo bridges and one μ_4-oxo bridge linking the "dangling" Mn4 (Figure 8B). We note that calculations of

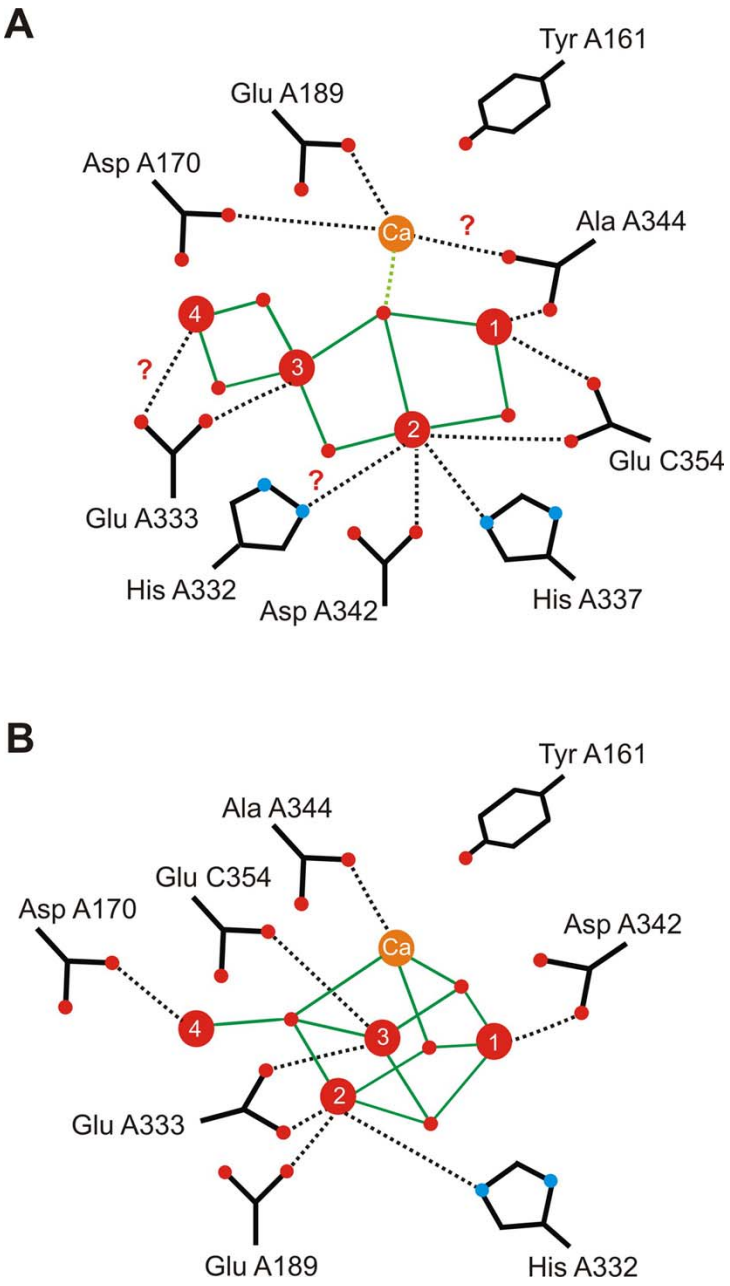

Figure 8. (A) Tentative ligand sphere of the Mn_4Ca cluster as a result of placing model IIa of Yano *et al.* (22) derived fom polarized EXAFS on PSIIcc single crystals into the 2.9 Å resolution structure (15). The question marks indicate problems of reconciling the EXAFS model with the crystal structure as discussed in the text. (B) Ligand sphere of the Mn_4Ca cluster according to the R-QM/MM model of Sproviero *et al.* (233) based on the 3.5 Å resolution structure (12). μ-oxo bridges between metal ions are drawn as small red spheres and green lines. Tyr 161 (Y_Z) is shown to indicate the orientation with respect to the reaction center, but is not a direct metal ligand.

this kind require assumptions to be made concerning the positions of water molecules, counter ions etc. due to the lack of experimental information about these details. Also, the original QM/MM model contained a Cl^- ion ligating Ca (232) in contrast to more recent experimental information (see subsection 5.1 and section 7). Nonetheless, Sproviero *et al.* could demonstrate that a heterocubane structure is principally in agreement with the polarized EXAFS data from single crystals. An advantage of this model is that there is no mismatch between the inorganic core and the proteinogeneous ligands. However, there is no ligation of a Mn ion by Ala A344, but ligation of the Ca^{2+} ion instead, which is in disagreement with spectroscopic data (see subsection 5.5). So, there remain discrepancies that require

further research. A promising route to more information about the structure of the WOC is polarized EXAFS on the recently obtained crystals of monomeric PSIIcc (28). In this new crystal form, there are only four different orientations of PSIIcc monomers in the unit cell, and for all of these orientations, the membrane normal makes an angle of ~90° with the crystallographic *b*-axis. This particular arrangement could facilitate the discrimination between absorber-backscatterer vectors oriented parallel and perpendicular to the membrane normal. Work along these lines is in progress.

5.3. Ca site and Ca/Sr exchange

The binding of Ca^{2+} to PSIIcc and its role in water oxidation has been the subject of numerous studies; see (157) and references therein. Biochemical studies revealed several Ca^{2+} binding sites in PSIIcc in accordance with the most recent crystallographic model (15), but Ädelroth *et al.* (237) could demonstrate by using radioactive $^{45}Ca^{2+}$ that a single exchangeable Ca^{2+} ion per RC is sufficient to restore oxygen-evolution activity in Ca-depleted PSIIcc. The close interaction of this Ca^{2+} ion with Mn in the WOC was actually established prior to the anomalous X-ray scattering experiments on single crystals of PSIIcc. One line of evidence originates from the requirement of Ca^{2+} besides Mn^{2+} for the photoassembly of the WOC; for reviews, see (238-241). Another set of experiments showed that the inactivation of the WOC by chemical reductants is retarded by Ca (186, 242-244). These data were tentatively interpreted *inter alia* in terms of a binding site, in which Ca^{2+} blocks access of bulky reductants to Mn (157). We shall return to this interesting aspect in section 6. A more direct evidence for Mn-Ca interaction is provided by EXAFS at the Ca K-edge showing backscattering from Mn at a distance of 3.4 Å (245) and complementing the data obtained at the Mn K-edge (see subsection 5.2).

A number of metals have been tested for their ability to functionally replace Ca^{2+} in the WOC. Apparently, the WOC has a preference for di- and trivalent metals whose ionic radii are not too different from that of Ca^{2+}, which is 0.99 Å (157). Among these ions, only Sr^{2+} (1.13 Å) is an activator of oxygen evolution activity (~40 % according to (246)), whereas Cd^{2+} (1.03 Å) and La^{3+} (1.04 Å) are competitive inhibitors. Notably, Mn^{2+} (0.80 Å) is a weak inhibitor in this type of experiment (~20 % activity (246)). We note that reconstitution with Ca^{2+} itself only restores about 80 % of the oxygen evolution activity. The decrease of activity in Sr^{2+}-reconstituted material can be traced back to a slowdown of the S-state transitions, but a significant retardation is also observed for Ca^{2+}-reconstituted samples compared to untreated PSII membranes (247) pointing to a disturbance of the WOC by the depletion/reconstitution procedure. Notwithstanding, the possibility to perform experiments on an essentially active WOC containing a different metal ion triggered spectroscopic studies on Sr^{2+}-reconstituted plant PSII. EXAFS at the Sr K-edge confirmed that Sr^{2+} is incorporated in the vicinity of Mn at a distance of ~3.5 Å with the slightly larger distance compared to Ca^{2+} (see above) likely originating from the larger ionic radius of Sr^{2+} (248). Corresponding experiments on oriented membranes revealed an orientation of the Mn-Sr vector along the membrane normal with an error of 23° (249) in accordance with the results on native, Ca^{2+}-containing PSIIcc discussed in subsection 5.2. The proximity of Sr to Mn was also explored with ^{87}Sr ESEEM spectrosocopy (250). The weak magnetic coupling between the $I = {}^{9}/_{2}$ ^{87}Sr nucleus and Mn was interpreted in terms of an upper limit for the Mn-Sr (and by analogy Mn-Ca) distance of 3.8 – 5.0 Å in reasonable agreement with the EXAFS-data.

A breakthrough concerning Ca/Sr-exchange was the development of a biosynthetic procedure by Boussac *et al.* (251). Cells of the thermophylic cyanobacterium *T. elongatus* were grown under continous illumination in a medium containing Sr^{2+}-salt instead of the normally used Ca^{2+}-salt. Surprisingly, the cells grew at the same rate in either case, demonstrating impressively the ability of Sr^{2+} to replace Ca^{2+} in the photosynthetic light reactions of these bacteria. The isolated PSIIcc showed the same reduction in oxygen-evolution as for biochemical Ca/Sr exchange when measured under continuous illumination, which was again traced back to a retardation of the S-state transitions. However, the oxygen evolution per flash was similar to Ca-containing samples indicating full activity. Moreover, the isolation of PSIIcc had to be performed in the presence of normal amounts of Ca^{2+}-salt to avoid loss of activity. The finally obtained core complexes contained 1 Sr/4 Mn. This result has two interesting implications: (i) Apparently, the Sr^{2+}-ion responsible for the restoration of oxygen-evolution activity is essentially nonexchangeable under the preparation conditions (i.e., in the presence of betaine protecting against the loss of extrinsic protein subunits) in contrast to other Sr^{2+}-ions that might have been biosynthetically incoporated into PSIIcc. This result is principally in agreement with earlier biochemical work indicating that one slowly exchangeing Ca^{2+} per RC is necessary for water oxidation (157). Ädelroth *et al.* (237) found a dissociation half-time for this Ca^{2+} of 80 h in intact plant PSIIcc. Furthermore, Sr^{2+} might be bound more tightly to the WOC than Ca^{2+} (for reasons to be discussed in section 6). (ii) The loss of activity in media lacking Ca^{2+} then points to a structure-stabilizing role of other Ca^{2+}-ions bound to PSIIcc such as Ca^{2+}-PsbK and/or Ca^{2+}-PsbO (see Figure 1 B, C). In the following, we shall refer to preparations from biosynthetically exchanged bacteria as Sr-PSIIcc.

An attempt was made to crystallize Sr-PSIIcc, but crystals diffracting to 3.9 Å were only obtained in the absence of betaine, resulting in a back-exchange of about 50 % of the Sr^{2+} to Ca^{2+} (252). Anomalous X-ray scattering around the Sr K-edge was applied to locate the Sr^{2+} ion in the structure, but radiation damage limited the datasets to a resolution of 6.5 Å. Nonetheless, an anomalous difference electron density map was reported (252) showing a peak attributed to Sr^{2+} at a distance of 1.88 Å and 1.65 Å, respectively, from the Ca^{2+} positions indicated in the crystal structures at 3.5 Å (12) and 3.0 Å (14) resolution.

Isotropic samples of Sr-PSIIcc were investigated with EXAFS in all amenable S-states at both

the Mn and Sr K-edge (253). The Mn K-edge data confirmed that there are no major structural changes concerning Mn-Mn vectors in the $S_1 \rightarrow S_2$ transition. However, the data suggested a lengthening of one Mn-Mn distance in S_3 from ~2.75 Å to ~2.85 Å that persisted until S_0, but was shortened again in the $S_0 \rightarrow S_1$ transition. Deprotonation of a hydroxo- to an oxo-bridge was discussed as a possible origin of the latter effect. More significant were the observed changes in Sr K-edge EXAFS. There are two major peaks in the FT-amplitude spectrum assigned to Sr-O (peak I) and Sr-Mn (peak II) vectors. Peak II is relatively narrow in S_1, broadens in S_2, is split into two peaks in S_3, and these two peaks change their relative amplitude upon going to S_0. These data were interpreted as a movement of the Sr^{2+} ion (and by analogy also of the Ca^{2+} ion in native PSIIcc) relative to the Mn-ions during the catalytic cycle of water oxidation. On the basis of model II (or IIa, see Figure 8A) of Yano *et al.* (22), the oxidation of the central μ_4-oxo bridge (also called "μ_3-oxo" considering only the Mn ions (253)) during $S_2 \rightarrow S_3$ was proposed as a possible cause for the structural changes.

5.4. EPR/ENDOR spectroscopy

In order to simulate the EPR and ENDOR spectra of the WOC, one has to specify the spin-Hamiltonian, which contains among others contributions the isotropic exchange interaction *J* between unpaired electrons on *different* Mn ions; for details, see (134, 146, 176). The exchange interaction causes delocalization of spin density between Mn ions and, hence, influences the effective g- and hfc-matrices determining the spectra. Since *J* can be expected to depend on the interaction between Mn ions, i.e., the mode of μ-oxo bridging, the EPR/ENDOR spectra contain, in principle, information about the structure of the WOC. However, this information is not easy to extract. Rather, independent structural information is used to constrain the parameters used in the spectral simulation. Not surprisingly, a number of *J*-coupling schemes for the WOC have been discussed in the literature (see (176) and references therein).

The coupling schemes can be divided into "dimer-of-dimers" models, in which the Mn_4-part of the WOC is separated into two dimers of strongly antiferromagnetically coupled Mn ions, "trimer-monomer" or "3 + 1" models, in which one Mn ion (e.g., the "dangling manganese") is segregated and "tetramer" (T) models, in which there is no obvious separation of the Mn-cluster. Based on a tetramer model, Kulik *et al.* (176) attempted an assignment of oxidation states to individual Mn ions. They found suitable solutions only for the single Mn^{III}-ion in the S_2-state (cf. Figure 4C) being either Mn4 or Mn2 (also called MnC). Their analysis of the S_0-state suggests that there is only a medium antiferromagnetic coupling between Mn4 and Mn3, which can be explained by the protonation of a μ_2-oxo bridge in accordance with interpretations of EXAFS-data (see subsections 5.2 and 5.3).

EPR/ENDOR spectroscopy has been performed also on oriented samples. Hasegawa *et al.* (145) studied the S_2-state multiline signal with EPR on oriented PSII-membranes from spinach. They attributed the observed hfc-anisotropy to the single Mn^{III}-ion in the S_2-state and arrived at an estimate for the orientation of the 2.7 Å Mn-Mn vector relative to the membrane normal of $\theta \geq 40°$. This result is roughly in agreement with the EXAFS-models (Figure 8A) and the preferred redox-state assignment and coupling scheme of Kulik *et al.* (176), if we identify the Mn^{III}-ion with Mn4. Teutloff *et al.* (177) investigated the S_2-state with ^{55}Mn-ENDOR on single crystals of dimeric PSIIcc from *T. elongatus* and suggested that the Mn^{III}-ion is Mn2. Apparently, there is at present no unique interpretation of EPR/ENDOR spectra as regards the structure of the WOC, and further work needs to be done. Measurements on single crystals of monomeric PSIIcc might be helpful in the future, since the peculiar arrangement of Mn_4Ca-clusters in this new crystal form (28) could facilitate the interpretation of spectra.

5.5. Ligand sphere of the Mn_4Ca-cluster

5.5.1. Asp A170

The crystal structures clearly show that Asp A170 is in the vicinity of the Mn_4Ca-cluster, but it remains unclear, whether its side chain ligates a metal ion and if so, which metal ion. The modeling at 2.9 Å resolution (15, 18) implies that Asp A170 could be a bridging ligand between the Ca^{2+} ion and Mn4 (Figures 7A, B), but likewise it could be a unidentate ligand of Mn4 only as suggested on the basis of earlier crystallographic studies (12, 14), the R-QM/MM-model (Figure 8B) of Sproviero *et al.* (233), DFT-based models of Siegbahn (211, 254-256), or EXAFS model III of Yano *et al.* (22). Another possibility is that it solely ligates the Ca^{2+} ion as suggested by model IIa (Figure 8A).

Asp A170 was among the first residues related to the WOC that were extensively studied by site-directed mutagenesis in the mesophilic cyanobacterium *Synechocystis* sp. PCC 6803 (257-260) or the unicellular green alga *Chlamydomonas reinhardtii* (261). A first critical test for the role of a residue in water oxidation is the ability of the mutated strain to grow photoautotrophically. Among the many mutations made at position A170, apparently, only the exchange to Glu, His and Val did not abolish the photoautotrophic growth (258, 259) with normal growth in the Glu case, but slow growth in the other two cases. The O_2 evolution activity was 40 – 60% of wild type in these mutants. Other mutants could be cultured heterotrophically and then still biosynthesized PSIIcc, so that O_2-evolution activities of 10 – 30% compared to wild type could be detected for Arg, Leu, Ile, Cys but none for Ala, Gly, Ser, Thr, Tyr, Pro and almost none (~5%) for Asn and Trp. In the O_2-evolving mutants, a significant fraction of PSIIcc (20 – 60%) lacks the Mn_4Ca cluster *in vivo*. These results demonstrate that Asp A170 is important for assembly and proper function of the WOC. However, the fact that Asp A170 can be replaced by non-ligating residues such as Val, Ile or Leu and oxygen is still evolved at 20 – 40 % of the wild type level is actually an argument against Asp A170 being an indispensable structural component of the assembled WOC. To uphold the idea that Asp A170 is a metal ligand, structural changes in the Val, Ile and Leu mutants have been invoked that would allow another residue or water molecule to act as an alternative ligand (259, 262).

To further deal with the ligation problem, the D(A170)H mutant was investigated by using EPR and ESEEM spectroscopy in X-band (263). The basic idea is that if Asp A170 is a ligand to Mn and as such is functionally replaced with His in the mutant, the hfc between one of the histidyl nitrogen nuclei and the unpaired electrons of a Mn ion should show up in spectra of the S_1 or S_2 states by analogy with His A332 (see subsection 5.5.3). However, no additional signal was detected. This result is in line with studies using FTIR spectrosopy (reviewed by Noguchi (264, 265)), which showed that all S_{n+1}-minus-S_n FTIR difference spectra (n = 0 – 2) of D(A170)H are essentially unchanged from that of wild type (262, 266, 267). In FTIR spectroscopy, one expects a frequency shift of characteristic vibrational modes of a carboxyl group, if it ligates a Mn ion that undergoes a change of its oxidation state or charge density during a $S_n \rightarrow S_{n+1}$ transition. The corresponding feature in the S_{n+1}-minus-S_n FTIR difference spectrum should vanish, if the carboxyl group is replaced with a histidyl group. As discussed by Debus (262), there are several explanations for the lack of any such spectral changes: (i) Asp A170 ligates a Mn ion that does not increase its charge or oxidation state during any of the $S_0 \rightarrow S_1$, $S_1 \rightarrow S_2$, or $S_2 \rightarrow S_3$ transitions. (ii) Charge delocalization in the Mn_4Ca-cluster as suggested by RXES (see subsection 4.2) renders the carboxyl modes of ligating residues insensitive to oxidation state changes in the WOC. (iii) Asp A170 does not ligate the assembled Mn_4Ca-cluster. (iv) Asp A170 in the wild type ligates a Mn ion, but His A170 in the mutant does not. This explanation would explain the lack of nitrogen hfc signals in the ESEEM experiments, but would work for the FTIR data only, if points (i) and/or (ii) apply. (v) Deprotonation events or changes in tautomeric equilibria compensate for the charge changes in the vicinity of Asp A170 due to oxidation of the WOC.

We would like to add two further points: (vi) Asp A170 ligates the Ca^{2+}-ion. This possibility is suggested by model IIa of Yano *et al.* (22) when placed into the 2.9 Å resolution structure of Guskov *et al.* (15) and would explain the lack of signals in both FTIR and ESEEM spectroscopy. (vii) Asp A170 functions as a proton acceptor, possibly forming a hydrogen bond to either a terminal water ligand or a μ-hydroxo bridge. Note that points (vi) and (vii) are not mutually exclusive. Also, a role of Asp A170 as proton transporter does not exclude the possibility of Mn-ligation as suggested by DFT-calculations of Siegbahn (256).

5.5.2. Glu A189

At 3.0 and 2.9 Å resolution (14, 15), Glu A189 is modeled as a bridging ligand between the Ca^{2+}-ion and the Mn-ion that is also ligated by His A332 (Figures 7A, B). This motif has been adopted by Siegbahn in his DFT-model (254). In contrast, Glu A189 is a unidentate ligand to a Mn-ion only in the heterocubane-models (Figure 8B) by Ferreira *et al.* (12) and Sproviero *et al.* (233). The EXAFS-models suggest that Glu A189 could be a unidentate (model IIa, Figure 8A) or bidentate (model III) ligand to Ca^{2+}.

Site-directed mutagenesis in *Synechocystis* sp. PCC 6803 revealed a situation of similar complexity as found for Asp A170 (see subsection 5.5.1). Only the mutations of Glu A189 to either Gln, Lys, Arg, Leu, or Ile do not abolish photoautotrophic growth (268). In all other cases, there is essentially no O_2 evolution, although heterotrophically grown cells still synthesize PSIIcc with a significant amount of photooxidizable Mn ions. The fact that O_2 is still evolved, when Glu A189 is replaced with the non-ligating residues Leu or Ile (40 – 60% of wild type), argues against a structure-stabilizing role of Mn-ligation by this residue. Consequently, the interaction of Glu A189 with a Mn-ion inferred from the electron density in this region has been proposed to be an artifact of the radiation-induced reduction of the Mn_4Ca-cluster (262). It is also striking that the mutants with the highest O_2-evolution are those in which the side chain of Glu A189 is exchanged to the large basic side chains of Lys (~80% activity) or Arg (~70%). The highly active Gln mutant (~70%) exhibits normal EPR multiline signals in S_1 and S_2 (268), as well as normal kinetics of O_2 release and of electron transfer from Y_Z to P_{D1} and from the Mn_4Ca-cluster to Y_Z during the $S_1 \rightarrow S_2$, $S_2 \rightarrow S_3$, and $S_3 \rightarrow S_0$ transitions (269). The Lys and Arg mutants still exhibit normal rates of electron transfer from Y_Z to P_{D1} and from the Mn_4Ca-cluster to Y_Z during the $S_1 \rightarrow S_2$ and $S_2 \rightarrow S_3$ transitions (269).

Inspired by the crystallographic studies, two groups used FTIR difference spectroscopy to assess the ligation problem. Kimura *et al.* (270) detected effects of the E(A189)Q mutant, which they interpreted as evidence for a ligation of Mn by Glu A189. On the other hand, Strickler *et al.* (271) presented evidence that these changes arise from indirect structural perturbations and do not indicate loss of a metal-ligation. Instead, they demonstrated that like the D(A170)H-mutation, neither of mutations E(A189)Q or E(A189)R eliminates any carboxylate modes from any of the difference spectra pertaining to the $S_0 \rightarrow S_1$, $S_1 \rightarrow S_2$, or $S_2 \rightarrow S_3$ transitions. Again, there are several possibilities to explain these data: (i) Glu A189 does not ligate Mn, but only Ca^{2+}. (ii) Glu A189 ligates a Mn-ion that does not change its oxidation state during the $S_0 \rightarrow S_1$, $S_1 \rightarrow S_2$, or $S_2 \rightarrow S_3$ transitions. (iii) The carboyxlate mode of Glu A189 is insensitive to oxidation state changes of the Mn_4Ca-cluster, presumably because of charge delocalization.

5.5.3. His A332

His A332 is a ligand to the same Mn-ion as Glu A189 in all crystallographic (12, 14, 15) and DFT-based (233, 254) models (Figures 7B, 9B), but this ligation is more difficult to accomplish with the EXAFS-models (22) placed into the latest crystal structure (15) with N_ε-Mn distances of 3.5 – 3.7 Å. Direct experimental evidence for Mn-ligation by at least one histidine was provided earlier on the basis of X-band ESEEM studies on PSIIcc preparations containing ^{15}N-labeled histidine (272).

The importance of His A332 for water oxidation is evident from the fact that of the many mutants at position A332 (made in *Synechocystis* sp. PCC 6803), none is able to promote photoautotrophic growth (273). Only the mutants H(A332)Q and H(A332)S, when cultured heterotrophically, evolve O_2, but only at 10 – 15% of the

wild type rates. Among the non-O_2-evolving mutants, H(A332)D and H(A332)E still biosynthesize large amounts of PSIIcc (273), which can be isolated for spectroscopic studies. An X-band ESEEM study of the H(A332)E mutant was interpreted as providing evidence that the histidyl ligand to Mn is indeed due to His A332 (274). The diminished amplitude of a characteristic histidyl nitrogen modulation in the mutant compared to wild type can be explained straightfowardly by the loss of metal-ligation in the mutant or the replacement of the ligating nitrogen with a glutamate oxygen. However, the possibility was not ruled out that His A332 does not ligate the Mn_4Ca-cluster and that the mutation merely modifies another His-Mn interaction by structural perturbations. A possible second candidate for a histidyl ligand is His A337 (see subsection 5.5.5). We note that according to the crystal structure (15), His A332 and His A337 are close to each other with a distance between the N_ε-atoms of ~4 Å, so that such a perturbation is conceivable. More recent ESEEM studies of ^{14}N- and ^{15}N-containing PSIIcc in K_a – and Q-band support the idea that there is at least one histidine ligating Mn, and the N-Mn distance was estimated to be in the range of 2.00 – 2.92 Å (172, 173).

FTIR experiments were conducted on spinach PSII-membranes containing ^{15}N and *Synechocystis* PSIIcc with ^{15}N-labeled histidine, and histidine signals were identified in S_2-minus-S_1 FTIR difference spectra (275). The vibrational signature indicated that this histidine is likely protonated at its N_δ-atom (also called N_π) and that this proton is involved in hydrogen bonding. Indeed, the crystal structure (15) suggests a hydrogen bond between N_δ of His A332 and the backbone carbonyl of Glu A329. The measurable influence of the $S_1 \rightarrow S_2$ transition on the vibrations of this histidine was interpreted as a possible evidence for this residue to ligate the Mn_4Ca-cluster (262, 275). This ligation then would be accomplished via the N_ε-atom (also called N_τ) in agreement with the crystal structures (12, 14, 15) and the DFT-based models (233, 254). A later study interpreted S_{n+1}-minus-S_n FTIR difference spectra (n = 0 – 2) as indicating that a single histidine residue coupled with structural changes of the WOC during the S-state cycle is responsible for the observed bands and that it is a Mn-ligand (276).

More recent mutagenesis experiments employ the thermophilic cyanobacterium *T. elongatus* (277, 278). The two mutants H(A332)Q and H(A332)S were constructed and characterized by different techniques (279). In striking contrast to the corresponding mutants of *Synechocystis* sp. PCC 6803, both *T. elongatus* mutants were able to grow photoautotrophically, and PSIIcc could be isolated with an O_2-evolution capacity corresponding to ~80% of the wild type value. As in the case of Ca/Sr-exchange (see subsection 5.3), the decrease in activity was traced back to kinetic limitations, while absorbance difference spectroscopy indicated normal cycling through the S-states. Among the various experiments performed was an X-band ESEEM study of the H(A332)S-mutant revealing no significant difference to wild type. Consequently, it was conluded that the observed nitrogen signals do not arise from His A332 and that the effects of the H(A332)E mutant of *Synechocystis* originate from structural perturbations of another His-Mn interaction corresponding to the second possible interpretation considered by Debus *et al.* (274). So, there is spectroscopic evidence that a Mn in the WOC is ligated by a histidine, but no clear evidence that it is His A332.

5.5.4. Glu A333

In all crystallographic structures, Glu A333 is a ligand to Mn, either unidentate (12) or as a bidentate bridge (14, 15). Interestingly, it is also a bidentate bridge in the heterocubane R-QM/MM model (233) and Siegbahn´s DFT-model (254). In the EXAFS-models (22), placed into the 2.9 Å resolution structure, it is close enough to Mn to be a unidentate ligand to Mn3 (models IIa and III) or probably even a bidentate bridge between Mn3 and Mn4 (model IIa, Figure 8A). Mutations at position A333 have been constructed in *Synechocystis* sp. PCC 6803 (273, 280). Remarkably, only the E(A333)Q mutant supports photoautotrophic growth and shows O_2-evolution at a non-negligible rate (20 – 30% of wild type). No FTIR results of a Glu A333 mutant have yet been reported. On the basis of this limited information, we conclude that Glu A333 is an indispensible structural component of the Mn_4Ca-cluster, likely a metal ligand, and can only partly be replaced by Gln in its function.

5.5.5. His A337

His A337 is close to His A332 (see subsection 5.5.3.), but is not a ligand to any metal ion of the Mn_4Ca-cluster in any crystal structure (12, 14, 15) or any DFT-based model (233, 254). However, the EXFAS-models (22) combined with the 2.9 Å resolution structure (15) suggest that it could be a ligand to Mn2 (Figure 8A) with the N_ε-Mn distance of 2.8 – 3.0 Å being significantly shorter than that of His A332. At the mutagenesis side, the situation is again complicated: Phototrophic growth is supported only by Arg and weakly so by Gln, Asn, and Phe (273). O_2 is evolved to a significant extent (> 5% of wild type) in the cases of Arg (~51 %), Gln (30 – 40%), Phe (~40%) as well as Glu, Asn, and Leu (10 – 20%). In all His A337 mutants, 10 – 50% of PSIIcc lack photooxidizable Mn ions *in vivo* (273). Therefore, His A337 has been considered as a possble Mn-ligand, but also as a possible hydrogen bond donor. To our knowledge, no spectroscopic study of any His A337 mutant has yet been reported. We note that according to the crystal structure (15), the N_δ-atom of His A337 is likely engaged in hydrogen bonding to the backbone O of Glu A333. Thus, the observations made by Noguchi *et al.* (275) discussed in subsection 5.5.3. in the context of His A332 could likewise apply to His A337.

5.5.6. Asp A342

Asp A342, close to the C-terminus of PsbA, is suggested to be a ligand to Mn in all crystal structures and DFT-based models, either as bidentate bridge (14, 15, 254) or unidentate (12, 233). EXFAS-model IIa suggests a unidentate ligation to Mn2 (Figure 8A). Five site-directed mutations of Asp A342 in *Synechocystis* sp. PCC 6803 have been reported (262, 273). Among these, only D(A342)E supports photoautotrophic growth, and O_2-evolution is possible in D(A342)E, D(A342)N, and

D(A342)H at rates corresponding to ~20%, ~30%, and ~6%, respectively, of the wild type. No O_2-evolution is possible, if Asp A342 is replaced with the non-ligating residues Ala or Val. Furthermore, 20 – 50 % of PSIIcc in theAsp A342 mutants lack photooxidizable Mn ions. This surprisingly clear situation strongly suggests a role for Asp A342 as Mn-ligand. However, S_{n+1}-minus-S_n FTIR difference spectra (n = 0 – 2) of the D(A342)N mutant are essentially identical to that of the wild type (281). This again suggests that either Asp A342 is not a Mn-ligand or it is a ligand, but insensitive to the oxidation of the Mn_4Ca-cluster.

5.5.7. C-terminal Ala A344

Ala A344 is unique among the ligands to the Mn_4Ca-cluster as it has no ligating side chain, but uses the C-terminal carboxyl group of PsbA instead. In most organisms, PsbA (D1) is biosynthesized as a precursor protein (termed pD1) with a C-terminal extension that has to be cleaved to allow for a functional assembly of the WOC (282-284). In the 3.5 Å resolution structure (12), the C-terminal residue of PsbA is located close to the Ca^{2+}-ion. Consequently, it was considered as ligand to Ca^{2+} (Figure 8C) in the R-QM/MM-model (233). At 3.0 and 2.9 Å resolution (14, 15), the C-terminus of PsbA adopts a different conformation, so that a bridging, bidentate ligation of Mn and Ca^{2+} becomes possible (Figures 7A, B, C). The EXAFS-models suggest a close proximity of the C-terminal carboxyl group to Mn1 (Figure 8A), and Siegbahn models Ala A344 as a unidentate ligand to Mn (254).

In contrast to the Asp and Glu residues discussed above, FTIR difference spectroscopy provided clear evidence for a close interaction of Ala A344 with the Mn_4Ca-cluster. To this end, S_{n+1}-minus-S_n FTIR difference spectra were recorded of PSIIcc from *Synechocystis* sp. PCC 6803 either unlabeled or labeled with L-[1-^{13}C]-alanine in two independent studies (285, 286). A band characteristic of a symmetric carboxylate stretching vibration was found to be downshifted during the $S_1 \rightarrow S_2$ transition and restored during $S_3 \rightarrow S_0$. The data were interpreted in terms of Ala A344 being a *unidentate* ligand to a Mn-ion that is oxidized (or whose charge increases) during $S_1 \rightarrow S_2$.

The publication of the 3.5 Å resolution structure (12) triggered a re-investigation of the possibility that Ala A344 ligates Ca^{2+}. Inspired by the work of Boussac *et al.* (251), cells of *Synechocystis* sp. PCC 6803 were cultured in a medium containing $SrCl_2$ instead of the normally used $CaCl_2$ to achieve biosynthetic Ca/Sr exchange (287). In addition, cells were labeled with L-[1-^{13}C]-alanine. The data demonstrated that several symmetric and asymmetric carboxylate stretching modes, that show up in S_{n+1}-minus-S_n FTIR difference spectra (n = 0 – 2), are affected by Ca/Sr exchange, but *not* that of the C-terminal carboxyl group of Ala A344. This was taken as evidence that Ala A344 does not ligate Ca^{2+}. Also, the modes that are perturbed by Ca/Sr exchange are neither due to Asp A170 nor Glu A189 or Asp A342, as these residues are insensitive to the investigated S-state changes (see above). This implies that any changes of carboxylate modes of Asp A170 or Glu A189 due to Ca/Sr exchange, that would be expected, if any of these two residues ligated Ca^{2+}, would likely escape detection, so that a Ca^{2+}-ligation by these groups can not be ruled out.

More recently, ^{13}C-ENDOR spectroscopy was applied to the S_2-state of L-[1-^{13}C]-alanine labeled PSIIcc from *Synechocystis* sp. PCC 6803, and a strong magnetic interaction of a ^{13}C-nucleus with unpaired electrons of the WOC was detected (288). This is further clear evidence that Ala A344 ligates a Mn-ion.

5.5.8. Glu C354

The only potential ligand to the Mn_4Ca-cluster that is not from PsbA is Glu C354. It is suggested to be a unidentate ligand to a Mn-ion (Figure 8B) in the heterocubane structures (12, 233), but a bidentate, bridging ligand between two Mn-ions in the 3.0 and 2.9 Å structures (14, 15) as well as in the DFT-model of Siegbahn (254). In the EXAFS-models, it is at a position, which would allow for a bridging ligation between Mn1 and Mn2 (Figure 8A) according to models IIa and III or between Mn2 and Mn3 (see Figure 4 in (18)) according to model IIa.

So far, only the mutant E(C354)Q has been constructed in *Synechocystis* sp. PCC 6803 and investigated spectroscopically (289-291). According to an earlier study, this mutant does not support photoautotrophic growth, evolves no O_2, and is not even able to accumulate PsbC (CP43) in the thylakoid membrane (289). The more recent studies report different phenotypes. Strickler *et al.* (290) were able to isolate PSIIcc from thylakoid membranes of their E(C354)Q mutant that evolved O_2 at 10 – 18% compared to wild type. The mutant PSIIcc was able to normally cycle through the S-states, but apparently only in a small fraction of centers. However, about 75% of centers were able to reach the S_2-state upon flash illumination, but were unable to advance beyond the S_2- or S_3-states. The S_2-minus-S_1 FTIR difference spectrum indicated a significant effect of the E(C354)Q mutation on a number of modes in the mid-frequency region. The data were taken as evidence that Glu C354 strongly interacts with the Mn_4Ca-cluster. One possible interpretation suggested by Strickler *et al.* (290) is that Glu C354 is a bridging ligand between two metal ions in the S_1-state, but changes to a *unidentate* ligand to a single metal ion in the S_2-state. However, other interpretations are possible due to the complexity of spectral changes induced by the mutation, so that further work is necessary to arrive at a better understanding of structural and functional implications.

Shimada *et al.* (291), in an independent study, were also able to isolate PSIIcc from the E(C354)Q mutant and found 21% O_2-evolution activity. Their data indicated a slightly lower efficiency of the $S_2 \rightarrow S_3$ transition compared to wild type and significantly retarded transitions beyond the S_3-state. The S_2-minus-S_1 FTIR difference spectrum of Shimada *et al.* is similar to that of Strickler *et al.*, but Shimada *et al.* arrived at a different interpretation: They proposed that Glu C354 changes from a bridging ligand between two Mn-ions in the S_1-state to a *chelating bidentate* ligand to a single Mn-ion in the S_2-state. They

also reported a S_3-minus-S_2 FTIR difference spectrum and concluded that none of the modes affected by the $S_2 \rightarrow S_3$ transition is due to Glu C354. This likely implies that the mode of ligation of a Mn-ion by Glu C354 is not changed during $S_2 \rightarrow S_3$ and that this Mn-ion does not change its oxidation state in this transition. Shimada *et al.* also reported evidence for an effect of the E(C354)Q mutation on vibrations of a water molecule.

6. EDUCT AND PRODUCT CHANNELS

6.1. Channel proposals

The crystal structures show that the WOC is buried within the protein (Figure 1) suggesting that there are channels within the protein matrix that allow for the delivery of substrate water (the educt) to the Mn_4Ca-cluster as well as the removal of protons and dioxygen (the products). Even prior to the crystal structures, the existence of such channels was proposed; for a recent review, see (292). One line of argumentation originates from earlier efforts to identify a possible metal peroxide intermediate in the reaction cycle of the WOC. It was recognized that certain treatments of plant PSIIcc, involving *inter alia* depletion of extrinsic subunits (293) or Cl^- (294, 295), stimulate the formation of hydrogen peroxide (H_2O_2) instead of O_2. Besides singlet oxygen, H_2O_2 is among the reactive oxygen species (ROS) that cause photo-oxidative damage of PSIIcc (296-298) and might be responsible for the requirement of a fast PsbA turnover (for reviews on photoinhibition, see (299-302)). The apparent correlation of H_2O_2 formation with an O_2-production deficit led Wydrzynski *et al.* (303) to formulate the "water accessibility hypothesis". According to this hypothesis, the accessibility of water to the WOC is controlled by the protein matrix and determines the reaction path of water oxidation. Depletion of extrinsic subunits or Cl^- disturbs the structural integrity of this protein matrix and leads to an uncontrolled water access to the WOC, which opens alternative reaction paths that result in an incomplete water oxidation with H_2O_2 as the product

A second line of evidence has its roots in studies with substrate water analogs. Radmer and Ollinger (304) investigated the activity of substituted hydroxylamines as reductants of the WOC and interpreted the observed dependence of the activity on the size of the reductant molecule as evidence that the substrate water binding sites reside in a cleft. Later work confirmed the size dependence and showed that the inhibitory effect of the reductants is diminished by the presence of extrinsic subunits (243) as well as Cl^- (243, 305) or Ca^{2+} (157, 242, 244), suggesting an influence of these components of PSIIcc on the integrity and/or width of inlet channels or on the accessibility of the Mn ions. Force *et al.* (306) studied the interaction of deuterated alcohols with the WOC by using ESEEM spectrosocopy to detect alkyl deuterons in the vicinity of Mn. They found evidence that the smaller alcohols methanol and ethanol and to a certain extent the slim *n*-propanol bind near the Mn_4Ca cluster, but the bulkier 2-propanol and dimethyl sulfoxide (DMSO) do not. On the basis of these data, they considered the existence of an access channel of limited size.

Complementing the water accessibility hypothesis, an "oxygen accessibility hypothesis" has been formulated (307, 308). According to this hypothesis, O_2 formed by the Mn_4Ca-cluster is directed into the lumen by a specific pathway whose purpose is to prevent the PSII-RC from coming into contact with O_2. The reason, why such a contact has to be avoided, is the occurrence of charge recombination reactions in the RC. Since the quinone exchange reactions in the RC are slow compared to EET and primary ET, it may happen under high-light conditions that the foward ET is blocked, e.g., Q_A reduced and the Q_B-site empty. Under these circumstances, the radical pair $P_{D1}^{\bullet+}Pheo_{D1}^{\bullet-}$ is still formed and lives long enough to be to a certain extent converted from its original singlet form $^1[P_{D1}^{\bullet+}Pheo_{D1}^{\bullet-}]$ to its triplet form $^3[P_{D1}^{\bullet+}Pheo_{D1}^{\bullet-}]$. The latter recombines to a Chl triplet state ^{3}Chl, which is likely localized on Chl_{D1} and P_{D1} at ambient temperatures (37). Neither $^3Chl_{D1}$ nor $^3P_{D1}$ can be quenched by carotenoids, as these are too far away for triplet – triplet energy transfer (Figure 2). However, there is evidence that the radical anion $Q_A^{\bullet-}$ is able to act as triplet quencher (309, 310). Nonetheless, ^{3}Chl formation in the RC could promote photosensitized production of singlet oxygen (311). As this process requires contact between ^{3}Chl in the RC with the triplet oxygen produced by the WOC, rapid egress of O_2 into the lumen would avoid singlet oxygen formation. Since singlet oxygen is the major ROS being responsible for photo-oxidative damage (297, 298), a special O_2-egress channel would contribute to the protection of PSIIcc.

Another aspect is the possible reversibility of the last, O_2-producing step of water oxidation, i.e., $[S_4] \rightarrow S_0 + O_2 + n\,H^+$, to be further discussed in subsection 10.3. Clausen *et al.* (312, 313) reported evidence that this step has a low driving force and, hence, can be suppressed or reversed at increased O_2-pressure. The significance and implications of this finding were debated in the literature (314-318). The important point in the present context is that reversibility of the last step would necessitate efficient removal of the product O_2 from the catalytic site and protection of this site against the atmospheric O_2-pressure. Both tasks could be perfomed by a specially designed transport channel, which directs O_2 outward, while the surrounding protein matrix prevents O_2 diffusion towards the Mn_4Ca cluster. In other words, the protein has to be "O_2-proof", but at the same time, has to act as an O_2-outlet valve. As suggested by Renger (102), an oxygen channel could help to prevent a reversal of electron transport that would turn the WOC in an "oxidase reaction mode".

Like an electron, the product "H^+" of water oxidation is an elementary particle and no molecule, so that it needs a carrier molecule rather than a channel. Therefore, it is more appropriate to talk about "H^+ exit pathways". On the other hand, these pathways are likely associated with channels, in which water molecules are placed. The widely accepted mechanism of proton transfer along water chains is that one proton "hops" from a water molecule to the next, then another proton from the second water molecule to the third and so forth. This is usually called the "Grotthuss mechanism", although it differs somewhat from de

Grotthuss´ original ideas (319, 320). Illustrations of this mechanism, including also protonatable amino acid side chains that contribute to proton transfer in proteins, can be found in earlier reviews (292, 321-323). The Grotthuss mechanism requires the involved water molecules and amino acid side chains to be arranged in an optimal way to promote proton transfer. Moreover, the side chains have to have suitable pK_a values to provide the driving force for directed proton transport (324). Also, the inscribed water molecules may have a tuned pK_a due to their interaction with the protein. These arrangements of proton carriers have to work under conditions of varying electric field (e.g., charge accumulation in the Mn_4Ca cluster, see subsection 4.6) and against the proton activity in the lumen, which is increased by the action of the WOC itself. It is, therefore, beyond dispute that specific H^+ exit pathways exist in PSIIcc.

6.2. Channel calculations

With the appearance of more detailed crystal structures, attempts have been made to identify possible educt and product channels of water oxidation by structure-based calculations. Different methods have been applied to the structures at 3.5 Å (325), 3.0 Å (324, 326, 327), and 2.9 Å (15, 200) resolution. Methods and work up to 2008 have been reviewed (292) and a brief comparison of this work with studies at 2.9 Å resolution given (18). In the following, we concentrate on the most recent work applying cavity search algorithms (200) and molecular dynamics (MD) simulations (327). Proton exit is further discussed in section 9.

In the cavity search algorithm applied, routes that a (spherical) particle of a given size can take from the interior of the protein to the bulk solvent are identified (328). For application to PSIIcc, the Mn, Ca^{2+} and Cl^- ions are removed, and possible trajectories for a sphere of specified radius starting from the WOC-site are evaluated (15, 325). A drawback of this method is that calculations are carried out on a static crystal structure and protein dynamics such as breathing motions that might be of importance for molecule transport through channels (292) are not considered. Therefore, the cavity search algorithm only allows for an initial characterization of possible channels. The most recent results obtained in this way on the basis of the 2.9 Å resolution structure (200) are summarized in Figure 9. Nine channels were identified and classified according to their width, length and hydrophobicity. The wider channels A1, A2, B1 and B2 were assigned to possible molecule (H_2O, O_2) transport channels, whereas the narrower channels C – G (yellow) were considered too tight for molecule transport and assigned to possible proton exit pathways (see the discussion below). The channels C – G form a complex network merging into three different exits to the lumen (Figure 9B), but only into two channels approaching the Mn_4Ca-cluster (Figure 9C). To demonstrate the principle ability of channels C – G to act as proton exit pathways, Gabdulkhakov *et al.* (200) modeled water molecules into these channels. One water molecule is situated between Mn4 and Cl^-, which is also "seen" as a blob of electron density in the 2.9 Å structure (Figure 7D). However, it is not clear from this analysis, whether all of these channels are really proton exit pathways. Moreover, there might be additional pathways that can not be traced by the cavity search algorithm simply because they involve mainly amino acid side chains or water molecules situated in cavities that are not connected by a trajectory with the WOC-site. Finally, it should be recalled that the calculations were performed on one PSIIcc-monomer. In the PSIIcc-dimer, the opening of channels CD, which points towards the monomer-monomer interface, is largely blocked by the second dimer half. This is not the case for the other channels.

The wider channels A1, A2, B1 and B2 all originate from one region on the other side of the WOC and allow access to Ca^{2+}, Mn1 and Mn2. Channels A1 and A2 were tentatively assigned to water inlet channels and B1 and B2 to O_2 egress channels (200), but this assignment is merely based on the assumption that O_2 transport requires a broader channel profil. Such a distinction is difficult on the basis of a static structure and given the coordinate error of about 0.26 Å. The channel B2 is actually blocked by Lys U134, but it could be demonstrated that a conformational change of this residue would open it (200).

Channels A2 and B1 are the most suitable candidates for entry paths allowing access of small molecules to the WOC. Their limited diameters provide a straightfoward explanation for the results of Force *et al.* (306) concerning the interaction of deuterated alcohols of different size with the Mn_4Ca-cluster (see subsection 6.1). Removal of Ca^{2+} would open an additional path from the wider channels to Mn4 and thus likely increase the susceptibility of the WOC against reductants in accordance with experimental observations (157). These channels could also provide size-limited pathways for Ca^{2+} exchange, which is slow in intact PSIIcc (237). The larger Sr^{2+} would probably be even slower, if not arrested, providing an explanation for the apparent inability to exchange biosynthetically incorporated Sr^{2+} (see subsection 5.3). We note that the channels in the vicinity of the WOC are determined by conserved protein subunits and thus are likely similar in cyanobacterial and plant PSIIcc.

To obtain a more realistic picture of possible water flow in PSIIcc, Vassiliev *et al.* (327) performed MD simulations based on the 3.0 Å structure (14) supplemented with more than 900 buried water molecules and the quantum chemical WOC-model of Sproviero *et al.* (329). Note that this model contains a Cl^- ion as ligand to Ca^{2+}, which may have an influence on charge distribution and dynamics. The ingenious idea of Vassiliev *et al.* was to employ mathematical techniques originating from fluid dynamics and used in magnetic resonance imaging to analyse water tracts in tissues (330). They applied these techniques to information on water diffusion in PSIIcc obtained from the MD simulation in order to identify highly anisotropic motions called streamlines. Water streamlines were found in spaces free of protein backbone atoms and in most cases also free of heavy atoms of amino acid side chains. These streamlines are generally located in the same regions as the channels suggested by analyses

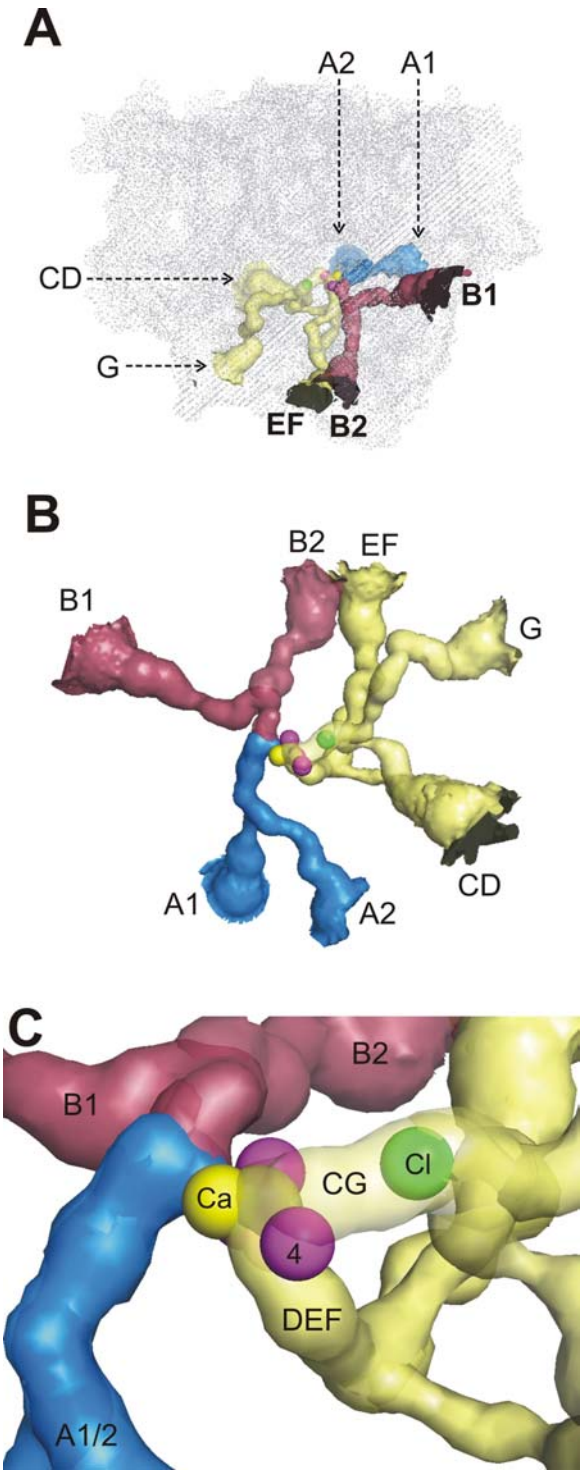

Figure 9. Channels connceting the Mn_4Ca cluster with the lumen according to the cavity search analysis performed by Gabdulkhakov *et al.* (200) based on the 2.9 Å resolution structure (15): (A) Side view of one PSIIcc monomer along the membrane plane (light grey, orientation as in Figure 1A) showing openings of the channels towards the lumen (A1, A2 blue, back side; B1, B2 red, front; joint opening of C and D, yellow, back side; joint opening of E and F, yellow, front; G yellow, back side). (B) View from the cytoplasmic side onto the membrane plane. The spheres represent ion positions (Mn, violet; Ca^{2+}, yellow; Cl^{-}, green)) according to the 2.9 Å resolution structure (15). (C) A closer look onto the channels in the vicinity of the Mn_4Ca cluster according to the 2.9 Å resolution structure (15).

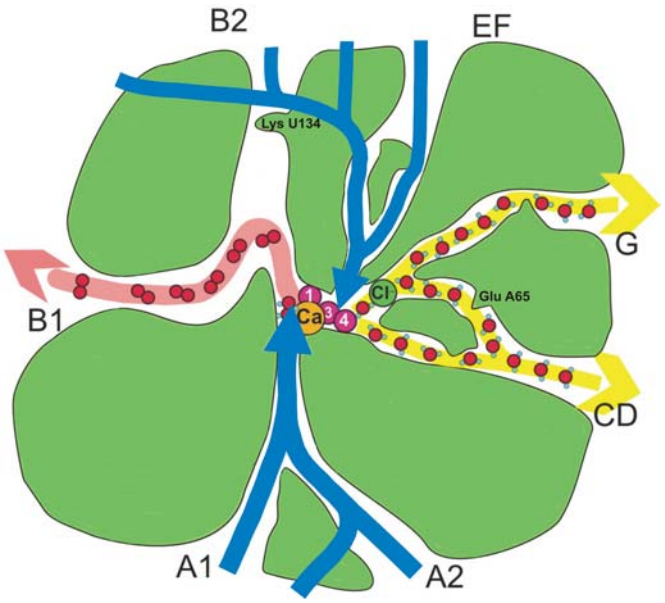

Figure 10. Schematic view of educt and product channels in PSIIcc connecting the Mn_4Ca cluster with the lumen (adapted from Gabdulkhakov *et al.* (200), same orientation as in Figure 9B) merging the ideas from ref. (200) and (327). According to this hypothetical model, water can reach the catalytic site from two different directions (blue arrows). Water molecules inscribed to channels C, D, and G probably serve as proton exit pathways, but water flow along channel G is possible depending on the effect of Cl^- on the dynamics. Channel B1 is suggested as a possible O_2 egress pathway. There is crystallographic evidence that channel B1 and the inner part of B2 are accessible to small molecules (200).

based on the static structure, indicating that the latter are a reasonable first approximation. However, there are also streamlines in spaces transiently occupied by amino acid side chains, demonstrating that side chain movements can promote water diffusion through regions, which from the viewpoint of the cavity search algorithms appear "waterproof". Also, thermal motions of the protein can open and close channels.

One major streamline region connects the "calcium side" of the WOC via channels A1 and A2 with the protein surface close to the membrane, supporting the idea that these are water inlet channels. The streamlines appear broader than the channels, indicating that water can leak through the channel walls because of thermal motion. These differences point to the limits of analyses based on static structures. Details of how the streamlines approach the Mn_4Ca-cluster may depend on the WOC-model used and are difficult to assess in the absence of a clear-cut structure. Therefore, the significance of differences between streamlines and channels in this region remain unclear. A second major streamline region is associated with channels C and G. Interestingly, these streamlines do not reach the protein surface, but seem to be blocked by narrow regions of channels C, D, and G (although in the case of channel G not at the narrowest pass). In particular, there are no streamlines in channel D and in channel C beyond the narrow pass at Glu A65. This residue is likely of importance for proton transfer as discussed in section 9. In contrast, there is significant water flow in the major part of channel G and in regions around channel G and the WOC. It is important to note that the Cl^- ion is lacking in the calculations based on the 3.0 Å structure. As hypothesized earlier (200), the Cl^- in this position could block water flow. In any case, the channels C, D, and G appear to be less suitable for water inlet than the region around channels A1 and A2.

The MD simulations showed an abundance of mobile water molecules around channels B1 and B2 with several entry possibilities. One entry coincides with the mouth of channel B2, but there are also other paths due to protein dynamics. Interestingly, there is no significant water stream in the opening region of the widest channel, B1. In contrast to the suggestions based on cavity analysis, there is a significant water migration in the EF channel system reaching the WOC region. In addition, there are shortcuts between the EF and B2 channels allowing water to bypass the barrier made up in the B2 channel by the salt-bridge between Lys U134 and Val V79.

To summarize, we present an updated working model of educt and product channels in Figure 10, merging the ideas from ref (200) and (327). According to this model, there are two major pathways for water inlet approaching the WOC from different sides. The details of how the water streams make contact with the Mn_4Ca-cluster can not be fixed at present due to the lack of a reliable structure in this region. The main entry points are around the mouths of channels A1, A2, B2, and EF. Although, there might be additional water motions in the inner parts of channels B1 and B2, we hypothesize channel B1 to be a likely O_2 egress pathway in agreement with earlier suggestions (200, 326). Channels CD are the prototype H^+ exit pathways, but there might by additional paths not associated with them. The G channel is indicated

as an additional proton path, but water motion in this region can not be ruled out depending on the effect of the Cl^- ion on the dynamics.

6.3. Noble gas pressurization

To identify possible hydrophobic pathways for dioxygen transfer, PSIIcc crystals have been investigated with X-ray diffraction that were derivatized with Xe (15, 200, 331) or Kr (200) under pressure. Noble gas pressurization is a well-known tool in X-ray crystallography to explore hydrophobic sites (332, 333) and especially to track O_2 transport channels (334, 335) in proteins. The idea behind Xe derivatization is that the Xe atom has a van-der-Waals radius of 2.16 Å (336) similar to that of the O_2 molecule (2.13 Å along the O=O bond) and is likewise nonpolar. Therefore, Xe should prefer the same environment as O_2, but can be detected by means of anomalous X-ray scattering (cf. subsection 5.1). However, the Xe-O_2-analogy is limited by two facts: (i) O_2 is not spherical, but has a smaller effective radius of 1.5 – 1.7 Å normal to the double bond axis (336). Hence, it could in principle enter channels from which Xe is excluded. (ii) Binding of atoms and nonpolar molecules to proteins depends not only on size, but also on polarizability (332, 333). As Xe has a significantly higher polarizability (4.04 $Å^3$ (337)) than O_2 (1.58 $Å^3$ (338)), it may prefer different binding niches. Moreover, there is recent evidence that O_2 may also bind to a polar site (339). In view of these facts, it is actually not surprising that no Xe atom was found in any of the proposed channels (15, 200, 331). Instead, Xe atoms mostly occupied niches amongst the lipid acyl chains in the membrane spanning part of PSIIcc. These sites were interpreted in terms of hypothetical pathways allowing O_2 to escape from the lumen via the membrane phase (200).

The pressurization experiments were repeated with Kr with the hope that the smaller radius of this atom (2.02 Å (336)) would allow for a tracking of channels (200). Despite the smaller anomalous signal of Kr, 23 binding sites could be identified in the PSIIcc dimer (11 per monomer and one on the C2-axis). Whereas most Kr atoms again occupied the lipid phase of PSIIcc, one was found in channel B1 (close to Phe C419) and another one in the inner part of channel B2 (close to Ile V71). In addition, PSIIcc was cocrystallized with DMSO, and two DMSO molecules were found in these channels close to the Kr sites (200). These data provide the first crystallographic evidence that channel B1 is accessible to small molecules and a likely pathway to approach the Mn_4Ca cluster or to egress.

7. CHLORIDE BINDING SITES

The requirement of Cl^- for activity of the WOC is known for quite some time and has been studied extensively; for reviews, see (157, 340). The earlier studies resulted in two general hypotheses on the role of Cl^- in water oxidation: (i) Cl^- ions are ligands to Mn, either as a bridging ligand (341, 342) or as an exchangeable anion helping to maintain charge neutrality during the S-state cycle (343). The idea of manganese ligation by chloride has been taken up in recent theoretical studies (344). Since the identification of calcium as a constituent of the WOC, a variant of the charge neutralization hypothesis has been suggested, in which Cl^- is a ligand to Ca^{2+} (232, 329, 345). The presently available crystallographic information including native (15) (see above) as well as bromide-substituted PSIIcc (15, 346, 347) (see below) provides no evidence for chloride ligating any metal ion of the WOC. (ii) Cl^- ions are bound to specific sites in the protein matrix close to the WOC and serve to facilitate deprotonation of water (348-350). The latter hypothesis was also incorporated into theoretical work (212, 256) and is more in line with the recent crystallographic studies (15, 346, 347).

The evidence from the earlier biochemical work for a physiological role of chloride in water oxidation was questioned, because the methods used for Cl^- depletion at that time were suspected to cause irreversible changes in the properties of PSIIcc (351). The seminal work of Andréasson and co-workers provided a clearer picture (350, 352-354). They labeled spinach PSII membranes with radioactive $^{36}Cl^-$ and applied extensive dialysis for Cl^- depletion to preserve the integrity of the protein matrix. In this way, they could demonstrate the following: (i) There is about one slowly exchanging Cl^- per WOC and no non-exchangeable Cl^- bound. (ii) Cl^- is needed to establish full water oxidation activity, but 35 – 55 % oxygen evolution is still obtained after Cl^- depletion by dialysis. (iii) The reduced activity can be traced back to a retardation of the S-state transitions reminiscent of the effect of Ca/Sr-exchange (see subsection 5.3), that is, full S-state cycling is possible in the absence of Cl^- (see also (355)). (iv) Oxygen evolution activity can be immediately (< 15 s) restored to 85 – 90% of the original value by addition of high concentrations of Cl^- corresponding to a dissociation constant of K_d = 0.5 – 0.8 mM (depending on whether sucrose or glycerol is present in the buffer), but is rapidly lost in Cl^--free media. Long-term incubation in Cl^- results in a conversion to slow Cl^- exchange behavior ($t_{1/2}$ = 1 h) characterized by a dissociation constant of K_d = 13 – 20 μM. The interconversion takes place on a time scale of minutes. These results have been interpreted in terms of a "one-site two-state" model (354), in which there is one Cl^- binding site close to the WOC that can exist in an "open" conformation (O-state) characterized by low affinity and rapid exchange and after Cl^- binding is transformed into a "closed" conformation (C-state) characterized by high affinity and slow exchange. Alternatively, one may consider a "two-site" model (355), in which one site is weakly binding and rapidly exchanging, while the other is tightly binding and only slowly exchanging. In this case, the interconversion between the two forms would likely occur by diffusion of Cl^- through the protein rather than dissociation and rebinding, since the interconversion is faster than the exchange at the high-affinity site. (v) In accordance with earlier studies (119, 356), Cl^- is found to be required for the formation of the S_2-state multiline signal at g = 2.0 (see subsection 4.3). In fact, binding of Cl^- in both modes (O- and C-state) stabilizes the multiline signal, whereas Cl^- depletion shifts the equilibrium towards the g = 4.1 signal (350, 354, 355). This result seems to indicate that in both modes Cl^- binds to the same site, in which it influences the magnetic properties of the WOC in a specific

manner, in line with the one-site two-state model. On the other hand, the two-site model would require to postulate that Cl^- binding to both sites affects the spin system in the WOC in the same way. (vi) The slowly exchanging Cl^- binding was found to depend on pH with an apparent pK_a of ~7.5 (353). Earlier work has indicated the presence of lysine residues in PSIIcc with an anomalously low pK_a near 7.8 (357-359). So, it was suggested that Cl^- may participate in a structure involving such a lysine (350). We note that all these experiments have been performed on plant thylakoid membranes. The situation is less clear in the case of cyanobacterial PSIIcc. In the following, we shall first discuss these data on the basis of the single "native" Cl^- binding site identified in the 2.9 Å resolution structure (15) and later turn to the possibility of additional halide binding sites following from work on Br^--substituted PSIIcc (346, 347). For consistency, we shall refer to the former Cl^- site as "Cl_1-site".

Assuming that the Cl^- binding behavior observed in plant PSIIcc resembles that of cyanobacterial PSIIcc, it is tempting to assign the Cl_1-site to the slowly exchanging high-affinity Cl^- binding site. There are three aspects that support such an assignment: (i) Cl_1 is bound to Lys D317 (Figure 7). According to the electrostatic calculations performed by Ishikita *et al.* (324) on the basis of the 3.0 Å resolution structure, this lysine has a pK_a value of 1.5 – 9.6 in the absence of Cl^- depending on the charge distribution assigned to the Mn_4Ca cluster. Thus, it likely falls into the category of low pK_a lysines and its deprotonation could significantly destabilize Cl^- binding. (ii) Cl_1 resides deeply buried in the protein, and chloride exchange requires a channel. A possible candidate is channel G. The MD simulations of Vassiliev *et al.* (327) show that channel G is rather flexible in the absence of Cl^- allowing for some water flow that could support fast chloride transport. It would be interesting to repeat these calculations with chloride bound to the Cl_1-site in order to reveal a possible influence on the protein dynamics that could result in a retardation of water and chloride transport. Also, an evaluation of Cl^--induced pK_a shifts of nearby residues and concomitant structural changes would be important to develop a molecular basis of the one-site two-state model. (iii) Cl_1 is bound to the backbone of Glu A333, which is a ligand to Mn, and a water molecule in contact with Mn (Figure 7D). Removal of chloride from this position would change the charge distribution in this region and also likely cause structural alterations of at least Mn4 and its environment. These changes could be responsible for the shift from the $g = 2.0$ multiline to the $g = 4.1$ signal in the S_2-state and also cause a retardation of S-state cycling without a complete loss of water oxidation activity.

We now turn to the more complicated picture emerging from studies on bromide-substituted PSIIcc. A number of anions has been tested for the ability to compete with $^{36}Cl^-$ for the slowly exchanging chloride binding site in plant PSIIcc (353). Among the competing anions, only Br^-, NO_3^-, and I^- support an oscillation of the S_2 multiline signal under a series of laser flashes. The oscillation pattern is somewhat weaker in the case of NO_3^- and I^-, whereas Br^- shows activation properties very similar to Cl^- (350). As an alternative to the chemical exchange procedure, Boussac and co-workers (360) developed a biosynthetic method for Cl/Br-exchange in cyanobacterial PSIIcc related in spirit to the Ca/Sr-exchange technique (see subsection 5.3) and allowing also for a combination of the two replacements. They confirmed that the ion replacements resulted in a fully intact but kinetically limited WOC and showed that the effects of the Ca^{2+}/Sr^{2+} and Cl^-/Br^- exchanges were additive. These data clearly indicate the importance of both, Ca^{2+} and Cl^-, for optimizing the photosynthetic water oxidation.

The possibility to replace Cl^- with functionally competent Br^- paved the way to employ X-ray techniques for a further study of the anion under physiologically relevant conditions. XAS studies at the Br K-edge in Cl^- depleted and Br^- substituted PSII membranes from spinach excluded the presence of metal ions in the first and second coordination sphere of Br^- (361). EXAFS analysis provided tentative evidence of at least one metal ion at a distance of about 5 Å from Br^- and a Br-O/N distance of ~3.3 Å (361), which would be in reasonable agreement with a bromide ion occupying the Cl_1-site (henceforth referred to as "Br_1"). X-ray crystallography exploiting the anomalous dispersion of Br^- was applied by three independent groups resulting in partially conflicting results: The first publication was by Murray *et al.* (346), who employed both, chemical (Br-infiltrated) and biosynthetical (Br-physiologically) exchange to PSIIcc from *T. elongatus* and found two bromide sites, Br_1 and Br_2, close to the WOC. This result was confirmed shortly thereafter by Kawakami *et al.* (347) based on chemical Cl/Br exchange in PSIIcc from *T. vulcanus* (Figure 11B). The Br_1-site is identical to Cl_1. The anion in Br_2 is ligated by the backbone NH-groups of Glu C354 (likely ligating Mn, see above) as well as Asn A338 and might be stabilized by interaction with the OH-dipole of Thr C355. In contrast, Guskov *et al.* (15) used biosynthetical exchange with PSIIcc from *T. elongatus* and found clear evidence for Br^- in the difference density map only for the Br_1-site as shown explicitly in Figure 11A. On the basis of these data and the 2.9 Å resolution structure, the presence of a second Cl^- binding site in native PSIIcc was questioned (18). However, irrespective of the existence of a Cl_2-site, the conflicting data obtained with bromide-substituted PSIIcc hint at the possibility of several halide binding sites that are differentially occupied under various conditions. The challenge for future research will be to find out, which factors control the occupation of the sites and which sites are of functional relevance.

8. REDOX ACTIVE TYROSINES

It is known for a long time that there is an ET intermediate between the WOC and the RC of PSIIcc (362) that retains an unpaired electron after being oxidized, giving rise to a signal detectable by EPR techniques (118). The signal has the characteristics of an organic radical and has been identified as a tyrosine radical on the basis of isotopic labelling experiments (103). The matter is complicated by the fact that there are two redox active tyrosines in PSIIcc, Y_Z and Y_D, which are located at symmetry-related positions close to the RC (Figure 2, for a

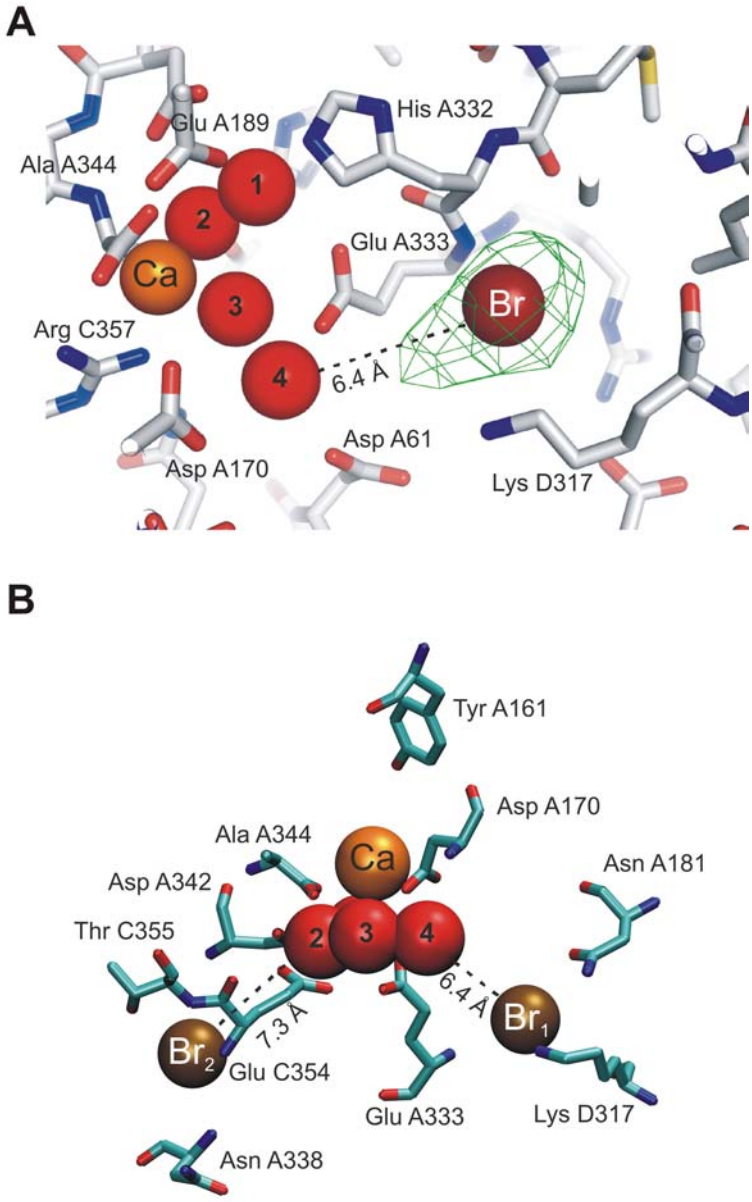

Figure 11. (A) Bromide binding site (Br_1) identified by Guskov *et al* (15) in a 3.9 Å data set of biosynthetically bromide-substituted PSIIcc of *Thermosynechococcus elongatus*, corresponding to the chloride binding site (Cl_1) identified in the native data set at 2.9 Å resolution. Figure made with PyMOL (493). (B) Bromide binding sites (Br_1 and Br_2) identified by Kawakami *et al* (347) in a 3.7 Å data set of chemically bromide-substituted PSIIcc of *Thermosynechococcus vulcanus*. Both binding sites were identified earlier by Murray *et al.* (346). Figure made with VMD (492).

review, see (363)). Only Y_Z (Tyr A161) is situated between P_{D1} and the WOC (Figure 12), whereas Y_D (Tyr D160) sits at a significant distance to the latter.

8.1. Y_Z

The identity of Tyr A161 with Y_Z was demonstrated by site-directed mutagenesis (364-366) long before its location in the vicinity of the Mn_4Ca cluster became apparent from the crystal structures. Besides the role of Y_Z as the intermediate electron acceptor between the WOC and P_{D1}, other functions have been attributed to it such as being a hydrogen abstractor (367), an electrostatic promoter of water splitting (368) or involved in proton release from the WOC (369). At present, these additional roles can not be settled. Here, we focus on the effect of hydrogen bonding between Tyr A161 and His A190.

In aqueous solution, the mid-point potential E_m of the phenolic side chain of tyrosine depends on pH (370, 371), since the group is deprotonated with different pK_a values pK_{red} and pK_{ox} in the reduced and oxidized form, respectively (Figure 12A). The oxidation of the neutral

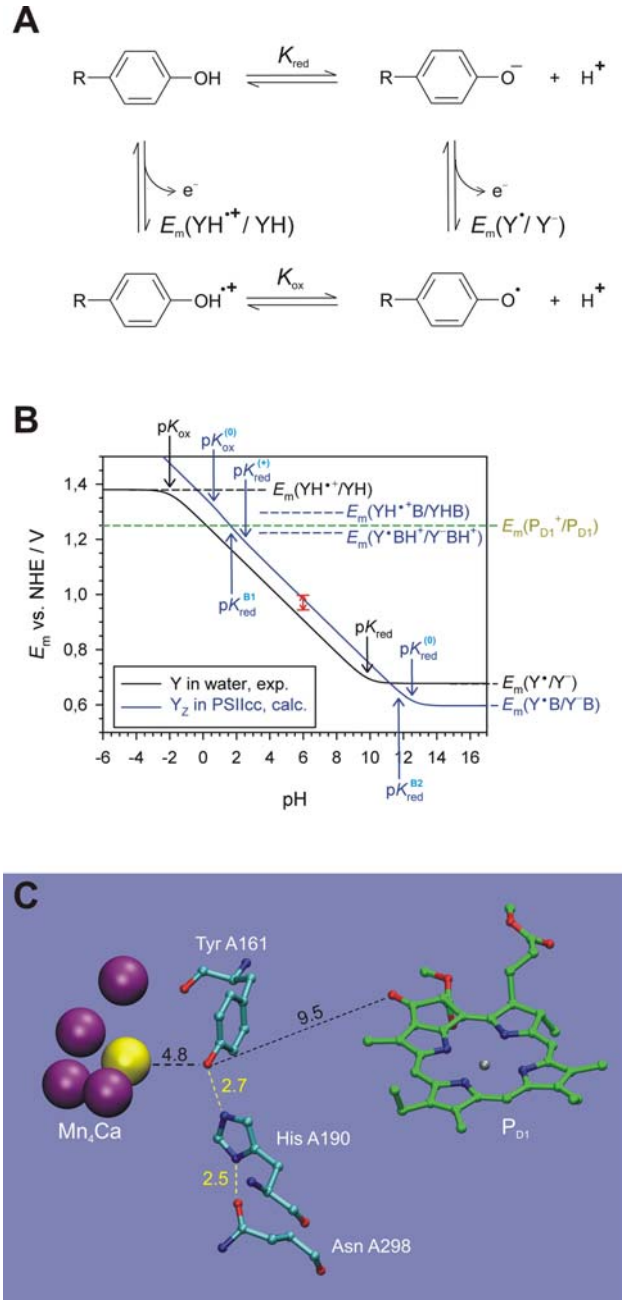

Figure 12. (A) Thermodynamic cycle relating redox and protonation reactions of a phenolic moiety (e.g., a tyrosine side chain) to the redox midpoint potentials $E_m(YH^{\bullet+}/YH)$ and $E_m(Y^{\bullet}/Y^-)$ of the protonated and deprotonated form, respectively, as well as to the acid constants K_{red} and K_{ox} of the reduced and oxidized form, respectively. (B) Pourbaix diagram of a tyrosine model compound (Y) in water (black) and of Y_Z in PSIIcc (blue). $pK_{red} = 9.9$ and $E_m(Y^{\bullet}/Y^-) = 650$ mV of Y are directly determined experimentally (373), while $pK_{ox} \approx -2$ is estimated from EPR of phenol radicals (374). The blue curve is an implementation of equation [2] with the following parameters/assumptions: $E_m(Y^{\bullet}BH^+/Y^-BH^+) = 1216$ mV (378), $pK_{red}^{(0)} - pK_{red}^{(+)} = pK_{ox}^{(0)} - pK_{ox}^{(+)}$, and the parameters listed in the caption to Figure 13B. The green dashed line indicates the estimated redox midpoint potential of P_{D1} (36) and the red double arrow the redox potential range of Y_Z estimated experimentally by Vass and Styring (379). (C) Location of Tyr A161 (Y_Z) relative to His A190, Asn A298, P_{D1}, and the Mn_4Ca cluster. The yellow dashed lines indicate hydrogen bond distances and the black dashed lines atom-atom distances. The numbers are distances in units of Å. Figure made with VMD (492).

protonated tyrosine YH to the neutral deprotonated tyrosine radical $Y^{\bullet}$ can proceed via two principle routes involving either the anion Y^{-} or the radical cation $YH^{\bullet+}$ depending on whether deprotonation or oxidation occurs first. The free energy differences for the four individual processes are determined by the redox mid-point potentials $E_m(YH^{\bullet+}/YH)$ and $E_m(Y^{\bullet}/Y^{-})$ as well as the two dissociation constants K_{red} and K_{ox} and are related to each other by the thermodynamic cycle depicted in Figure 12A. This cycle implies that if, e.g., $E_m(YH^{\bullet+}/YH)$, K_{red}, and K_{ox} are given, $E_m(Y^{\bullet}/Y^{-})$ is uniquely determined. The pH-dependence of E_m is shown in the Pourbaix diagram, i.e., a potential-pH-plot (372), in Figure 12B (black curve) and is given by the Nernst-Clark equation:

$$E_m = E_m(YH^{\bullet+}/YH) + (59\ \text{mV})\,\lg\left(\frac{10^{-pH}+K_{red}}{10^{-pH}+K_{ox}}\right) \quad [1]$$

valid at room temperature. To obtain the behavior of the tyrosine side chain in aqueous solution, reactions of the backbone amino and carboxy groups have to be avoided. Therefore, measurements have been performed on the model compound N-acetyl-L-tyrosinamid resulting in $E_m(Y^{\bullet}/Y^{-}) = +650$ mV and $pK_{red} = 9.9$ (373). The value of pK_{ox} is fairly low and more difficult to measure, but can be estimated on the basis of EPR experiments on phenol radical cations in aqueous sulphuric acid to be ~–2 (374). The value of $E_m(YH^{\bullet+}/YH)$ is then fixed to about +1.38 V, which is higher than the estimated potential of P_{D1} (36). But what is the actual redox mid-point potential of Y_Z in PSIIcc?

The protein environment can have a strong influence on E_m of Y_Z, in particular, a hydrogen bond to a nearby base B such as His A190 (Figures 7A, 12C). To describe such a scenario, we have to consider at least eight states: four with reduced ("red") and four with oxidized ("ox") Y_Z. The four states in each case are with both Y_Z and B deprotonated, both protonated as well as only Y_Z or only B protonated. For simplicity, we assume His A190 to be protonatable only at N_ε, while the proton at N_δ is engaged in a stable hydrogen bond to Asn A298 (Figure 12C), and neglect the influence of other titratable groups. First, we consider the pH-dependent population of the four states pertaining to reduced Y_Z that are shown in the thermodynamic cycle of Figure 13A. Within this minimal model, the Tyr A161/His A190/Asn A298 system is described formally as a diprotic acid. Y_Z has two different pK_a values ($pK_{red}^{(0)}$ and $pK_{red}^{(+)}$) depending on the protonation state of B and *vice versa* (pK_{red}^{B1} and pK_{red}^{B2}; we dropped the index "red" in Figure 13 for simplicity). A titration curve of this system would exhibit two steps determined by the lowest and the highest of the four pK_a values. Between these two pK_a values, one of the titratable protons remains in the system and is distributed between the two moieties as determined by the free energy difference for proton transfer (PT) from B to Y, $\Delta G_{red}^{PT} = (RT\ln 10)pK_{red}^{PT}$ with $pK_{red}^{PT} = pK_{red}^{B1} - pK_{red}^{(+)} = pK_{red}^{B2} - pK_{red}^{(0)}$. That is, Y is protonated for $pK_{red}^{(0)} > pK_{red}^{B2}$, and B is protonated for $pK_{red}^{(0)} < pK_{red}^{B2}$. These two cases are shown in Figures 13 B and C, respectively, where the mole fractions X of the individual states are plotted as a function of pH.

Experimental information on the protonation state of Y_Z may be obtained from spectroscopy (363, 371). While data from UV/VIS spectroscopy remained inconclusive, FTIR measurements argue strongly that Y_Z is protonated at pH 6 (375), implying $pK_{red}^{(0)} > pK_{red}^{B2}$. Very recently, Rappaport *et al.* (376) investigated PSIIcc, in which 3-fluorotyrosine (3F-Y) was incorporated biosynthetically. In aqueous solution, the pK_a of the corresponding model compound N-acetyl-3-fluorotyrosinamid is shifted by –1.5 to 8.4 (377). Rappaport *et al.* investigated *inter alia* the pH-dependence of the kinetics of $P_{D1}^{\bullet+}$ reduction in labeled and unlabeled, Mn-depleted PSIIcc from *T. elongatus*. As discussed below, their data suggest that $pK_{red}^{(0)} > 12$ for unlabeled Y_Z (at least in Mn-depleted samples). The electrostatic calculations of Ishikita and Knapp (378) suggest (according to our interpretation) that $pK_{red}^{(0)} \approx 12.5$, $pK_{red}^{(+)} \approx 2.5$, and $pK_{red}^{PT} = -0.8$. On the basis of these parameters, we calculated the titration curves in Figure 13B to illustrate a possible pH-dependence of the various states. Note in particular, that in the absence of a strong influence by another titratable group, the protonation states of both, Tyr A161 and His A190, are expected to be pH-independent in a wide range between pK_{red}^{B1} and $pK_{red}^{(0)}$. If Y_Z is fluorinated, the pK_a values of Y_Z are expected to decrease by 1.5, while those of B remain unaffected. If $pK_{red}^{PT} > -1.5$ as in the present model, fluorination can be expected to change the protonation state of reduced Y_Z at physiological pH (Figure 13C). Therefore, FTIR experiments on such labeled samples could give information about pK^{PT}.

Turning back to the redox potential, we can write down a scheme analogous to Figure 13A also for oxidized Y_Z with appropriate pK_a values $pK_{ox}^{(0)}$, $pK_{ox}^{(+)}$, pK_{ox}^{B1}, pK_{ox}^{B2}, and $pK_{ox}^{PT} = \Delta G_{ox}^{PT}/(RT\ln 10)$, and connect the two schemes by mid-point potentials for the various redox couples. The Nernst-Clark equation of this minimal-model reads

$$E_m = E_m(YH^{\bullet+}BH^{+}/YHBH^{+}) + (59\ \text{mV})\,\lg\left(\frac{10^{-2pH}+(K_{red}^{(+)}+K_{red}^{B1})\,10^{-pH}+K_{red}^{(0)}K_{red}^{B1}}{10^{-2pH}+(K_{ox}^{(+)}+K_{ox}^{B1})\,10^{-pH}+K_{ox}^{(0)}K_{ox}^{B1}}\right) \quad [2]$$

Here, $E_m(YH^{\bullet+}BH^{+}/YHBH^{+})$ is the mid-point potential for the left redox couple in Figure 12A, but in the presence of a protonated (positively charged) His A190. The blue curve in Figure 12B respresents equation [2] in the relevant pH range for the parameters listed in the figure caption. We made use again of the calculations by Ishikita and Knapp (378), suggesting $E_m(Y^{\bullet}BH^{+}/Y^{-}BH^{+}) = 1216$ mV (lower blue dashed line in Figure 12B). Furthermore, we assumed that the pK_a shift due to the oxidation of Y_Z is the same in protein and solution, i.e., $\Delta pK_a = -11.9$, and that

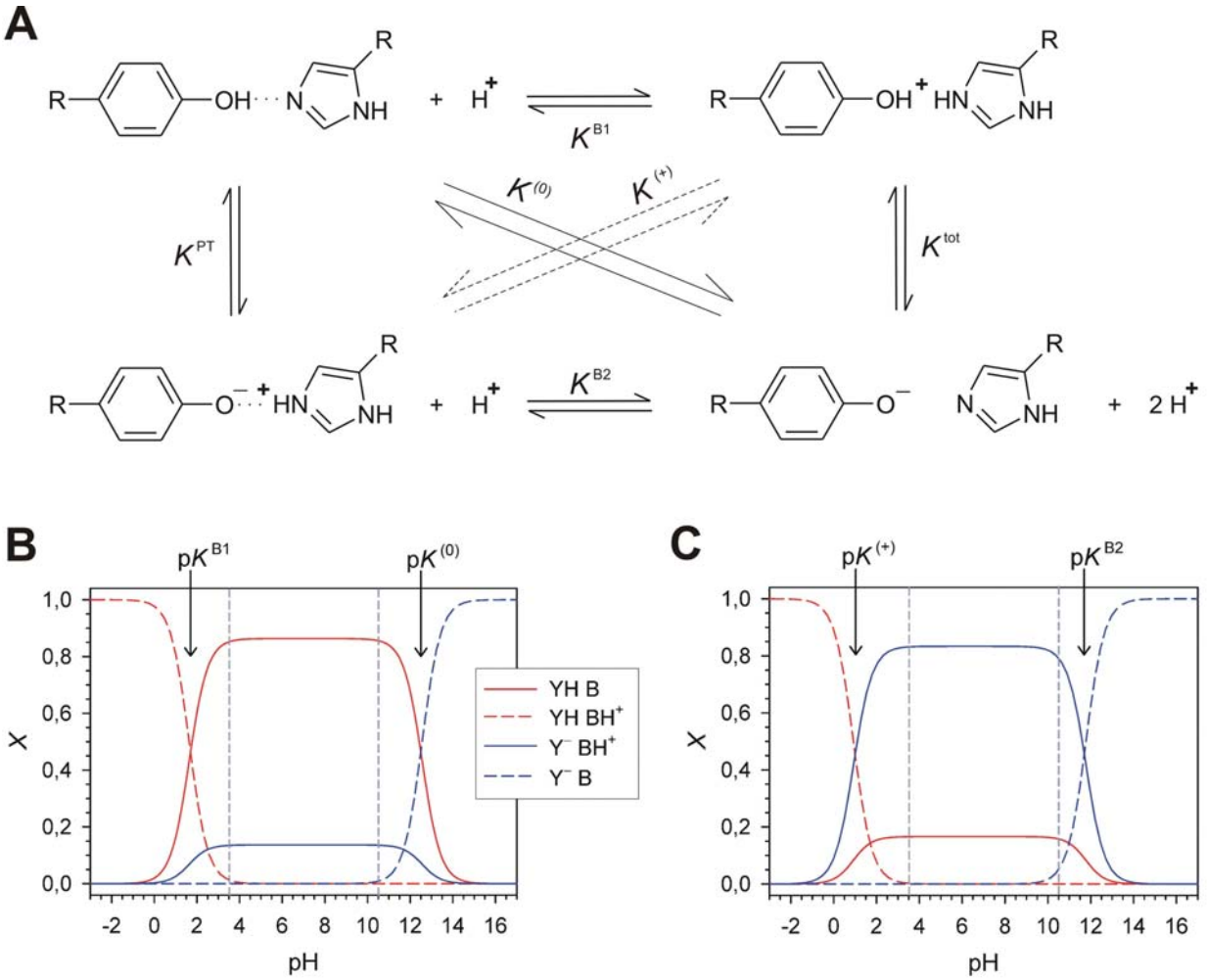

Figure 13. (A) Thermodynamic cycle defining acid and equilibrium constants of the Tyr A161 – His A190 pair modeled as a diprotic acid, written for the reduced form of Y_Z (index "red" omitted for simplicity). A similar cycle can be written for the oxidized form of Y_Z. (B) Theoretical pH titration of the Tyr A161 – His A190 pair with Y_Z reduced (X = mole fraction of the indicated species) assuming the following parameters: $pK_{red}^{PT} = -0.8$, $pK_{red}^{(0)} = 12.5$, $pK_{red}^{(+)} = 2.5$. (C) Same as in B, but with $pK_{red}^{PT} = +0.7$, $pK_{red}^{(0)} = 11.0$, $pK_{red}^{(+)} = 1.0$.

$pK_{red}^{(0)} - pK_{red}^{(+)} = pK_{ox}^{(0)} - pK_{ox}^{(+)}$. With these settings, we can define the eight-state model completely. Clearly, these parameters are preliminary, and a more precise evaluation awaits a reliable WOC structure at a higher resolution and further experiments. Nonetheless, the following insight may be gained: (i) At physiological conditions, i.e., pH 6, the equilibrium mid-point potential of Y_Z is calculated to be +986 mV in agreement with Ishikita and Knapp (378) and with experimental estimates by Vass and Styring (379) placing the potential in the range of 950 – 990 mV (red double arrow in Figure 12B). The potential depends on pH as expected ($dE_m/d(pH) = -59$ mV) between $pK_{red}^{(+)}$ and pK_{red}^{B2}. The situation may become more complicated, if the influence of other titratable residues (e.g., Arg C357) or an S-state dependence is taken into account. (ii) In the present model, the pK_a-values of Tyr A161 are $pK_{red}^{(0)} = 12.5$ and $pK_{ox}^{(0)} = 0.6$, which are increased by 2.6 compared to tyrosine in aqueous solution. This shift is not only due to the hydrogen bond to His A190, but also depends on other parts of PSIIcc as do the redox potentials. In particular, electrostatic calculations suggest that there is an influence of the protonation state of Arg C357 and the charges assigned to the WOC, where the former is affected by the latter (378). This implicates that pK_a values and redox potentials may be S-state-dependent and influenced by Mn- or Ca-depletion procedures. Notably, the charge state of P_{D1} has only a small effect (< 10 mV). (iii) In the present model, $pK_{red}^{PT} < 0$ and $pK_{ox}^{PT} > 0$, meaning that Y_Z becomes deprotonated and His A190 protonated upon oxidation of Y_Z in equilibrium. This result does not

necessarily indicate that a concerted proton-electron transfer (CPET) takes place. (iv) If ET precedes PT (ET-PT mechanism) the relevant redox potential in the present model is $E_m(YH^{\bullet+}B/YHB)$ = 1299 mV, which is higher than the estimated potential of the $P_{D1}^{\bullet+}/P_{D1}$ couple by about 50 mV. Given the uncertainty of these numbers, an ET-PT mechanism cannot be excluded on purely energetic grounds, at least within this model. (v) If proton transfer to His A190 precedes ET to $P_{D1}^{\bullet+}$ (PT-ET mechanism), the relevant redox potential is $E_m(Y^{\bullet}BH^+/Y^-BH^+)$ = 1216 mV (378), and the driving force for ET is rather small (< 40 meV).

The kinetics of $P_{D1}^{\bullet+}$ reduction by Y_Z is complex; for recent reviews, see (21, 380, 381). A reasonable description involves at least three exponential kinetics with a "fast" ns, a "slow" ns, and a µs component, and this general picture is obtained from experiments on a variety of sample and organism types (199, 277, 368, 376, 382-386). To unravel the complexity of Y_Z oxidation, experiments have been performed on intact and Mn-depleted PSIIcc. In intact PSIIcc, the amplitude of the "fast" ns phase is larger in S_0 and S_1 compared to S_2 and S_3, while that of the "slow" ns component is smaller, i.e., shows the opposite behavior (199, 382, 383). This S-state dependence could be due to an electrostatic effect of the presumed surplus charge on the WOC in S_2 and S_3 (see subsection 4.6) or originate from conformational changes (381). In contrast to the ns phases that lack any kinetic H/D isotope exchange effect (368, 383, 387, 388), the µs component is significantly different in H_2O compared to D_2O (383, 389). Therefore, the µs component is assigned to proton rearrangements in the neighborhood of Y_Z, while the "slow" ns component is ascribed to protein relaxation not involving proton shifts. The "fast" ns component is interpreted as reflecting the actual ET from Y_Z to $P_{D1}^{\bullet+}$, but the observed rate constant (35 – 70 ns) does not necessarily correspond to the instrinsic rate constant for forward ET as discussed in (386). The absence of an isotope effect indicates that if this ET is coupled to PT, the latter is not rate-limiting. Another interesting feature of the "fast" phase is its pH-dependence, i.e., the amplitude declines at acidic pH with an apparent pK_a of 4.6 (368, 390-392) and in the alkaline range with pK_a ~ 8 (368). Since the population of the state YH B in the model outlined above shows a similar behavior (albeit with different pK_a values used in the modeling, see Figure 13B), it is tempting to identify the two apparent pK_a´s as pK_{red}^{B1} = 4.6 and $pK_{red}^{(0)}$ = 8.0. In particular, the identification of pK_{red}^{B1} would be in line with the proposal of Kühn *et al.* (392) that protonation of the Tyr A161/His A190 pair at the N_ε of the imidazole would inhibit Y_Z oxidation due to suppression of the necessary PT. However, such an interpretation is premature as other titratable groups could affect the kinetics (cf. discussion of Y_D below), and further studies are required to explain the pH-dependence at a molecular level. Mn-depletion causes a drastic change in the characteristic of $P_{D1}^{\bullet+}$ reduction by Y_Z (381), and it remains unclear at present, what actually can be learned from these experiments about intact PSIIcc.

8.2. Metalloradical signals of Y_Z

During the last decade, EPR signals were detected that represent light-induced $Y_Z^{\bullet}$ interacting magnetically with the Mn_4Ca-cluster. These so-called metalloradical signals can be induced at helium temperatures by illumination with visible (VIS) or near-infrared (NIR) light; for reviews, see (393, 394). In this context, it should be recalled that S-state progression is inhibited at cryogenic temperatures with characteristic half-inhibition temperatures for the individual transitions between 135 and 235 K (395). Also, reduction of Q_B is blocked, so that VIS-illumination of the RC will create the state $P_{D1}^{\bullet+}Q_A^{\bullet-}$. Under these circumstances, $P_{D1}^{\bullet+}$ is apparently able to oxidize Y_Z at helium temperatures, if PSIIcc is poised in the S_0 or S_1 state prior to freezing, but not in S_2 or S_3. However, Y_Z oxidation occurs only in 40 – 50% of the centers (396). The ability to oxidize Y_Z appears to be correlated with the charge state of the WOC, i.e., the presumed surplus charge in S_2 and S_3 (see subsection 4.6) seems to inhibit the reaction. More recently, it could be demonstrated that Y_Z oxidation by VIS-illumination in centers poised in the S_2 state is possible at nitrogen temperatures (77 – 190 K) indicating a thermal barrier (397).

The Mn_4Ca cluster poised in the S_2 or S_3 state is sensitive to NIR light (398-401). Illumination at 10 K in the presence of $Q_A^{\bullet-}$ produces a metalloradical signal that resembles $S_1Y_Z^{\bullet}Q_A^{\bullet-}$ (402). Illumination of the state $S_3Q_A^{\bullet-}$ at 4 – 50 K also results in a metalloradical signal (169, 403, 404) with an action spectrum peaking around 760 nm (401) that is interpreted as $S_2'Y_Z^{\bullet}Q_A^{\bullet-}$, where S_2' is assigned to a proton-deficient variant of S_2 based on its pH-dependence (405). The state $S_2'Y_Z^{\bullet}Q_A^{\bullet-}$ recombines to $S_2'Y_ZQ_A$, which in turn can be transformed into $S_2'Y_Z^{\bullet}Q_A^{\bullet-}$ by VIS-illumination at helium temperatures (393, 405, 406). Note that NIR-illumination of $S_2Q_A^{\bullet-}$ and $S_3Q_A^{\bullet-}$ apparently leads to backward ET from Y_Z to the WOC. The suggested mechanisms of NIR sensitivity involve intervalence charge transfer transitions between Mn^{III} and Mn^{IV}, NIR-induced spin state transitions or d-d transitions in Mn^{III} causing a spin change (394). The presence of Mn-ions with the "correct" oxidation state seems to be crucial.

An important property of the metalloradical signals is the pH-dependence, which has beeen studied recently for S_0 (407), S_1 (408) and S_3 (394). While the pH-dependence of S-state turnover at room temperature (409) is not necessarily indicative of Y_Z activity, formation of metalloradical signals is a more direct indicator. Indeed, the results from the different experiments do not always agree, Whereas both, S-state progression and metalloradical formation, decline at acidic pH with essentially the same apparent pK_a for S_0 and S_3, this is not the case for S_1. The $S_1 \rightarrow S_2$ transition at ambient temperatures is pH-independent between pH 3.5 and 9.5 (409), but the formation of $S_1Y_Z^{\bullet}Q_A^{\bullet-}$ at cryogenic temperatures is inihibited at low pH with an apparent pK_a of ~4.7 (408). It

should be noted that in all these low-temperature studies of PSIIcc, it is implicitly assumed that the protonation probabilities of groups are only weakly temperature-dependent. This assumption remains untested.

Havelius *et al.* (394, 407, 408) provided a tempting explanation for the apparent discrepancy between $S_1 \rightarrow S_2$ transition activity and formation of $S_1Y_Z^{\bullet}Q_A^{\bullet-}$ at low pH: They interpreted the apparent pK_a ~4.7 of the metalloradical signal as pK_{red}^{B1} in accordance with the interpretation of Kühn *et al.* (392) for the ns kinetics of Y_Z oxidation. At pH > pK_{red}^{B1}, the state YH B prevails, and the normal proton-coupled ET proceeds. At pH < pK_{red}^{B1}, the state YH BH^+ is present, and oxidation of Y_Z is only possible, if the phenolic proton is taken up by another group, albeit slower (µs kinetics). The latter process is coupled to proton movements not confined to a single hydrogen bond. It, therefore, only proceeds at elevated temperatures and may be responsible for the H/D isotope exchange effect. The group accepting the proton is likely important for proton release from the WOC. Then, its protonation by Y_Z blocks proton release and consequently those S-state progressions that are accompanied by proton egress. Since no protons are expelled in the $S_1 \rightarrow S_2$ transition (see section 9), the latter can proceed at high temperature at all pH, while Y_Z is oxidized fast at pH > pK_{red}^{B1} and slow at pH < pK_{red}^{B1}. Accordingly, the $S_0 \rightarrow S_1$ and $S_3 \rightarrow S_0$ transitions that require the proton acceptor are blocked below pK_{red}^{B1} at any temperature. This model awaits further testing by studies of the pH-dependent formation of the metalloradical associated with the S_2 state.

8.3. Y_D

We now turn to the second player in the tyrosine game. Despite its remote position relative to the WOC (Figure 2), Y_D (i.e., Tyr D160) is not unimportant (363, 410). In mutants of *Synechocystis* PCC 6803 with Tyr D160 replaced by Phe, photoautotrophic growth is slowed down (411), which may be related to a retardation and reduced efficiency of the photoassembly of the Mn_4Ca-cluster (412). Y_D is apparently able to donate electrons to $P_{D1}^{\bullet+}$ in Mn-depleted PSIIcc (413) and is in redox equilibrium with P_{D1}, Y_Z and the WOC in intact PSIIcc (379). To disentangle the various contributions, Mn-depleted PSIIcc of a Y_Z-lacking mutant was investigated with time-resolved EPR and optical techniques (414). This study revealed electron donation of Y_D to $P_{D1}^{\bullet+}$ with sub-µs kinetics that is pH-dependent, i.e., rises at high pH with an apparent pK_a of 7.7. To explain the unexpectedly fast ET, an involvement of P_{D2} (i.e., partial delocalization of P^+ on P_{D2}) was proposed. The pH-dependence was confirmed in low-temperature studies showing that Y_D can be oxidized at 15 K (415). These results imply that there is a pH-dependent competition between Y_Z and Y_D as demonstrated recently in studies of the Y_Z metalloradical signals (394, 408).

In intact PSIIcc, oxidized Y_D (termed $Y_D^{\bullet}$ in the following, as it is likely a deprotonated radical, see below) is able to oxidize the S_0 state of the Mn_4Ca cluster up to S_1 (Figure 4B) as shown by using EPR spectrosocpy (410, 416). This ET has a half life time between 2 and 50 min. depending on the species and sample type (416-418). It has been proposed that Y_D could serve to stabilize the WOC by maintaining it in a higher oxidation state (416). This also suggests a role of Y_D in the photoactivation process (412), in which Mn^{2+} is incorporated into apo-PSIIcc by light-triggered oxidation (238-241). Further support for this idea comes from the observation that $Y_D^{\bullet}$ is able to oxidize the overreduced states S_{-1} and S_{-2} of the Mn_4Ca-cluster (183). However, there is also evidence that reduced Y_D is able to reduce the S_2 and S_3 states (419), thereby effectuating a back-stepping in the Kok-cycle down to S_1 (Figure 4B). These processes are characterized by half life times between 0.8 and 5.5 s (417, 418). The redox mid-point potential of the $Y_D^{\bullet}/Y_D$ H couple has been estimated from direct chemical oxidation of Mn-depleted PSIIcc to be 760 mV (420), which is in agreement with estimates based on kinetic measurements on intact PSIIcc (379). The difference of ~200 mV with respect to Y_Z is also reproduced by electrostatic calculations (378) and can be considered as compatible with the structural information about PSIIcc.

Like Y_Z, Y_D is believed to be protonated in its reduced form and to deliver a proton to a nearby base upon oxidation ("proton rocking motion" model (421)). EPR spectroscopy combined with site-directed mutagenesis provided evidence that this base is His D189 (422-424), and ENDOR data indicated the presence of an exchangeable proton hydrogen-bonded to $Y_D^{\bullet}$ (425) and bound to N_ε of His A189 (426). Such a hydrogen bond is also in agreement with FTIR data (375). The crystal structure confirms the presence of His D189 in the vicinity of Tyr D160 (Figure 14). Unlike its counterpart in PsbA, His D189 is, at the N_δ-side, not hydrogen bonded to an asparagine side chain, but to the protonatable side chain of Arg D294, which in turn is in hydrogen bonding distance to a chain of titratable residues. Moreover, there is a hydrogen bond between two amide side chains close to and "parallel" to the hydrogen bond between Tyr D160 and His D189. It remains to be clarified, how this arrangement affects the dynamics of proton-coupled ET. A recent FTIR study (427) indicates that reduced YD remains protonated between pH 6 and 10, i.e., the state YDH B prevails. However, in the oxidized form $Y_D^{\bullet}$, His D189 remains neutral and its protonation state is *not* responsible for the pH-dependence of Y_D oxidation. The measured apparent pK_a of 7.7 (see above) is, therefore, to be assigned to other groups. A likely explanation is that after accepting a proton from Tyr D160 at N_ε, His D198 deprotonates at N_δ by virtue of its interaction with Arg D294, which in turn delivers a proton to the hydrogen bonded network of titratable groups (Figure 14). This explanation is in agreement with very recent QM/MM computations (428) suggesting that the measured hfc of $Y_D^{\bullet}$ are more in line with hydrogen bonding to a neutral than to a charged histidine. However, the functional role of the hydrogen-bond network around Y_D remains still elusive.

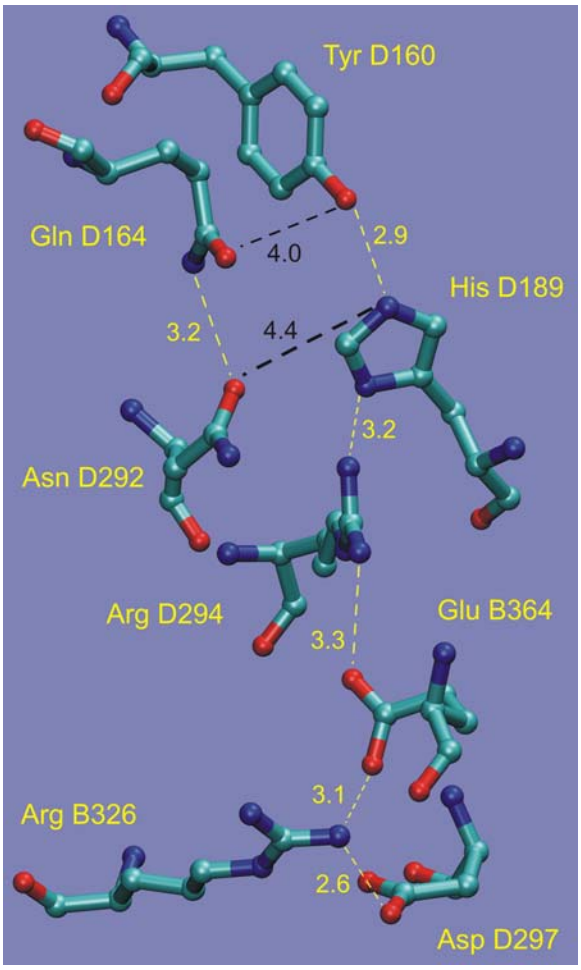

Figure 14. Hydrogen bonding network around Y_D (Tyr D160) as evident from the crystal structure at 2.9 Å resolution (15). The yellow dashed lines indicate hydrogen bond distances and the black dashed lines atom-atom distances. The numbers are distances in units of Å. Note that the 4.0 Å distance is between the phenolic oxygen of Tyr D160 and the amide nitrogen of Gln D164. Figure made with VMD (492).

9. PROTON RELEASE

A key aspect in the understanding of biological water oxidation is the proton release pattern, i.e., the number of protons released in each of the S-state transitions. Accordingly, there have been many studies aiming at a determination of the proton release stoichiometry applying various techniques (371, 429-431). The pioneering work of Fowler (432) indicated a release pattern for $S_0 \rightarrow S_1 \rightarrow S_2 \rightarrow S_3 \rightarrow S_0$ of 0.75 : 0 : 1.25 : 2 measured by using a pH electrode. This principle pattern was confirmed by other groups using optical techniques (433-437) and more recently by Schlodder and Witt (438) using a pH electrode and by Suzuki *et al* (431) using FTIR spectrosopy (see Figure 4A). Based on the expectation that the proton stoichiometry should be represented by a set of integers, these results were interpreted as a pattern of 1 : 0 : 1 : 2. Other studies on various sample types challenged this view and arrived at a simple stoichiometry of 1 : 1 : 1 : 1 (429, 439-441). However, one has to distinguish carefully between the actual number of protons expelled in each S-state transition (intrinsic proton release pattern) and the number of protons reaching the outer medium and being detectable by pH-electrodes, indicator dyes etc. (extrinsic proton release pattern) (442).

In the following, we shall concentrate on the more recent data obtained with isolated PSIIcc from *T. elongatus* (431, 438). The first problem to deal with is the proton uptake by the artificial electron acceptor (e.g., dichloro-*p*-benzoquinone, DCBQ) used to maintain light-induced RC turnover. This can be circumvented by the addition of (non-protonatable) ferricyanide as final electron acceptor, ensuring reoxidation of DCBQ (438). Then, two complications remain: (i) The sequence of proton release as a function of flash number n is given by (437)

$$\Delta H(n) = \sum_{i=0}^{3} \varepsilon_i T_i(n) \qquad [3]$$

where ε_i is the number of protons liberated in the $S_i \rightarrow S_{i+1}$ transition and $T_i(n)$ the weight of transition $S_i \rightarrow S_{i+1}$ upon flash n. As discussed in subsection 4.1., $T_i(n)$ depends on the Kok-parameters, i.e., the number of "double-hits" and "misses". These parameters have to be determined by analysis of an independent observable or by fitting. (ii) If we denote the number of protons expelled from the WOC in the $S_i \rightarrow S_{i+1}$ transition with k_i (intrinsic proton release pattern), then in general, $\varepsilon_i \neq k_i$, i.e. the extrinsic proton release pattern may be different. This can be understood by considering the presence of a titratable amino acid side chain in the vicinity of the WOC. Similar to the effect of Y_Z oxidation on the pK_a of His A190 discussed in subsection 8.1, oxidation of the WOC may shift the pK_a of this nearby group by virtue of their electrostatic interaction. If the pK_a shift is large enough, S-state progression may cause the group to deprotonate and hence a proton to be liberated even though $k_i = 0$. Under these conditions, one expects the ε_i to be pH-dependent and not necessarily integer numbers.

Schlodder and Witt (438) performed experiments on crystallizable PSIIcc from *T. elongatus* and found a pH-dependent proton release pattern. While $\varepsilon_0 = \varepsilon_2 = 1$ at all pH between 5.5 and 7.5, $\varepsilon_1 = m$ and $\varepsilon_3 = 2 - m$, where m is approximately a sigmoidal function of pH with an inflection point around 5.7. As a consequence, the pattern is 1 : 0 : 1 : 2 at pH 7.5, but tends towards 1 : 1 : 1 : 1 below pH 5.5. The simplest interpretation of this feature is that there is one titratable group in the vicinity of the WOC (called AH in Figure 4C) with a p$K_a \sim 5.7$ in the S_0 and S_1 states and a shifted p$K_a < 5.5$ in states S_2 and S_3, where the pK_a shift is caused by the positive surplus charge in the latter two states (see subsection 4.6). Then, m is the protonation probability of AH. On the basis of these data, it is believed that the intrinsic proton release pattern is indeed 1 : 0 : 1 : 2 and the deviations of the extrinsic pattern originate from deprotonation of (at least) one amino acid side chain.

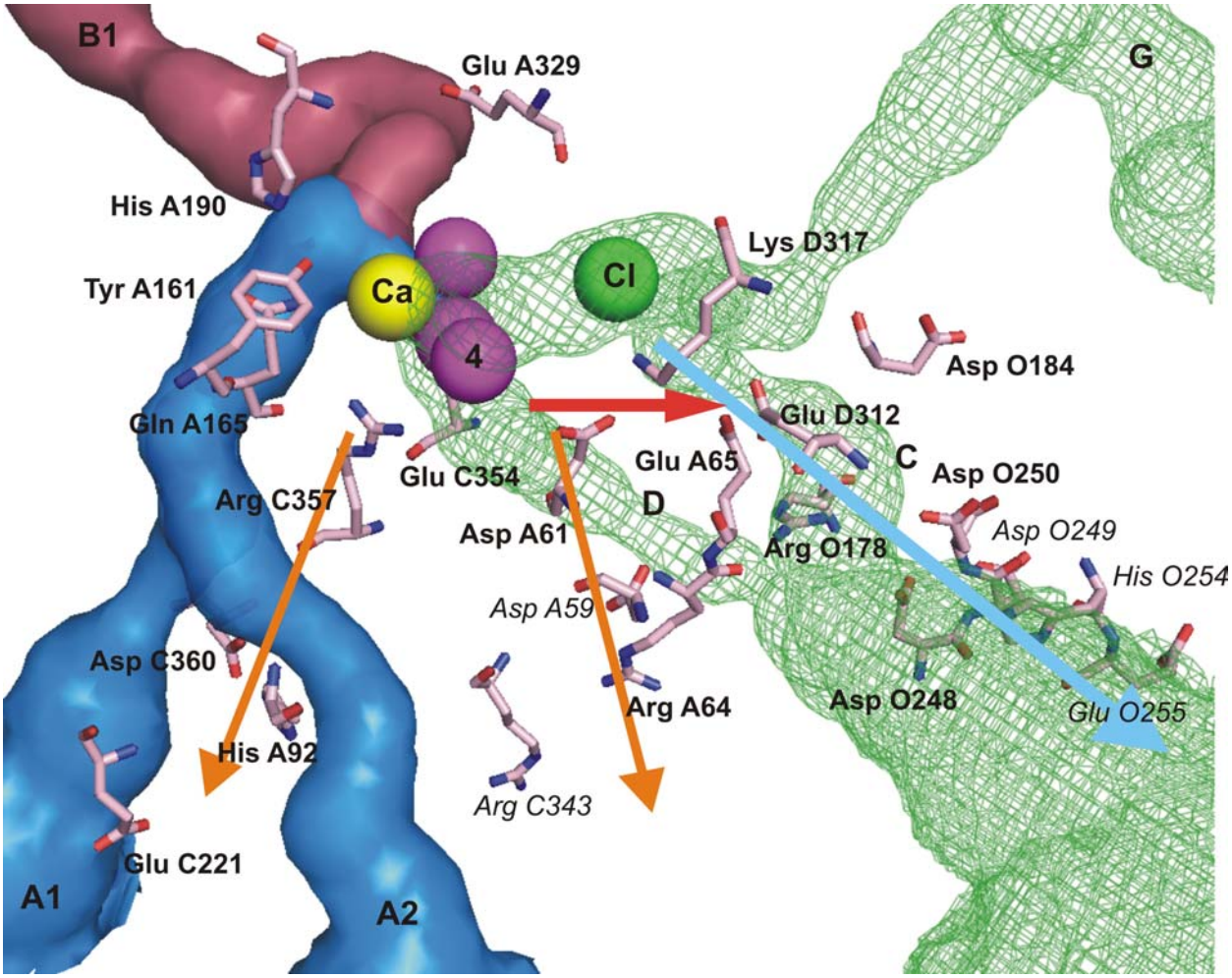

Figure 15. Amino acid residues around the Mn_4Ca cluster in PSIIcc proposed to be involved in proton egress in relation to the channels of Gabdulkhakov *et al.* (200). The blue arrow indicates the originally proposed pathway involving residues of PsbO (447-449). Note that the residues labeled in italics are not adjoint to the channels. Electrostatic (324) and quantum chemical calculations (329) suggest additional pathways indicated by the orange and red arrows, respectively. Figure made with PyMOL (493).

A problem of the earlier proton release measurements is that they are conducted at low or even zero buffer concentration. Under these conditions, protons may be trapped by buffering groups of the protein, which could disturb the determination of liberated protons. Suzuki *et al.* (431) circumvented this problem by using high buffer concentrations to ensure trapping of all liberated protons by the buffer and exploited the FTIR-response of isotopically labeled buffer to quantitate the proton uptake. In this way, they comfirmed the results of Schlodder and Witt for pH 6 and approved the reliability of the data. The FTIR-data also indicated that the amino acid residue responsible for the pH-dependence is neither Asp, Glu, His nor Cys, and left only Arg, Lys and Tyr as candidates. The only groups of this kind within ~10 Å of the Mn_4Ca-cluster are Arg A334, Arg C357, Lys D317, and Tyr A161. The latter is Y_Z discussed in section 8 and is unlikely to titrate at pH 5.7. Also, the interaction with His A190 suggests a response of His vibrations upon deprotonation that is not observed. Lys D317 interacts with the chloride ion Cl_1 (see section 7), which likely upshifts its pK_a. However, a loss of chloride from the Cl_1-site or a reorganiztaion of the protein in this region as suggested by the "one-site two-state" model could change the titration behavior of Lys D317 and/or the nearby Arg A334. The currently most interesting candidate is Arg C357, which is located very close to the Mn_4Ca-cluster (see Figure 15) and has been proposed to be directly involved in the reaction mechanism of water oxidation, viz. as proton abstractor (23, 443). Mutants of *Synechocystis* sp. PCC 6803 have been constructed, in which Arg C357 is replaced with Ser (444, 445) or Lys (446). Both mutations cause a severe impairment of O_2 evolution, but still contain 60 – 80 % of PSIIcc. Most strikingly, the R(C357)K mutant evolves ~10 % O_2 compared to wild type and does not show any oscillations of O_2 yield as a function of flash number (446). This feature has been interpreted tentatively

as representing a "miss" factor of 46 % indicating that Arg C357 is extremely important for S-state turnover and can not be fully replaced in its function with the different base Lys. These findings are principally in agreement with a role of Arg C357 as proton abstractor, but do not yet prove it. Electrostatic calculations confirm qualitatively that the protonation state of Arg C357 depends on the net charge of the Mn_4Ca-cluster and demonstrate an influence of this protonation state on the redox mid-point potential of Y_Z (378). So, in principle, Arg C357 could be responsible for the pH-dependence of the proton release pattern, the "fast" ns phase of Y_Z oxidation and the S-state turnover for S_2 to S_0 (see section 8). However, according to our present knowledge, the apparent pK_a values of all these processes are different, so that Arg C357 is probably not the sole origin of the pH-dependence.

As apparent from section 6, proton egress pathways connecting the Mn_4Ca-cluster with the lumen have not yet been identified. However, proposals for such pathways have been made based on visual inspection of the crystal structure (12, 447-449), channel calculations as described in subsection 6.2, electrostatic calculations of pK_a values (324), and QM/MM calculations (232, 329). The first proposals were based upon the 3.5 Å structure and assigned an important role in proton egress to titratable residues of PsbO (blue arrow in Figure 15). Later electrostatic calculations based upon the 3.0 Å structure confirmed this assignment by revealing a gradient of pK_a values to be established by these residues, but also identfied additional possible pathways (orange arrows in Figure 15). On the basis of their QM/MM calculations using the heterocubane structure, Sproviero *et al.* (232, 329) suggested proton exit from the Mn_4Ca-cluster via Asp A61 and Glu A65 (red arrow in Figure 15) leading to the originally proposed pathway involving PsbO. Glu A65 was also discussed by Gabdulkhakov *et al.* (200), as it was found to be located close to a narrow pass of a designated "proton channel" (Figure 10). They demonstrated in particular, that channel C (Figure 9) can be filled with water molecules connecting Mn4 (with one water molecule detected experimentally, see Figure 7D) via the chloride ion in the Cl_1-site with Glu A65, and proposed this as a possible proton egress pathway in agreement with earlier suggestions concerning the role of Cl^- (350). Note that this pathway also leads to the originally proposed PsbO-path, but that the PsbO-path deviates from the further joint course of channels C and D (Figure 15).

Central residues in these paths are Asp A61, Glu A65, and Glu D312 (Figure 15). Asp A61 was mutated in *Synechocystis* sp. PCC 6803 to either Glu, Asn or Ala (259). The mutants D(A61)N and D(A61)A exhibit only slow photoautotrophic growth and 20 % O_2-evolution activity despite a high apparent PSIIcc-content. In contrast, the mutation D(A61)E grows normally and evolves O_2 at 60 % of the wild type level. A similar feature was obtained with Glu A65, where the mutation to either Gln or Ala slowed down the photoautotrophic growth and reduced the O_2-evolution to 20 %, whereas the mutation to Asp allowed for normal growth and 90 % O_2-activity (259). These data suggest that titratable residues are required in these positions in line with their presumed roles as intermediate proton acceptors. Very recently, Glu D312 has been mutated to Ala (450). This mutant is photoautotrophic and evolves O_2 at 30 % of the wild type level. Notably, the three mutations D(A61)A, E(A65)A and E(D312)A perturb the properties of the Mn_4Ca-cluster far more than many mutations of the putative ligands discussed in subsection 5.5. In all three mutants, the efficiency of the $S_2 \rightarrow S_3$ transition was found to be lower than in the wild type, and the effciency of the $S_3 \rightarrow S_0$ transition was even more substantially lowered (450). Since according to the likely intrinsic proton release pattern discussed above, the $S_1 \rightarrow S_2$ transition requires no proton abstraction, whereas the $S_2 \rightarrow S_3$ and $S_3 \rightarrow S_0$ transitions do (cf. Figure 4C), this finding is consistent with a role of the three residues in proton egress.

10. WATER BINDING, WATER CONSUMPTION, AND OXYGEN RELEASE

10.1. Water binding sites

The binding of substrate water to the WOC has been reviewed recently (451), so that we give only a brief overwiew here, focussing on two points: spectroscopic analysis and mass spectrometry. One spectroscopic approach to water in PSIIcc is vibrational spectroscopy, in particular FTIR (265, 452), and will be discussed in subsection 10.2. The second important group of spectroscopic experiments is based on magnetic resonance. Earlier NMR experiments demonstrated an S-state dependence of proton spin relaxation rates ascribed to different oxidation states of bound manganese, but it was not possible to distinguish water protons from other exchangeable protons (453). The S_2-state multiline EPR signal (see subsection 4.3) exhibits line broadening upon incubation of PSIIcc with $H_2{}^{17}O$ due to hyperfine coupling with the $I = {}^5/_2$ nucleus ^{17}O, indicating binding of water to the catalytic center in the S_0, S_1 or S_2 state with oxygen coordinating Mn (454). The ^{17}O-Mn interaction was later confirmed by ESEEM (455) and a pulse EPR technique known as hyperfine sublevel correlation (HYSCORE) spectroscopy (456).

ESEEM was also used to study manganese-deuterium hfc and the ability of d_3-labeled methanol to displace D_2O (457). Four classes of exchangeable deuterons were identified in S_2 and S_0. The two classes with the strongest hfc were interpreted as one water molecule that is closely bound to a Mn and is not displaced by methanol. The other two classes represent water molecules that are not closely bound to Mn (Mn-D distance ~3.7–4.7 Å) and protein matrix protons (Mn-D distance ~4 Å), where the latter are variably exchanged in different preparations. The effect of H/D-exchange on Mn-H hfc was studied with ENDOR and evidence was presented for different proton exchange rates in different S-states ascribed to a variation of water binding affinities with the oxidation state of the Mn_4Ca-cluster (458).

A more direct approach to ligand exchange at the Mn_4Ca-cluster applies mass spectrometry (451). In this type of experiment, the incorporation of ^{18}O from

isotopically labeled water into the product O_2 of water oxidation is monitored by detecting the various formed O_2 species using a mass spectrometer. Crucial to the success of this method was the development of a rapid mixing system by Wydrzynski, Messinger and co-workers, setting the limit for detectable exchange rates to 175 s^{-1} (459, 460). In this way, it could be demonstrated that there is a slow ($t_{½} \approx$ 500 ms at 10 °C) and a fast ($t_{½}$ < 25 ms at 10 °C) exchanging substrate water in the S_3 state. Note that this result implies that ^{18}O-labeled water injected after poising the WOC in the S_3-state can still exchange oxygen isotopes with the substrate water that finally gives rise to the produced dioxygen. The two different rates indicate that there are two inequivalent sites concerning this exchange process. Later work uncovered the complete S-state dependence of the exchange rates (461). The two sites are inequivalent throughout the whole catalytic cycle. The rapidly exchanging substrate water is progressively more tightly bound in S_1, S_2, and S_3, but can be kinetically resolved only in the S_2 and S_3 states. On the other hand, the slowly exchanging substrate water is tightly bound in S_1, less so in S_2 and S_3, and most loosely bound in S_0 (451). Also, the two substrate water molecules do not exhibit interconversion between their sites. A comparison with exchange rates in di-μ-oxo dimanganese complexes suggests that these two binding sites do not correspond to the position of a μ-oxo bridge between two manganese ions at least in S_0, S_2 and S_3 (462, 463). However, the data are consistent with the slowly exchanging substrate being a bridge in S_1. Another hint to the slow-binding site is the effect of chemical Ca^{2+}/Sr^{2+} exchange, which consistently increases the exchange rate in S_1, S_2, and S_3 (464). A possible explanation is that this slow-exchange site corresponds to a terminal or bridging ligand to Ca^{2+}.

Recently, the ^{18}O exchange rates have been measured in two site-directed mutants (465). Upon replacement of Asp A170, one of the likely ligands to Mn4 (see subsection 5.5), with His, the exchange rates in S_3 are only marginally affected. This was interpreted as indication that Mn4 does not bind substrate water, but binding of non-substrate water to this Mn ion was not excluded. Replacement of Asp A61 with Asn, known to suppress S-state advancement beyond S_2 (see section 9), causes a decrease of both exchange rates in S_3. This result suggests an interaction of Asp A61 with both substrate water molecules, probably via a hydrogen bonding network.

10.2. Water insertion and consumption

FTIR spectroscopy is a suitable tool to investigate water reactions (265, 452). Water molecules in biological systems can always be expected to be engaged in hydrogen bonding to a certain extent. These hydrogen bonds affect the stretching vibrations of the OH groups. The vibrations of weakly hydrogen bonded groups occur in the range 3700 – 3500 cm^{-1} and are thus well separated from other vibrations (466). However, strongly hydrogen bonded OH groups vibrate at lower frequencies (3500 – 3000 cm^{-1}) and are thus superimposed to NH stretching vibrations of the peptide backbone (467), which makes the analysis more difficult. Analysis of $S_{i+1} - S_i$ difference FTIR spectra in the region of weakly hydrogen bonded OH stretching modes revealed significant differences between the transitions (468). In the $S_1 \rightarrow S_2$ transition one observes a shift of a frequency from 3588 to 3617 cm^{-1}, which is assigned to a water molecule with an asymmetry in hydrogen bonding that becomes more pronounced upon formation of the S_2 state. In contrast, the $S_i \rightarrow S_{i+1}$ transitions for i = 0, 2 as well as the $S_3 \rightarrow S_0$ transition exhibit a clear decrease in OH oscillator absorption intensity, which is twice as large in the latter as in the two former transitions. The negative signal can be interpreted in any of the following two ways: (i) A weak hydrogen bond of water or hydroxid turns into a strong one or (ii) a proton is released from a weakly hydrogen bonded OH group. The intensities suggest that two weakly hydrogen bonded OH groups undergo a reaction in the $S_3 \rightarrow S_0$ transition, whereas only one weakly hydrogen bonded OH group reacts in any of the transitions $S_0 \rightarrow S_1$ and $S_2 \rightarrow S_3$. If we interpret the changes in the vibrational spectra as deprotonation, they are in nice agreement with the intrinsic proton release pattern of 1 : 0 : 1 : 2 discussed in section 9 (see Figure 4C for m = 0). Thus, it seems that FTIR monitors the deprotonation of substrate water. Note that this interpretation implies that a hydroxid ion is bound to the Mn_4Ca-cluster in S_1 and S_2. The possible lack of a Mn-centered oxidation in the $S_2 \rightarrow S_3$ transition could be related to the oxidation of a water or hydroxid ligand accompanied by deprotonation of this ligand.

One way to analyse water insertion is to probe the need of the individual S-state transitions for water. This has been done in an FTIR study by variation of the hydration extent of a *T. elongatus* PSIIcc film sample through a change of the relative humidity in a sealed infrared cell (469). In the range of 73 – 99% relative humidity, the efficiencies of the $S_2 \rightarrow S_3$ and $S_3 \rightarrow S_0$ transitions were found to decrease faster than those of the $S_1 \rightarrow S_2$ and $S_0 \rightarrow S_1$ transitions upon lowering the water content, which was interpreted as indication of water insertion into the WOC in the former two transitions (452). At lower relative humidities, all S-state transitions are severely impaired, demonstrating that one has to be careful with procedures involving dehydration of samples. The interpretation of the effects of humidity suggests that one substrate water molecule is already inserted into the WOC early in the catalytic cycle, that is, prior to the formation of the S_0 state (and presumably after O_2 release from the preceding cycle). This is in line with the interpretation of the proton release during the $S_0 \rightarrow S_1$ transition as reflecting deprotonation of substrate water. However, there is a problem with the second water molecule: The humidity data seem to imply that it is inserted during the $S_2 \rightarrow S_3$ transition. This is in conflict with the detection of two inequivalent ^{18}O exchange rates in the S_2 state (see subsection 10.1), suggesting that the second water molecule is already bound at this stage (470).

Another indicator of water reactions could be the HOH bending mode appearing around 1640 cm^{-1}. However, the absorption of this mode shows only weak intensity relative to the OH stretching vibration (471) and is overlapping with peptide backbone vibrations. In D_2O, the

DOD bending mode is shifted to ~1200 cm^{-1}, where the protein does not absorb strongly. Therefore, D_2O bound to the WOC was investigated with FTIR in the bending region (1100 – 1300 cm^{-1}) as well as in the region of the OD stretch (2530 – 2730 cm^{-1}) (472). All amenable difference spectra exhibited six to eigth peaks in the bending region, indicating that at least two fully deuterated D_2O molecules are coupled to each S-state transition. Besides peak shifts, some signals represented loss of absorption intensity in agreement with water consumption. A negative peak at ~1240 cm^{-1} was used to identify the $S_2 \rightarrow S_3$, $S_3 \rightarrow S_0$, and $S_0 \rightarrow S_1$ transitions as possible substrate insertion steps. Analysis of the OD stretching region showed the presence of a negative peak at 2694 cm^{-1} mainly due to the $S_2 \rightarrow S_3$ and $S_3 \rightarrow S_0$ transitions in agreement with the idea that these are substrate insertion steps. Altogether, these data suggest that there are always more than two water molecules bound to the WOC, and that some substrate water may be inserted in one cycle, but is not consumed until the next cycle. This would also help to reconcile the FTIR data with the ^{18}O exchange experiments.

10.3. Dioxygen formation and release

As stated by McEvoy and Brudvig (23), there are so many proposals for the mechanism of water oxidation that it is impossible to examine or even mention them all. For completeness, we give here a brief summary of aspects concerning the question of how dioxygen is actually formed. The hypothetical mechanisms can be grouped roughly into "radical mechanisms", "coupling of oxo-ligands", "nucleophilic attack", and "S_3 state peroxide".

The possibility that the $S_2 \rightarrow S_3$ transition does not involve oxidation of Mn triggered mechanistic proposals, in which the oxidation is oxygen-centered and the formed oxyl radical attacks a second oxygen species in the S_4 state (473-475). The radical could actually be a μ-oxo bridge linking Mn and Ca^{2+} ions, which would explain the more pronounced changes in metal distances upon S_3 formation as observed with EXAFS (253).

"Coupling of oxo-ligands" here refers to studies of Mn_4O_4 cubane structures (476-478) advocating a model, in which two oxo-vertices of the cubane are covalently linked by an intermolecular pathway, and the release of the two bridges as O_2 effectuates an opening of the cubane to a "butterfly" structure. Since the opening implies a relaxation of strain in the structure, this is also referred to as the "Jack-in-the-Box" hypothesis of dioxygen formation (23). Although the original mechanism is unlikely to describe biological water oxidation, the "Jack-in-the-Box" aspect is intriguing. If at least one of the substrate water molecules ultimately forms a μ-oxo bridge as discussed above, and provided the remaining metal ligands (i.e., the other μ-oxo bridges and the amino acid side chains) impose a strain on the metal cluster, the stepwise oxidation/deprotonation of the cluster could weaken this bridge, until it is finally too weak to resist the strain, and the cluster is opened under ejection of O_2. Relaxation of strain could be an important aspect of dioxygen release, making a back reaction unfavorable.

Based on their ^{18}O exchange data (see subsection 10.1), Wydrzynski and coworkers (461) proposed that both substrate water molecules are terminal ligands to manganese and are bound in the form of hydroxide ligands to Mn^{III} in the S_3 state. After a further oxidation/deprotonation event in the $S_3 \rightarrow S_4$ transition, one of the hydroxides turns into a terminal oxo-ligand that by virtue of its intercation with Mn^{IV} is electron-depleted and thus allows for a "nucleophilic attack" by the second, neighboring hydroxide to form an O-O bond. In variants of this mechanism, the attacking hydroxide is bound to Ca^{2+} (479), or a Ca^{2+}-bound water molecule or hydroxide ion attacks an oxo-ligand to a Mn^{V} (480, 481). However, at present, it seems rather unlikely that there is a Mn^{V} in the WOC.

A common feature of these mechanisms is that O-O bond formation is associated with the kinetically elusive S_4 state. In contrast, there are also mechanistic proposals, in which this linkage is already established in the S_3 state in the form of a bound peroxide, i.e., O-O bond formation precedes the final deprotonation steps. We refer the reader to the review by Renger (380) for an in-depth discussion of these variants.

Since the formulation of the S-state model by Kok and co-workers (99, 100), there has been a quest for the S_4 state, which remained clouded in secrecy. Formally, such a state has to exist, as four oxidation equivalents are needed to produce O_2 from H_2O, but apparently, this state is not stable. One has to distinguish carefully between the states $S_3Y_Z^{\bullet}$, in which Y_Z is oxidized, and S_4Y_Z, in which ET from the WOC to Y_Z has taken place. In the following, we concentrate on experiments that aimed at the identification of a reaction intermediate between $S_3Y_Z^{\bullet}$ and S_0Y_Z that could be S_4Y_Z.

The temperature dependence of S-state advancement was investigated by following the kinetics with UV spectroscopy. In contrast to the $S_1 \rightarrow S_2$ and $S_2 \rightarrow S_3$ transitions, the $S_3 \rightarrow S_0$ transition showed a pronounced break in the Arrhenius plot for PSIIcc from *T. vulcanus* (482). Similar results were obtained with different preparations from spinach (483, 484), but no break could be detected in other studies employing pea (388) and *Synechocystis* sp. (485). Therefore, the general significance of the non-Arrhenius behavior remains unclear. As a possible explanation, it has been proposed that the break point represents the presence of different redox isomers of the S_3 state (482-484) rather than a redox intermediate and that it is species dependent (109).

A metastable intermediate (S_4Y_Z) that has different spectroscopic properties than the final state (S_0Y_Z) should eventually be detectable as a lag phase in the time course of a spectroscopic signal. Rappaport *et al.* (486) investigated absorption transients at 295 nm to monitor ET to $Y_Z^{\bullet}$ and at 424 – 440 nm interpreted as probing ET and proton release. They found a simple monophasic kinetics for $S_1Y_Z^{\bullet} \rightarrow S_2Y_Z$ and $S_2Y_Z^{\bullet} \rightarrow S_3Y_Z$, but more

complicated biphasic transients for $S_3Y_Z^{\bullet} \rightarrow S_0Y_Z$ and $S_0Y_Z^{\bullet} \rightarrow S_1Y_Z$. We note that a similarly complex kinetics indicating a lag phase in $S_3Y_Z^{\bullet} \rightarrow S_0Y_Z$ had been observed earlier (482, 487, 488). Rappaport *et al.* (486) interpreted the lag phase (30 µs) as a proton release (or OH^- binding) step preceding the actual ET, so that it is circumstantial evidence for a reaction intermediate, but not necessarily for a redox intermediate. Razeghifard and Pace (489) measured the dioxygen release kinetics by using time-resolved EPR oximetry. In this technique, the paramagnetic O_2 is detected by virtue of its effect on the EPR spectra of stable radicals (e.g., deuterated tempone). The O_2 release kinetics was directly compared with the EPR-detected reduction of $Y_Z^{\bullet}$. The data were interpreted in terms of a sequential reaction scheme $S_3Y_Z^{\bullet} \rightarrow$ intermediate $\rightarrow S_0Y_Z$, where the intermediate could be either S_4Y_Z or the modified S_3 state as proposed by Rappaport *et al.* (486). Razeghifard and Pace (489) came to the conclusion that the most likely explanation for the delayed O_2 release (50 – 200 µs) is the modification (e.g., deprotonation) of S_3, implying again that S_4 remained kinetically elusive.

Another way to detect O_2 is polarography. Clausen *et al.* (485) detected a lag phase (450 µs) in the polarographic transient that was, however, not detectable in the UV kinetics. They concluded that the lag phase was not indicative of S_4, but rather due to O_2 transiently bound to the protein. Haumann *et al.* (110) used time-resolved XAS to monitor shifts of the Mn K-edge during the S state transitions. For $S_i \rightarrow S_{i+1}$ with i = 0, 1, 2, an absorption decrease is observed in agreement with oxidation of the Mn_4Ca cluster by $Y_Z^{\bullet}$. In the $S_3 \rightarrow S_0$ transition, the absorption increases as expected for Mn reduction to S_0, but with a lag phase of about 250 µs. Since the reduction of $Y_Z^{\bullet}$ in this step is slower, it was concluded that the Mn_4Ca-cluster does not change its redox state during the lag phase. As an explanation, earlier proposals of a preceding proton release were taken up. The deprotonated S_3 state was originally termed "S_4", which is somewhat misleading as discussed in subsection 4.1. In fact, the XAS transient after the third flash is essentially biphasic and besides the lag phase shows no sign of any redox intermediate that could be assigned to S_4.

If the final step of dioxygen production is reversible, an increase of the O_2 pressure should shift the equilibrium towards educts and intermediate. This idea was exploited by Clausen and Junge (312, 490), who analyzed UV transients and reported evidence for the O_2-induced stabilization of an intermediate B. Their data yielded a free energy change for the final, O_2-releasing step of ΔG_{BC} = – 8.6 kJ mol^{-1}. It should be noted that the nature of B was not strictly specified and that there is no evidence for an additional oxidation step of the Mn_4Ca cluster. Instead, the data were analysed by assuming B = $S_2Y_ZH_2O_2$, where H_2O_2 is a hypothetical peroxide intermediate. These data were later supported by delayed fluorescence measurements, where B was called S_2^* (313). The results were debated in the literature (314-316). As pointed out by Penner-Hahn and Yocum (315), the interpretation $B = S_2^*$ is difficult to reconcile with the data of Haumann *et al.* (110), as there is no evidence for a redox intermediate, neither with oxidized nor reduced Mn. Of course, there could be more intermediates, and any of these could have too short a life time to be detected. This debate triggered a study of the O_2-pressure effect with time-resolved XAS (318). It was concluded that elevated O_2 pressure rather causes an artificial Mn oxidation (e.g., by ROS) than a thermodynamic product inhibition. This result calls into question the formerly estimated ΔG_{BC}. A recent study on whole cells, leaves and thylakoid membranes also questions the reversibility of the last, O_2-forming step that would allow for product inhibition (317). We conclude, that there is presently no evidence for an S_4 state in terms of a resolvable redox intermediate, and it is still unknown, how O_2 is actually formed in photosynthetic water oxidation.

11. CONCLUSION AND PERSPECTIVES

PSIIcc is a complex molecular machinery. This complexity is intriguing, but also quite demanding. In the present review, we have made an attempt to collect experimental facts that along with insight from theoretical computations may help to uncover the operating principles of Nature´s water oxidation device on the basis of recent crystallographic information. Clearly, the growth of our knowledge about PSIIcc before and after the advent of crystal structures is enormous, but there are still too many white spots on the map. The ultimate goal is to further improve the quality of the crystal structure, which might be attained soon (491). However, this structure will not mark the end of the struggle for understanding, but rather open a new stage. The focus will then likely shift to obtain direct structural information about different functional states of PSIIcc, viz. the S-states. As X-rays will always cause some damage (at least Mn-reduction), X-ray crystallography will have ultimate limits in this respect, but nonetheless important insight may be gained, not the least concerning the surrounding of the WOC (e.g., the chloride cofactors). Spectroscopic methods such as FTIR, EXAFS or EPR/ENDOR will remain important. A challenge for future research will be to improve crystals and/or technical facilities to allow for the study of PSIIcc by using neutron diffraction. This non-invasive technique could bring us the desired mechanistic details of efficient light-induced water oxidation and the necessary inspiration for the design of commercially useful catalysts. In any case, PSIIcc will keep us busy.

12. ACKNOWLEDGEMENTS

We thank A. Gabdulkhakov for providing figure material and G. Renger for critial reading of the manuscript. This work benefitted from financial support by the Deutsche Forschungsgemeinschaft through Sfb 429 (to F. M.) and Center of Excellence "UniCat" coordinated by the Technische Universität Berlin (to A. Z.).

13. REFERENCES

1. M. Hambourger, G. F. Moore, D. M. Kramer, D. Gust, A. L. Moore and T. A. Moore: Biology and technology for photochemical fuel production. *Chem Soc Rev* 38, 25-35 (2009)

2. G. Renger: Primary Processes of Photosynthesis - Principles and Apparatus. In: *Comprehensive Series in Photochemistry and Photobiology*. Ed D. P. Häder and G. Jori. RSC Publishing, Cambridge (2008)

3. P. Jordan, P. Fromme, H. T. Witt, O. Klukas, W. Saenger and N. Krauss: Three-dimensional structure of cyanobacterial photosystem I at 2.5 Å resolution. *Nature* 411, 909-917 (2001)

4. A. Amunts, O. Drory and N. Nelson: The structure of a plant photosystem I supercomplex at 3.4 Å resolution. *Nature* 447, 58-63 (2007)

5. A. Amunts, H. Toporik, A. Borovikova and N. Nelson: Structure Determination and Improved Model of Plant Photosystem I. *J Biol Chem* 285, 3478-3486 (2010)

6. G. Kurisu, H. Zhang, J. L. Smith and W. A. Cramer: Structure of the cytochrome b_6f complex of oxygenic photosynthesis: tuning the cavity. *Science* 302, 1009-1014 (2003)

7. D. Stroebel, Y. Choquet, J. L. Popot and D. Picot: An atypical haem in the cytochrome b_6f complex. *Nature* 426, 413-418 (2003)

8. Z. Liu, H. Yan, K. Wang, T. Kuang, J. Zhang, L. Gui, X. An and W. Chang: Crystal structure of spinach major light-harvesting complex at 2.72 Å resolution. *Nature* 428, 287-292 (2004)

9. J. Standfuss, A. C. Terwisscha van Scheltinga, M. Lamborghini and W. Kühlbrandt: Mechanisms of photoprotection and nonphotochemical quenching in pea light-harvesting complex at 2.5 Å resolution. *EMBO J* 24, 919-928 (2005)

10. A. Zouni, H. T. Witt, J. Kern, P. Fromme, N. Krauss, W. Saenger and P. Orth: Crystal structure of photosystem II from *Synechococcus elongatus* at 3.8 Å resolution. *Nature* 409, 739-743 (2001)

11. N. Kamiya and J. R. Shen: Crystal structure of oxygen-evolving photosystem II from *Thermosynechococcus vulcanus* at 3.7-Å resolution. *Proc Natl Acad Sci U S A* 100, 98-103 (2003)

12. K. N. Ferreira, T. M. Iverson, K. Maghlaoui, J. Barber and S. Iwata: Architecture of the photosynthetic oxygen-evolving center. *Science* 303, 1831-1838 (2004)

13. J. Biesiadka, B. Loll, J. Kern, K. D. Irrgang and A. Zouni: Crystal structure of cyanobacterial photosystem II at 3.2 Å resolution: a closer look at the Mn-cluster. *Phys Chem Chem Phys* 6, 4733-4736 (2004)

14. B. Loll, J. Kern, W. Saenger, A. Zouni and J. Biesiadka: Towards complete cofactor arrangement in the 3.0 Å resolution structure of photosystem II. *Nature* 438, 1040-1044 (2005)

15. A. Guskov, J. Kern, A. Gabdulkhakov, M. Broser, A. Zouni and W. Saenger: Cyanobacterial photosystem II at 2.9 Å resolution: role of quinones, lipids, channels and chloride. *Nat Struct Mol Biol* 16, 334 - 342 (2009)

16. D. M. Rees, A. G. W. Leslie and J. E. Walker: The structure of the membrane extrinsic region of bovine ATP synthase. *Proc Natl Acad Sci U S A* 106, 21597-21601 (2009)

17. D. Pogoryelov, O. Yildiz, J. D. Faraldo-Gomez and T. Meier: High-resolution structure of the rotor ring of a proton-dependent ATP synthase. *Nat Struct Mol Biol* 16, 1068-1073 (2009)

18. A. Guskov, A. Gabdulkhakov, M. Broser, C. Glöckner, J. Hellmich, J. Kern, J. Frank, F. Müh, W. Saenger and A. Zouni: Recent Progress in the Crystallographic Studies of Photosystem II. *ChemPhysChem* 11, 1160-1171 (2010)

19. T. Wydrzynski and K. Satoh: Photosystem II: the light-driven water:plastoquinone oxidoreductase. In: *Advances in Photosynthesis and Respiration*. Ed Govindjee. Springer, Dordrecht (2005)

20. J. Kern and G. Renger: Photosystem II: structure and mechanism of the water:plastoquinone oxidoreductase. *Photosynth Res* 94, 183-202 (2007)

21. G. Renger and T. Renger: Photosystem II: The machinery of photosynthetic water splitting. *Photosynth Res* 98, 53-80 (2008)

22. J. Yano, J. Kern, K. Sauer, M. J. Latimer, Y. Pushkar, J. Biesiadka, B. Loll, W. Saenger, J. Messinger, A. Zouni and V. K. Yachandra: Where water is oxidized to dioxygen: structure of the photosynthetic Mn_4Ca cluster. *Science* 314, 821-825 (2006)

23. J. P. McEvoy and G. W. Brudvig: Water-splitting chemistry of photosystem II. *Chem Rev* 106, 4455-4483 (2006)

24. J. Kern, J. Biesiadka, B. Loll, W. Saenger and A. Zouni: Structure of the Mn_4-Ca cluster as derived from X-ray diffraction. *Photosynth Res* 92, 389-405 (2007)

25. H. Dau and M. Haumann: The manganese complex of photosystem II in its reaction cycle – Basic framework and possible realization at the atomic level. *Coord Chem Rev* 252, 273-295 (2008)

26. J. Barber and J. W. Murray: Revealing the structure of the Mn-cluster of photosystem II by X-ray crystallography. *Coord Chem Rev* 252, 233-243 (2008)

27. A. Zouni: From Cell Growth to the 3.0 Å Resolution Crystal Structure of Cyanobacterial Photosystem II. In:

Primary Processes of Photosynthesis, Principles and Apparatus. Ed G. Renger. RSC Publishing, Cambridge, 2, 193 - 236 (2008)

28. M. Broser, A. Gabdulkhakov, J. Kern, A. Guskov, F. Müh, W. Saenger and A. Zouni: Crystal Structure of Monomeric Photosystem II from *Thermosynechococcus elongatus* at 3.6-Å Resolution. *J Biol Chem* 285, 26255-26262 (2010)

29. J. J. Eaton-Rye and C. Putnam-Evans: The CP47 and CP43 Core Antenna Components. In: *Photosystem II: The Light-Driven Water:Plastoquinone Oxidoreductase*. Ed T. Wydrzynski and K. Satoh. Springer, Dordrecht, 45-70 (2005)

30. F. Müh, T. Renger and A. Zouni: Crystal structure of cyanobacterial photosystem II at 3.0 Å resolution: a closer look at the antenna system and the small membrane-intrinsic subunits. *Plant Physiol Biochem* 46, 238-264 (2008)

31. L. X. Shi and W. P. Schröder: The low molecular mass subunits of the photosynthetic supracomplex, photosystem II. *Biochim Biophys Acta* 1608, 75-96 (2004)

32. L. E. Thornton, J. L. Roose, H. B. Pakrasi and M. Ikeuchi: The Low Molecular Weigth Proteins of Photosystem II. In: *Photosystem II: The Light-Driven Water:Plastoquinone Oxidoreductase*. Ed T. Wydrzynski and K. Satoh. Springer, Dordrecht, 121-137 (2005)

33. T. M. Bricker and R. L. Burnap: The Extrinsic Proteins of Photosystem II. In: *Photosystem II: The Light-Driven Water:Plastoquinone Oxidoreductase*. Ed T. Wydrzynski and K. Satoh. Springer, Dordrecht, 95-120 (2005)

34. J. L. Roose, K. M. Wegener and H. B. Pakrasi: The extrinsic proteins of Photosystem II. *Photosynth Res* 92, 369-387 (2007)

35. I. Enami, A. Okumura, R. Nagao, T. Suzuki, M. Iwai and J. R. Shen: Structures and functions of the extrinsic proteins of photosystem II from different species. *Photosynth Res* 98, 349-363 (2008)

36. F. Rappaport and B. A. Diner: Primary photochemistry and energetics leading to the oxidation of the (Mn)4Ca cluster and to the evolution of molecular oxygen in Photosystem II. *Coord Chem Rev* 252, 259-272 (2008)

37. T. Renger and E. Schlodder: Primary Photophysical Processes in Photosystem II: Bridging the Gap between Crystal Structure and Optical Spectra. *ChemPhysChem* 11, 1141-1153 (2010)

38. R. A. Khatypov, A. Y. Khmelnitskiy, M. M. Leonova, L. G. Vasilieva and V. A. Shuvalov: Primary light-energy conversion in tetrameric chlorophyll structure of photosystem II and bacterial reaction centers: I. A review. *Photosynth Res* 98, 81-93 (2008)

39. B. R. Green and W. W. Parson: Light-Harvesting Antennas in Photosynthesis. In: *Advances in Phothosynthesis and Respiration*. Ed Govindjee. Springer (Kluwer Academic Publishers), Dordrecht, The Netherlands (2003)

40. H. van Amerongen and R. Croce: Structure and Function of Photosystem II Light-Harvesting Proteins (Lhcb) of Higher Plants. In: Primary Processes of Photosynthesis, Principles and Apparatus. Ed G. Renger. RSC Publishing, Cambridge, U. K., 1, 329 - 367 (2008)

41. G. Raszewski and T. Renger: Light harvesting in photosystem II core complexes is limited by the transfer to the trap: Can the core complex turn into a photoprotective mode? J Am Chem Soc 130, 4431-4446 (2008)

42. Y. Miloslavina, M. Szczepaniak, M. G. Müller, J. Sander, M. Nowaczyk, M. Rögner and A. R. Holzwarth: Charge separation kinetics in intact photosystem II core particles is trap-limited. A picosecond fluorescence study. Biochemistry 45, 2436-2442 (2006)

43. G. Tumino, A. P. Casazza, E. Engelmann, F. M. Garlaschi, G. Zucchelli and R. C. Jennings: Fluorescence lifetime spectrum of the plant photosystem II core complex: photochemistry does not induce specific reaction center quenching. *Biochemistry* 47, 10449-10457 (2008)

44. E. G. Andrizhiyevskaya, D. Frolov, R. van Grondelle and J. P. Dekker: On the role of the CP47 core antenna in the energy transfer and trapping dynamics of Photosystem II. *Phys Chem Chem Phys* 6, 4810-4819 (2004)

45. J. Deisenhofer and H. Michel: The Photosynthetic Reaction Center from the Purple Bacterium *Rhodopseudomonas viridis*. *Science* 245, 1463-1473 (1989)

46. M. H. B. Stowell, T. M. McPhillips, D. C. Rees, S. M. Soltis, E. Abresch and G. Feher: Light-induced structural changes in photosynthetic reaction center: Implications for mechanism of electron-proton transfer. *Science* 276, 812-816 (1997)

47. J. Koepke, E. M. Krammer, A. R. Klingen, P. Sebban, G. M. Ullmann and G. Fritzsch: pH modulates the quinone position in the photosynthetic reaction center from *Rhodobacter sphaeroides* in the neutral and charge separated states. *J Mol Biol* 371, 396-409 (2007)

48. C. R. D. Lancaster: Structure of Reaction Centers in Anoxygenic Bacteria. In: *Primary Processes of Photosynthesis, Principles and Apparatus*. Ed G. Renger. RSC Publishing, Cambridge, 2, 5 - 56 (2008)

49. G. Döring, H. H. Stiehl and H. T. Witt: A 2nd Chlorophyll Reaction in Electron Chain of Photosynthesis - Registration by Repetitive Excitation Technique. *Z Naturforsch B* 22, 639-644 (1967)

50. J. Barber and M. D. Archer: P680, the primary electron donor of photosystem II. *J Photochem Photobiol A* 142, 97-106 (2001)

51. G. Raszewski, B. A. Diner, E. Schlodder and T. Renger: Spectroscopic properties of reaction center pigments in photosystem II core complexes: revision of the multimer model. *Biophys J* 95, 105-119 (2008)

52. W. Zinth and J. Wachtveitl: The first picoseconds in bacterial photosynthesis - Ultrafast electron transfer for the efficient conversion of light energy. *ChemPhysChem* 6, 871-880 (2005)

53. F. Müh, F. Lendzian, M. Roy, J. C. Williams, J. P. Allen and W. Lubitz: Pigment-protein interactions in bacterial reaction centers and their influence on oxidation potential and spin density distribution of the primary donor. *J Phys Chem B* 106, 3226-3236 (2002)

54. J. R. Reimers and N. S. Hush: Unified description of the electrochemical, charge distribution, and spectroscopic properties of the special-pair radical cation in bacterial photosynthesis. *J Am Chem Soc* 126, 4132-4144 (2004)

55. A. Warshel and W. W. Parson: Spectroscopic Properties of Photosynthetic Reaction Centers .1. Theory. *J Am Chem Soc* 109, 6143-6152 (1987)

56. M. E. Madjet, F. Müh and T. Renger: Deciphering the influence of short-range electronic couplings on optical properties of molecular dimers: application to "special pairs" in photosynthesis. *J Phys Chem B* 113, 12603-12614 (2009)

57. F. Müh, M. E. Madjet, J. Adolphs, A. Abdurahman, B. Rabenstein, H. Ishikita, E. W. Knapp and T. Renger: α-Helices direct excitation energy flow in the Fenna-Matthews-Olson protein. *Proc Natl Acad Sci U S A* 104, 16862-16867 (2007)

58. J. Adolphs, F. Müh, M. E. A. Madjet, M. Schmidt am Busch and T. Renger: Structure-Based Calculations of Optical Spectra of Photosystem I Suggest an Asymmetric Light-Harvesting Process. *J Am Chem Soc* 132, 3331-3343 (2010)

59. J. Bernarding, H. J. Eckert, H. J. Eichler, A. Napiwotzki and G. Renger: Kinetic Studies on the Stabilization of the Primary Radical Pair $P680^+$ $Pheo^-$ in Different Photosystem II Preparations from Higher Plants. *Photochem Photobiol* 59, 566-573 (1994)

60. M. E. van Brederode, M. R. Jones, F. van Mourik, I. H. M. van Stokkum and R. van Grondelle: A new pathway for transmembrane electron transfer in photosynthetic reaction centers of *Rhodobacter sphaeroides* not involving the excited special pair. *Biochemistry* 36, 6855-6861 (1997)

61. M. Brecht, V. Radics, J. B. Nieder and R. Bittl: Protein dynamics-induced variation of excitation energy transfer pathways. *Proc Natl Acad Sci U S A* 106, 11857-11861 (2009)

62. M. Brecht: Spectroscopic characterization of photosystem I at the single-molecule level. *Mol Phys* 107, 1955-1974 (2009)

63. V. I. Novoderezhkin, J. P. Dekker and R. van Grondelle: Mixing of exciton and charge-transfer states in Photosystem II reaction centers: Modeling of stark spectra with modified Redfield theory. *Biophys J* 93, 1293-1311 (2007)

64. E. Romero, I. H. M. van Stokkum, V. I. Novoderezhkin, J. P. Dekker and R. van Grondelle: Two Different Charge Separation Pathways in Photosystem II. *Biochemistry* 49, 4300-4307 (2010)

65. J. Myers and J. R. Graham: Enhancement in *Chlorella*. *Plant Physiol* 38, 105-116 (1963)

66. N. L. Greenbaum and D. Mauzerall: Effect of Irradiance Level on Distribution of Chlorophylls between PS II and PS I as Determined from Optical Cross-Sections. *Biochim Biophys Acta* 1057, 195-207 (1991)

67. H. Pettai, V. Oja, A. Freiberg and A. Laisk: The long-wavelength limit of plant photosynthesis. *FEBS Lett* 579, 4017-4019 (2005)

68. H. Pettai, V. Oja, A. Freiberg and A. Laisk: Photosynthetic activity of far-red light in green plants. *Biochim Biophys Acta* 1708, 311-321 (2005)

69. E. Krausz, J. L. Hughes, P. Smith, R. Pace and S. P. Arskold: Oxygen-evolving Photosystem II core complexes: a new paradigm based on the spectral identification of the charge-separating state, the primary acceptor and assignment of low-temperature fluorescence. *Photochem Photobiol Sci* 4, 744-753 (2005)

70. J. L. Hughes, P. Smith, R. Pace and E. Krausz: Charge separation in photosystem II core complexes induced by 690-730 nm excitation at 1.7 K. *Biochim Biophys Acta* 1757, 841-851 (2006)

71. A. Thapper, F. Mamedov, F. Mokvist, L. Hammarström and S. Styring: Defining the Far-Red Limit of Photosystem II in Spinach. *Plant Cell* 21, 2391-2401 (2009)

72. E. Schlodder, V. V. Shubin, E. El-Mohsnawy, M. Roegner and N. V. Karapetyan: Steady-state and transient polarized absorption spectroscopy of photosytem complexes from the cyanobacteria *Arthrospira platensis* and *Thermosynechococcus elongatus*. *Biochim Biophys Acta* 1767, 732-741 (2007)

73. F. Müh, J. Rautter and W. Lubitz: Two distinct conformations of the primary electron donor in reaction centers from *Rhodobacter sphaeroides* revealed by ENDOR/TRIPLE-spectroscopy. *Biochemistry* 36, 4155-4162 (1997)

74. R. N. Frese, M. Germano, F. L. de Weerd, I. H. M. van Stokkum, A. Y. Shkuropatov, V. A. Shuvalov, H. J. van Gorkom, R. van Grondelle and J. P. Dekker: Electric field effects on the chlorophylls, pheophytins, and β-carotenes in the reaction center of photosystem II. *Biochemistry* 42, 9205-9213 (2003)

75. M. Y. Okamura, M. L. Paddock, M. S. Graige and G. Feher: Proton and electron transfer in bacterial reaction centers. *Biochim Biophys Acta* 1458, 148-163 (2000)

76. M. L. Paddock, G. Feher and M. Y. Okamura: Proton transfer pathways and mechanism in bacterial reaction centers. *FEBS Lett* 555, 45-50 (2003)

77. E. Nabedryk and J. Breton: Coupling of electron transfer to proton uptake at the Q_B site of the bacterial reaction center: A perspective from FTIR difference spectroscopy. *Biochim Biophys Acta* 1777, 1229-1248 (2008)

78. S. Hermes, J. M. Stachnik, D. Onidas, A. Remy, E. Hofmann and K. Gerwert: Proton uptake in the reaction center mutant L210DN from *Rhodobacter sphaeroides* via protonated water molecules. *Biochemistry* 45, 13741-13749 (2006)

79. H. Cheap, S. Bernad, V. Derrien, L. Gerencsér, J. Tandori, P. de Oliveira, D. K. Hanson, P. Maróti and P. Sebban: M234Glu is a component of the proton sponge in the reaction center from photosynthetic bacteria. *Biochim Biophys Acta* 1787, 1505-1515 (2009)

80. T. Iwata, M. L. Paddock, M. Y. Okamura and H. Kandori: Identification of FTIR Bands Due to Internal Water Molecules around the Quinone Binding Sites in the Reaction Center from *Rhodobacter sphaeroides*. *Biochemistry* 48, 1220-1229 (2009)

81. M. L. Paddock, M. Flores, R. Isaacson, C. Chang, E. C. Abresch and M. Y. Okamura: ENDOR spectroscopy reveals light induced movement of the H-bond from Ser-L223 upon forming the semiquinone (Q_B^-*) in reaction centers from *Rhodobacter sphaeroides*. *Biochemistry* 46, 8234-8243 (2007)

82. H. Ishikita and E. W. Knapp: Variation of Ser-L223 hydrogen bonding with the Q_B redox state in reaction centers from *Rhodobacter sphaeroides*. *J Am Chem Soc* 126, 8059-8064 (2004)

83. H. Ishikita and E. W. Knapp: Control of quinone redox potentials in photosystem II: Electron transfer and photoprotection. *J Am Chem Soc* 127, 14714-14720 (2005)

84. A. Remy and K. Gerwert: Coupling of light-induced electron transfer to proton uptake in photosynthesis. *Nat Struct Biol* 10, 637-644 (2003)

85. S. Hermes, O. Bremm, F. Garczarek, V. Derrien, P. Liebisch, P. Loja, P. Sebban, K. Gerwert and M. Haumann: A time-resolved iron-specific X-ray absorption experiment yields no evidence for an $Fe^{2+} \rightarrow Fe^{3+}$ transition during $Q_A^- \rightarrow Q_B$ electron transfer in the photosynthetic reaction center. *Biochemistry* 45, 353-359 (2006)

86. J. Breton: Steady-state FTIR spectra of the photoreduction of Q_A and Q_B in *Rhodobacter sphaeroides* reaction centers provide evidence against the presence of a proposed transient electron acceptor X between the two quinones. *Biochemistry* 46, 4459-4465 (2007)

87. H. Ishikita, A. Galstyan and E. W. Knapp: Redox potential of the non-heme iron complex in bacterial photosynthetic reaction center. *Biochim Biophys Acta* 1767, 1300-1309 (2007)

88. V. Petrouleas and B. A. Diner: Identification of Q400, a High-Potential Electron-Acceptor of Photosystem II, with the Iron of the Quinone-Iron Acceptor Complex. *Biochim Biophys Acta* 849, 264-275 (1986)

89. R. Hienerwadel and C. Berthomieu: Bicarbonate binding to the non-heme iron of photosystem II investigated by Fourier transform infrared difference spectroscopy and 13C-labeled bicarbonate. Biochemistry 34, 16288-16297 (1995)

90. Govindjee and J. J. S. van Rensen: Photosystem II Reaction Center and Bicarbonate. In: The Photosynthetic Reaction Center Ed J. Deisenhofer and J. R. Norris. Academic Press, Orlando, 1, 357 - 389 (1993)

91. J. J. S. van Rensen, C. H. Xu and Govindjee: Role of bicarbonate in photosystem II, the water-plastoquinone oxido-reductase of plant photosynthesis. Physiol Plant 105, 585-592 (1999)

92. N. Cox, L. Jin, A. Jaszewski, P. J. Smith, E. Krausz, A. W. Rutherford and R. Pace: The semiquinone-iron complex of photosystem II: structural insights from ESR and theoretical simulation; evidence that the native ligand to the non-heme iron is carbonate. Biophys J 97, 2024-2033 (2009)

93. C. Berthomieu and R. Hienerwadel: Iron coordination in photosystem II: interaction between bicarbonate and the QB pocket studied by Fourier transform infrared spectroscopy. Biochemistry 40, 4044-4052 (2001)

94. K. Takizawa, J. A. Cruz, A. Kanazawa and D. M. Kramer: The thylakoid proton motive force in vivo. Quantitative, non-invasive probes, energetics, and regulatory consequences of light-induced pmf. Biochim. Biophys. Acta 1767, 1233-44 (2007)

95. A. N. Tikhonov, R. V. Agafonov, I. A. Grigor'ev, I. A. Kirilyuk, V. V. Ptushenko and B. V. Trubitsin: Spin-probes designed for measuring the intrathylakoid pH in chloroplasts. Biochim. Biophys. Acta 1777, 285-94 (2008)

96. T. Watanabe and M. Kobayashi: Electrochemistry of chlorophylls. In: Chlorophylls. Ed H. Scheer. CRC Press, Boca Raton, 287 - 315 (1991)

97. H. Ishikita, W. Saenger, J. Biesiadka, B. Loll and E. W. Knapp: How photosynthetic reaction centers control oxidation power in chlorophyll pairs P680, P700, and P870. *Proc Natl Acad Sci U S A* 103, 9855-9860 (2006)

98. P. Joliot, G. Barbieri and R. Chabaud: A New Model of Photochemical Centers in System II. *Photochem Photobiol* 10, 309-329 (1969)

99. B. Kok, B. Forbush and M. McGloin: Cooperation of charges in photosynthetic O_2 evolution – I. A linear four step mechanism. *Photochem Photobiol* 11, 457-475 (1970)

100. B. Forbush, B. Kok and M. P. McGloin: Cooperation of Charges in Photosynthetic O_2 Evolution – II. Damping of Flash Yield Oscillation, Deactivation. *Photochem Photobiol* 14, 307-321 (1971)

101. J. Messinger, U. Wacker and G. Renger: Unusual low reactivity of the water oxidase in redox state S_3 toward exogenous reductants. Analysis of the NH_2OH- and NH_2NH_2-induced modifications of flash-induced oxygen evolution in isolated spinach thylakoids. *Biochemistry* 30, 7852-7862 (1991)

102. G. Renger: Molecular mechanism of water oxidation. In: *Concepts in photobiology: photosynthesis and photomorphogenesis*. Ed G. S. Singhal, G. Renger, Govindjee, K. D. Irrgang and S. K. Sopory. Kluwer Academic Publisher (now Springer) and Narosa Publishing, Dordrecht, Delhi, 292-329 (1999)

103. B. A. Barry and G. T. Babcock: Tyrosine radicals are involved in the photosynthetic oxygen-evolving system. *Proc Natl Acad Sci U S A* 84, 7099-7103 (1987)

104. V. P. Shinkarev: Flash-induced oxygen evolution in photosynthesis: simple solution for the extended S-state model that includes misses, double-hits, inactivation, and backward-transitions. *Biophys. J* 88, 412-421 (2005)

105. P. Joliot, A. Joliot, B. Bouges and G. Barbieri: Studies of System II Photocenters by Comparative Measurements of Luminescence, Fluorescence, and Oxygen Emission. *Photochem Photobiol* 14, 287-305 (1971)

106. B. Bouges-Bocquet: Limiting Steps in Photosystem II and Water Decomposition in *Chlorella* and Spinach Chloroplasts. *Biochim Biophys Acta* 292, 772-785 (1973)

107. B. R. Velthuys and J. W. M. Visser: The Reactivation of EPR Signal II in Chloroplasts Treated with Reduced Dichlorophenol-Indophenol: Evidence against a Dark Equilibrium between Two Oxidation-States of the Oxygen Evolving System. *FEBS Lett* 55, 109-112 (1975)

108. W. F. J. Vermaas, G. Renger and G. Dohnt: The Reduction of the Oxygen-Evolving System in Chloroplasts by Thylakoid Components. *Biochim Biophys Acta* 764, 194-202 (1984)

109. J. Messinger and G. Renger: Photosynthetic Water Splitting. In: *Primary Processes of Photosynthesis, Principles and Apparatus*. Ed G. Renger. RSC Publishing, Cambridge, 2, 291-349 (2008)

110. M. Haumann, P. Liebisch, C. Müller, M. Barra, M. Grabolle and H. Dau: Photosynthetic O_2 formation tracked by time-resolved x-ray experiments. *Science* 310, 1019-1021 (2005)

111. H. Dau and M. Haumann: Eight steps preceding O-O bond formation in oxygenic photosynthesis – a basic reaction cycle of the Photosystem II manganese complex. *Biochim Biophys Acta* 1767, 472-483 (2007)

112. V. P. Shinkarev and C. A. Wraight: Oxygen evolution in photosynthesis: from unicycle to bicycle. *Proc Natl Acad Sci U S A* 90, 1834-1838 (1993)

113. V. P. Shinkarev: Binary oscillations in the Kok model of oxygen evolution in oxygenic photosynthesis. *Photosynth Res* 48, 411-417 (1996)

114. V. P. Shinkarev: Oxygen evolution in photosynthesis: simple analytical solution for the Kok model. *Biophys J* 85, 435-441 (2003)

115. J. Yano and V. K. Yachandra: X-ray absorption spectroscopy. *Photosynth Res* 102, 241-254 (2009)

116. U. Bergmann and P. Glatzel: X-ray emission spectroscopy. *Photosynth Res* 102, 255-266 (2009)

117. K. Sauer, J. Yano and V. K. Yachandra: X-ray spectroscopy of the photosynthetic oxygen-evolving complex. *Coord Chem Rev* 252, 318-335 (2008)

118. W. Lubitz, F. Lendzian and R. Bittl: Radicals, radical pairs and triplet states in photosynthesis. *Acc Chem Res* 35, 313-320 (2002)

119. A. Haddy: EPR spectroscopy of the manganese cluster of photosystem II. *Photosynth Res* 92, 357-368 (2007)

120. L. Kulik and W. Lubitz: Electron-nuclear double resonance. *Photosynth Res* 102, 391-401 (2009)

121. R. G. Shulman, Y. Yafet, P. Eisenberger and W. E. Blumberg: Observation and Interpretation of X-Ray Absorption Edges in Iron Compounds and Proteins. *Proc Natl Acad Sci U S A* 73, 1384-1388 (1976)

122. D. B. Goodin, V. K. Yachandra, R. D. Britt, K. Sauer and M. P. Klein: The State of Manganese in the Photosynthetic Apparatus .3. Light-Induced-Changes in X-Ray Absorption (K-Edge) Energies of Manganese in Photosynthetic Membranes. *Biochim Biophys Acta* 767, 209-216 (1984)

123. T. A. Roelofs, W. C. Liang, M. J. Latimer, R. M. Cinco, A. Rompel, J. C. Andrews, K. Sauer, V. K. Yachandra and M. P. Klein: Oxidation states of the manganese cluster during the flash-induced S-state cycle of the photosynthetic oxygen-evolving complex. *Proc Natl Acad Sci U S A* 93, 3335-3340 (1996)

124. J. Messinger, J. H. Robblee, U. Bergmann, C. Fernandez, P. Glatzel, H. Visser, R. M. Cinco, K. L. McFarlane, E. Bellacchio, S. A. Pizarro, S. P. Cramer, K. Sauer, M. P. Klein and V. K. Yachandra: Absence of Mn-centered oxidation in the S-2 → S-3 Transition: Implications for the mechanism of photosynthetic water oxidation. *J Am Chem Soc* 123, 7804-7820 (2001)

125. T. A. Ono, T. Noguchi, Y. Inoue, M. Kusunoki, T. Matsushita and H. Oyanagi: X-ray Detection of the Period-Four Cycling of the Manganese Cluster in Photosynthetic Water Oxidizing Enzyme. *Science* 258, 1335-1337 (1992)

126. L. Iuzzolino, J. Dittmer, W. Dörner, W. Meyer-Klaucke and H. Dau: X-ray absorption spectroscopy on layered photosystem II membrane particles suggests manganese-centered oxidation of the oxygen-evolving complex for the S_0-S_1, S_1-S_2, and S_2-S_3 transitions of the water oxidation cycle. *Biochemistry* 37, 17112-17119 (1998)

127. M. Haumann, C. Müller, P. Liebisch, L. Iuzzolino, J. Dittmer, M. Grabolle, T. Neisius, W. Meyer-Klaucke and H. Dau: Structural and oxidation state changes of the photosystem II manganese complex in four transitions of the water oxidation cycle ($S_0 \rightarrow S_1$, $S_1 \rightarrow S_2$, $S_2 \rightarrow S_3$, and $S_{3,4} \rightarrow S_0$) Characterized by X-ray absorption spectroscopy at 20 K and room temperature. *Biochemistry* 44, 1894-1908 (2005)

128. H. Dau, P. Liebisch and M. Haumann: X-ray absorption spectroscopy to analyze nuclear geometry and electronic structure of biological metal centers--potential and questions examined with special focus on the tetra-nuclear manganese complex of oxygenic photosynthesis. *Anal Bioanal Chem* 376, 562-583 (2003)

129. M. Kusunoki, T. Ono, T. Noguchi, Y. Inoue and H. Oyanagi: Manganese K-Edge X-Ray-Absorption Spectra of the Cyclic S-States in the Photosynthetic Oxygen-Evolving System. *Photosynth Res* 38, 331-339 (1993)

130. V. K. Yachandra, V. J. DeRose, M. J. Latimer, I. Mukerji, K. Sauer and M. P. Klein: Where Plants Make Oxygen - a Structural Model for the Photosynthetic Oxygen-Evolving Manganese Cluster. *Science* 260, 675-679 (1993)

131. G. Peng, F. M. F. Degroot, K. Hämäläinen, J. A. Moore, X. Wang, M. M. Grush, J. B. Hastings, D. P. Siddons, W. H. Armstrong, O. C. Mullins and S. P. Cramer: High-Resolution Manganese X-Ray-Fluorescence Spectroscopy - Oxidation-State and Spin-State Sensitivity. *J Am Chem Soc* 116, 2914-2920 (1994)

132. H. Visser, E. Anxolabéhère-Mallart, U. Bergmann, P. Glatzel, J. H. Robblee, S. P. Cramer, J. J. Girerd, K. Sauer, M. P. Klein and V. K. Yachandra: MnK-edge XANES and K beta XES studies of two Mn-oxo binuclear complexes: Investigation of three different oxidation states relevant to the oxygen-evolving complex of photosystem II. *J Am Chem Soc* 123, 7031-7039 (2001)

133. P. Glatzel, U. Bergmann, J. Yano, H. Visser, J. H. Robblee, W. W. Gu, F. M. F. de Groot, G. Christou, V. L. Pecoraro, S. P. Cramer and V. K. Yachandra: The electronic structure of Mn in oxides, coordination complexes, and the oxygen-evolving complex of photosystem II studied by resonant inelastic X-ray scattering. *J Am Chem Soc* 126, 9946-9959 (2004)

134. J. A. Weil, J. R. Bolton and J. E. Wertz: Electron paramagnetic resonance: Elementary theory and practical applications. John Wiley & Sons, Inc., New York (1994)

135. A. Haddy, W. R. Dunham, R. H. Sands and R. Aasa: Multifrequency EPR Investigations into the Origin of the S_2-State Signal at g = 4 of the O_2-Evolving Complex. *Biochim Biophys Acta* 1099, 25-34 (1992)

136. K. A. Ahrling and R. J. Pace: Simulation of the S_2 State Multiline Electron Paramagnetic Resonance Signal of Photosystem II: A Multifrequency Approach. *Biophys J* 68, 2081-2090 (1995)

137. P. Dorlet, A. Boussac, A. W. Rutherford and S. Un: Multifrequency high-field EPR study of the interaction between the tyrosyl Z radical and the manganese cluster in plant photosystem II. *J Phys Chem B* 103, 10945-10954 (1999)

138. G. C. Dismukes and Y. Siderer: Intermediates of a Polynuclear Manganese Center Involved in Photosynthetic Oxidation of Water. *Proc Natl Acad Sci U S A* 78, 274-278 (1981)

139. J. L. Zimmermann and A. W. Rutherford: EPR Studies of the Oxygen-Evolving Enzyme of Photosystem II. *Biochim Biophys Acta* 767, 160-167 (1984)

140. Ö. Hansson, R. Aasa and T. Vänngard: The Origin of the Multiline and g = 4.1 Electron-Paramagnetic Resonance Signals from the Oxygen-Evolving System of Photosystem II. *Biophys J* 51, 825-832 (1987)

141. H. Matsuoka, K. Furukawa, T. Kato, H. Mino, J. R. Shen and A. Kawamori: g-Anisotropy of the S_2-state manganese cluster in single crystals of cyanobacterial photosystem II studied by W-band electron paramagnetic resonance spectroscopy. *J Phys Chem B* 110, 13242-13247 (2006)

142. C. Teutloff, S. Kessen, J. Kern, A. Zouni and R. Bittl: High-field (94-GHz) EPR spectroscopy on the S_2 multiline signal of Photosystem II. *FEBS Lett* 580, 3605-3609 (2006)

143. A. Haddy, R. Aasa and L. E. Andréasson: S-Band EPR Studies of the S_2-State Multiline Signal from the Photosynthetic Oxygen-Evolving Complex. *Biochemistry* 28, 6954-6959 (1989)

144. M. Zheng and G. C. Dismukes: Orbital configuration of the valence electrons, ligand field symmetry, and manganese oxidation states of the photosynthetic water

oxidizing complex: Analysis of the S_2 state multiline EPR signals. *Inorg Chem* 35, 3307-3319 (1996)

145. K. Hasegawa, M. Kusunoki, Y. Inoue and T. A. Ono: Simulation of S_2-state multiline EPR signal in oriented photosystem II membranes: structural implications for the manganese cluster in an oxygen-evolving complex. *Biochemistry* 37, 9457-9465 (1998)

146. M. F. Charlot, A. Boussac and G. Blondin: Towards a spin coupling model for the Mn_4 cluster in photosystem II. *Biochim Biophys Acta* 1708, 120-132 (2005)

147. D. A. Berthold, G. T. Babcock and C. F. Yocum: A Highly Resolved, Oxygen-Evolving Photosystem II Preparation from Spinach Thylakoid Membranes - EPR and Electron-Transport Properties. *FEBS Lett* 134, 231-234 (1981)

148. J. K. Blasie, M. Erecinska, S. Samuels and J. S. Leigh: Structure of a Cytochrome Oxidase-Lipid Model Membrane. *Biochim Biophys Acta* 501, 33-52 (1978)

149. A. W. Rutherford: Orientation of EPR Signals Arising from Components in Photosystem II Membranes. *Biochim Biophys Acta* 807, 189-201 (1985)

150. J. L. Zimmermann and A. W. Rutherford: Electron Paramagnetic Resonance Properties of the S_2 State of the Oxygen-Evolving Complex of Photosystem II. *Biochemistry* 25, 4609-4615 (1986)

151. D. H. Kim, R. D. Britt, M. P. Klein and K. Sauer: The g = 4.1 EPR Signal of the S_2 State of the Photosynthetic Oxygen-Evolving Complex Arises from a Multinuclear Mn Cluster. *J Am Chem Soc* 112, 9389-9391 (1990)

152. D. H. Kim, R. D. Britt, M. P. Klein and K. Sauer: The Manganese Site of the Photosynthetic Oxygen-Evolving Complex Probed by EPR Spectroscopy of Oriented Photosystem II Membranes: The g = 4 and g = 2 Multiline Signals. *Biochemistry* 31, 541-547 (1992)

153. A. V. Astashkin, Y. Kodera and A. Kawamori: Pulsed EPR Study of Manganese g = 4.1 Signal in Plant Photosystem II. *J Magn Reson B* 105, 113-119 (1994)

154. O. Horner, E. Rivière, G. Blondin, S. Un, A. W. Rutherford, J. J. Girerd and A. Boussac: SQUID magnetization study of the infrared-induced spin transition in the S_2 state of photosystem II: Spin value associated with the g = 4.1 EPR signal. *J Am Chem Soc* 120, 7924-7928 (1998)

155. A. Haddy, K. V. Lakshmi, G. W. Brudvig and H. A. Frank: Q-band EPR of the S_2 state of photosystem II confirms an S = 5/2 origin of the X-band g = 4.1 signal. *Biophys J* 87, 2885-2896 (2004)

156. K. V. Lakshmi, M. J. Reifler, D. A. Chisholm, J. Y. Wang, B. A. Diner and G. W. Brudvig: Correlation of the cytochrome c_{550} content of cyanobacterial Photosystem II with the EPR properties of the oxygen-evolving complex. *Photosynth Res* 72, 175-189 (2002)

157. C. F. Yocum: The calcium and chloride requirements of the O_2 evolving complex. *Coord Chem Rev* 252, 296-305 (2008)

158. K. A. Ahrling, S. Peterson and S. Styring: An oscillating manganese electron paramagnetic resonance signal from the S_0 state of the oxygen evolving complex in photosystem II. *Biochemistry* 36, 13148-13152 (1997)

159. J. Messinger, J. H. Robblee, W. O. Yu, K. Sauer, V. K. Yachandra and M. P. Klein: The S_0 state of the oxygen-evolving complex in photosystem II is paramagnetic: Detection of EPR multiline signal. *J Am Chem Soc* 119, 11349-11350 (1997)

160. A. Boussac, H. Kuhl, E. Ghibaudi, M. Rögner and A. W. Rutherford: Detection of an electron paramagnetic resonance signal in the S_0 state of the manganese complex of photosystem II from *Synechococcus elongatus*. *Biochemistry* 38, 11942-11948 (1999)

161. K. A. Ahrling, S. Peterson and S. Styring: The S_0 state EPR signal from the Mn cluster in photosystem II arises from an isolated S = $^1/_2$ ground state. *Biochemistry* 37, 8115-8120 (1998)

162. S. L. Dexheimer and M. P. Klein: Detection of a Paramagnetic Intermediate in the S_1 State of the Photosynthetic Oxygen-Evolving Complex. *J Am Chem Soc* 114, 2821-2826 (1992)

163. R. D. Britt, J. M. Peloquin and K. A. Campbell: Pulsed and parallel-polarization EPR characterization of the photosystem II oxygen-evolving complex. *Annu Rev Biophys Biomol Struct* 29, 463-495 (2000)

164. T. Yamauchi, H. Mino, T. Matsukawa, A. Kawamori and T. Ono: Parallel polarization electron paramagnetic resonance studies of the S_1-state manganese cluster in the photosynthetic oxygen-evolving system. *Biochemistry* 36, 7520-7526 (1997)

165. K. A. Campbell, J. M. Peloquin, D. P. Pham, R. J. Debus and R. D. Britt: Parallel polarization EPR detection of an S_1-state "multiline" EPR signal in photosystem II particles from *Synechocystis* sp. PCC 6803. *J Am Chem Soc* 120, 447-448 (1998)

166. K. A. Campbell, W. Gregor, D. P. Pham, J. M. Peloquin, R. J. Debus and R. D. Britt: The 23 and 17 kDa extrinsic proteins of photosystem II modulate the magnetic properties of the S_1-state manganese cluster. *Biochemistry* 37, 5039-5045 (1998)

167. W. Y. Hsieh, K. A. Campbell, W. Gregor, R. D. Britt, D. W. Yoder, J. E. Penner-Hahn and V. L. Pecoraro: The first spectroscopic model for the S_1 state multiline signal of the OEC. *Biochim Biophys Acta* 1655, 149-157 (2004)

168. T. Matsukawa, H. Mino, D. Yoneda and A. Kawamori: Dual-mode EPR study of new signals from the S_3-state of oxygen-evolving complex in photosystem II. *Biochemistry* 38, 4072-4077 (1999)

169. N. Ioannidis and V. Petrouleas: Electron paramagnetic resonance signals from the S_3 state of the oxygen-evolving complex. A broadened radical signal induced by low-temperature near-infrared light illumination. *Biochemistry* 39, 5246-5254 (2000)

170. A. Boussac, M. Sugiura, A. W. Rutherford and P. Dorlet: Complete EPR Spectrum of the S_3-State of the Oxygen-Evolving Photosystem II. *J Am Chem Soc* 131, 5050-5051 (2009)

171. D. W. Randall, B. E. Sturgeon, J. A. Ball, G. A. Lorigan, M. K. Chan, M. P. Klein, W. H. Armstrong and R. D. Britt: ^{55}Mn ESE-ENDOR of a Mixed Valence Mn(III)Mn(IV) Complex: Comparison with the Mn Cluster of the Photosynthetic Oxygen-Evolving Complex. *J Am Chem Soc* 117, 11780-11789 (1995)

172. G. J. Yeagle, M. L. Gilchrist, L. M. Walker, R. J. Debus and R. D. Britt: Multifrequency electron spin-echo envelope modulation studies of nitrogen ligation to the manganese cluster of photosystem II. *Phil Trans R Soc B* 363, 1157-1166 (2008)

173. G. J. Yeagle, M. L. Gilchrist, R. M. McCarrick and R. D. Britt: Multifrequency pulsed electron paramagnetic resonance study of the S_2 state of the photosystem II manganese cluster. *Inorg Chem* 47, 1803-1814 (2008)

174. J. M. Peloquin, K. A. Campbell, D. W. Randall, M. A. Evanchik, V. L. Pecoraro, W. H. Armstrong and R. D. Britt: ^{55}Mn ENDOR of the S_2-state multiline EPR signal of photosystem II: Implications on the structure of the tetranuclear Mn cluster. *J Am Chem Soc* 122, 10926-10942 (2000)

175. L. V. Kulik, B. Epel, W. Lubitz and J. Messinger: ^{55}Mn pulse ENDOR at 34 GHz of the S_0 and S_2 states of the oxygen-evolving complex in photosystem II. *J Am Chem Soc* 127, 2392-2393 (2005)

176. L. V. Kulik, B. Epel, W. Lubitz and J. Messinger: Electronic structure of the Mn_4O_xCa cluster in the S_0 and S_2 states of the oxygen-evolving complex of photosystem II based on pulse ^{55}Mn-ENDOR and EPR Spectroscopy. *J Am Chem Soc* 129, 13421-13435 (2007)

177. C. Teutloff, S. Pudollek, S. Kessen, M. Broser, A. Zouni and R. Bittl: Electronic structure of the tyrosine D radical and the water-splitting complex from pulsed ENDOR spectroscopy on photosystem II single crystals. *Phys Chem Chem Phys* 11, 6715-6726 (2009)

178. B. Bouges: Action of Low Concentrations of Hydroxylamine on Oxygen Evolved by *Chlorella* and Spinach Chloroplasts. *Biochim Biophys Acta* 234, 103-112 (1971)

179. W. F. Beck and G. W. Brudvig: Reactions of hydroxylamine with the electron-donor side of photosystem II. *Biochemistry* 26, 8285-8295 (1987)

180. H. Kretschmann, S. Pauly and H. T. Witt: Evidence for a Chemical-Reaction of Hydroxylamine with the Photosynthetic Water Splitting Enzyme S in the Dark - Possible States of Manganese and Water in the S-Cycle. *Biochim Biophys Acta* 1059, 208-214 (1991)

181. P. J. Riggs, R. Mei, C. F. Yocum and J. E. Penner-Hahn: Reduced Derivatives of the Manganese Cluster in the Photosynthetic Oxygen-Evolving Complex. *J Am Chem Soc* 114, 10650-10651 (1992)

182. H. Kretschmann and H. T. Witt: Chemical-Reduction of the Water-Splitting Enzyme-System of Photosynthesis and Its Light-Induced Reoxidation Characterized by Optical and Mass-Spectrometric Measurements - a Basis for the Estimation of the States of the Redox Active Manganese and of Water in the Quaternary Oxygen-Evolving S-State Cycle. *Biochim Biophys Acta* 1144, 331-345 (1993)

183. J. Messinger and G. Renger: Generation, oxidation by the oxidized form of the tyrosine of polypeptide D2, and possible electronic configuration of the redox states S_0, S_{-1}, and S_{-2} of the water oxidase in isolated spinach thylakoids. *Biochemistry* 32, 9379-9386 (1993)

184. J. Messinger, G. Seaton, T. Wydrzynski, U. Wacker and G. Renger: S_{-3} state of the water oxidase in photosystem II. *Biochemistry* 36, 6862-6873 (1997)

185. J. Messinger, J. H. Robblee, U. Bergmann, C. Fernandez, P. Glatzel, S. Isgandarova, B. Hanssum, G. Renger, S. P. Cramer, K. Sauer and V. K. Yachandra: Manganese oxidation states in photosystem II. In: *12th International Congress on Photosynthesis, Brisbane*. CSIRO Publishing, Melbourne, Australia (2001)

186. R. Mei and C. F. Yocum: Comparative Properties of Hydroquinone and Hydroxylamine Reduction of the Ca^{2+}-Stabilized O_2-Evolving Complex of Photosystem-II - Reductant-Dependent Mn^{2+} Formation and Activity Inhibition. *Biochemistry* 31, 8449-8454 (1992)

187. U. Bergmann, M. M. Grush, C. R. Horne, P. DeMarois, J. E. Penner-Hahn, C. F. Yocum, D. W. Wright, C. E. Dube, W. H. Armstrong, G. Christou, H. J. Eppley and S. P. Cramer: Characterization of the Mn oxidation states in photosystem II by Kβ X-ray fluorescence spectroscopy. *J Phys Chem B* 102, 8350-8352 (1998)

188. J. Messinger, J. H. A. Nugent and M. C. W. Evans: Detection of an EPR multiline signal for the S_0* state in photosystem II. *Biochemistry* 36, 11055-11060 (1997)

189. V. Petrouleas and B. A. Diner: Formation by NO of Nitrosyl Adducts of Redox Components of the Photosystem II Reaction Center. I. NO Binds to the

Acceptor-Side Non-Heme Iron. *Biochim Biophys Acta* 1015, 131-140 (1990)

190. B. A. Diner and V. Petrouleas: Formation by NO of Nitrosyl Adducts of Redox Components of the Photosystem II Reaction Center. II. Evidence That HCO_3^-/CO_2 Binds to the Acceptor-Side Non-Heme Iron. *Biochim Biophys Acta* 1015, 141-149 (1990)

191. Y. Sanakis, C. Goussias, R. P. Mason and V. Petrouleas: NO interacts with the tyrosine radical $Y_D^{\cdot}$ of photosystem II to form an iminoxyl radical. *Biochemistry* 36, 1411-1417 (1997)

192. C. Goussias, N. Ioannidis and V. Petrouleas: Low-temperature interactions of NO with the S_1 and S_2 states of the water-oxidizing complex of photosystem II. A novel Mn-multiline EPR signal derived from the S_1 state. *Biochemistry* 36, 9261-9266 (1997)

193. J. Sarrou, N. Ioannidis, Y. Deligiannakis and V. Petrouleas: A Mn(II)-Mn(III) EPR signal arises from the interaction of NO with the S_1 state of the water-oxidizing complex of photosystem II. *Biochemistry* 37, 3581-3587 (1998)

194. N. Ioannidis, J. Sarrou, G. Schansker and V. Petrouleas: NO reversibly reduces the water-oxidizing complex of photosystem II through S_0 and S_1 to the state characterized by the Mn(II)-Mn(III) multiline EPR signal. *Biochemistry* 37, 16445-16451 (1998)

195. G. Schansker, C. Goussias, V. Petrouleas and A. W. Rutherford: Reduction of the Mn cluster of the water-oxidizing enzyme by nitric oxide: Formation of an S_{-2} state. *Biochemistry* 41, 3057-3064 (2002)

196. N. Ioannidis, G. Schansker, V. V. Barynin and V. Petrouleas: Interaction of nitric oxide with the oxygen evolving complex of photosystem II and manganese catalase: a comparative study. *J Biol Inorg Chem* 5, 354-363 (2000)

197. Ö. Saygin and H. T. Witt: On the Change of the Charges in the four Photo-induced Oxidation Steps of the Water-Splitting Enzyme System S - Optical Characterization at O_2-Evolving Complexes Isolated from *Synechococcus*. *FEBS Lett* 176, 83-87 (1984)

198. Ö. Saygin and H. T. Witt: Evidence for the Electrochromic Identification of the Change of Charges in the four Oxidation Steps of the Photoinduced Water Cleavage in Photosynthesis. *FEBS Lett* 187, 224-226 (1985)

199. K. Brettel, E. Schlodder and H. T. Witt: Nanosecond Reduction Kinetics of Photooxidized Chlorophyll-a_{II} (P-680) in Single Flashes as a Probe for the Electron Pathway, H^+-Release and Charge Accumulation in the O_2-Evolving Complex. *Biochim Biophys Acta* 766, 403-415 (1984)

200. A. Gabdulkhakov, A. Guskov, M. Broser, J. Kern, F. Müh, W. Saenger and A. Zouni: Probing the Accessibility of the Mn_4Ca Cluster in Photosystem II: Channels Calculation, Noble Gas Derivatization, and Cocrystallization with DMSO. *Structure* 17, 1223-1234 (2009)

201. A. A. Vaguine, J. Richelle and S. J. Wodak: SFCHECK: a unified set of procedures for evaluating the quality of macromolecular structure-factor data and their agreement with the atomic model. *Acta Crystallogr D* 55, 191-205 (1999)

202. R. B. G. Ravelli and E. F. Garman: Radiation damage in macromolecular cryocrystallography. *Curr Opin Struct Biol* 16, 624-629 (2006)

203. M. Weik, R. B. G. Ravelli, G. Kryger, S. McSweeney, M. L. Raves, M. Harel, P. Gros, I. Silman, J. Kroon and J. L. Sussman: Specific chemical and structural damage to proteins produced by synchrotron radiation. *Proc Natl Acad Sci U S A* 97, 623-628 (2000)

204. V. Adam, A. Royant, V. Nivière, F. P. Molina-Heredia and D. Bourgeois: Structure of superoxide reductase bound to ferrocyanide and active site expansion upon X-ray-induced photo-reduction. *Structure* 12, 1729-1740 (2004)

205. R. H. Baxter, B. L. Seagle, N. Ponomarenko and J. R. Norris: Specific radiation damage illustrates light-induced structural changes in the photosynthetic reaction center. *J Am Chem Soc* 126, 16728-16729 (2004)

206. J. Wuerges, J. W. Lee, Y. I. Yim, H. S. Yim, S. O. Kang and K. D. Carugo: Crystal structure of nickel-containing superoxide dismutase reveals another type of active site. *Proc Natl Acad Sci U S A* 101, 8569-8574 (2004)

207. L. M. Utschig, S. D. Chemerisov, D. M. Tiede and O. G. Poluektov: Electron paramagnetic resonance study of radiation damage in photosynthetic reaction center crystals. *Biochemistry* 47, 9251-9257 (2008)

208. H. Dau, P. Liebisch and M. Haumann: The structure of the manganese complex of Photosystem II in its dark-stable S_1-state – EXAFS results in relation to recent crystallographic data. *Phys Chem Chem Phys* 6, 4781-4792 (2004)

209. J. Yano, J. Kern, K. D. Irrgang, M. J. Latimer, U. Bergmann, P. Glatzel, Y. Pushkar, J. Biesiadka, B. Loll, K. Sauer, J. Messinger, A. Zouni and V. K. Yachandra: X-ray damage to the Mn4Ca complex in single crystals of photosystem II: a case study for metalloprotein crystallography. *Proc Natl Acad Sci U S A* 102, 12047-12052 (2005)

210. M. Grabolle, M. Haumann, C. Müller, P. Liebisch and H. Dau: Rapid loss of structural motifs in the manganese complex of oxygenic photosynthesis by X-ray irradiation at 10-300 K. *J Biol Chem* 281, 4580-4588 (2006)

211. M. R. Blomberg and P. E. Siegbahn: Quantum chemistry as a tool in bioenergetics. *Biochim Biophys Acta* 1797, 129-142 (2010)

212. M. Kusunoki: Mono-manganese mechanism of the photosytem II water splitting reaction by a unique Mn_4Ca cluster. *Biochim Biophys Acta* 1767, 484-492 (2007)

213. L. G. Parratt and C. F. Hempstead: Anomalous Dispersion and Scattering of X-Rays. *Phys Rev* 94, 1593-1600 (1954)

214. J. R. Helliwell: Synchrotron X-Radiation Protein Crystallography - Instrumentation, Methods and Applications. *Rep Prog Phys* 47, 1403-1497 (1984)

215. C. Mueller-Dieckmann, S. Panjikar, A. Schmidt, S. Mueller, J. Kuper, A. Geerlof, M. Wilmanns, R. K. Singh, P. A. Tucker and M. S. Weiss: On the routine use of soft X-rays in macromolecular crystallography. Part IV. Efficient determination of anomalous substructures in biomacromolecules using longer X-ray wavelengths. *Acta Cryst D* 63, 366-380 (2007)

216. M. Haumann, M. Barra, P. Loja, S. Löscher, R. Krivanek, A. Grundmeier, L. E. Andreasson and H. Dau: Bromide does not bind to the Mn_4Ca complex in its S_1 state in Cl^--depleted and Br^--reconstituted oxygen-evolving photosystem II: Evidence from X-ray absorption spectroscopy at the Br K-edge. *Biochemistry* 45, 13101-13107 (2006)

217. V. K. Yachandra, K. Sauer and M. P. Klein: Manganese cluster in photosynthesis: Where plants oxidize water to dioxygen. *Chem Rev* 96, 2927-2950 (1996)

218. J. A. Kirby, A. S. Robertson, J. P. Smith, A. C. Thompson, S. R. Cooper and M. P. Klein: State of Manganese in the Photosynthetic Apparatus. 1. Extended X-Ray Absorption Fine-Structure Studies on Chloroplasts and Di-μ-Oxo-Bridged Dimanganese Model Compounds. *J Am Chem Soc* 103, 5529-5537 (1981)

219. K. Wieghardt: The Active-Sites in Manganese-Containing Metalloproteins and Inorganic Model Complexes. *Angew Chem Int Ed* 28, 1153-1172 (1989)

220. G. Christou: Manganese Carboxylate Chemistry and Its Biological Relevance. *Acc Chem Res* 22, 328-335 (1989)

221. V. L. Pecoraro, M. J. Baldwin and A. Gelasco: Interaction of Manganese with Dioxygen and Its Reduced Derivatives. *Chem Rev* 94, 807-826 (1994)

222. S. Mukhopadhyay, S. K. Mandal, S. Bhaduri and W. H. Armstrong: Manganese clusters with relevance to photosystem II. *Chem Rev* 104, 3981-4026 (2004)

223. E. J. Larson, P. J. Riggs, J. E. Penner-Hahn and V. L. Pecoraro: Protonation of $[\{Mn^{IV}(saltn)(\mu_2\text{-}O)\}_2]$ Results in Significant Modification of Structure and Catalase-Like Reactivity. *J Chem Soc, Chem Commun* 102-103 (1992)

224. M. J. Baldwin, T. L. Stemmler, P. J. Riggs-Gelasco, M. L. Kirk, J. E. Penner-Hahn and V. L. Pecoraro: Structural and Magnetic Effects of Successive Protonations of Oxo Bridges in High-Valent Manganese Dimers. *J Am Chem Soc* 116, 11349-11356 (1994)

225. J. Yano, Y. Pushkar, P. Glatzel, A. Lewis, K. Sauer, J. Messinger, U. Bergmann and V. Yachandra: High-resolution Mn EXAFS of the oxygen-evolving complex in photosystem II: Structural implications for the Mn_4Ca cluster. *J Am Chem Soc* 127, 14974-14975 (2005)

226. K. Sauer and V. K. Yachandra: The water-oxidation complex in photosynthesis. *Biochim Biophys Acta* 1655, 140-148 (2004)

227. G. N. George, R. C. Prince and S. P. Cramer: The Manganese Site of the Photosynthetic Water-Splitting Enzyme. *Science* 243, 789-791 (1989)

228. I. Mukerji, J. C. Andrews, V. J. Derose, M. J. Latimer, V. K. Yachandra, K. Sauer and M. P. Klein: Orientation of the Oxygen-Evolving Manganese Complex in a Photosystem II: Membrane Preparation - an X-Ray Absorption Spectroscopy Study. *Biochemistry* 33, 9712-9721 (1994)

229. H. Schiller, J. Dittmer, L. Iuzzolino, W. Dorner, W. Meyer-Klaucke, V. A. Sole, H. F. Nolting and H. Dau: Structure and orientation of the oxygen-evolving manganese complex of green algae and higher plants investigated by X-ray absorption linear dichroism spectroscopy on oriented photosystem II membrane particles. *Biochemistry* 37, 7340-7350 (1998)

230. Y. Pushkar, J. Yano, P. Glatzel, J. Messinger, A. Lewis, K. Sauer, U. Bergmann and V. Yachandra: Structure and orientation of the Mn_4Ca cluster in plant photosystem II membranes studied by polarized range-extended X-ray absorption spectroscopy. *J Biol Chem* 282, 7198-7208 (2007)

231. P. Liebisch and H. Dau: Linear Dichroism in the XANES of Partially Oriented Samples: Theory and Application to the Photosynthetic Manganese Complex. *ChemPhysChem* 11, 1236-1247 (2010)

232. E. M. Sproviero, J. A. Gascón, J. P. McEvoy, G. W. Brudvig and V. S. Batista: Quantum mechanics/molecular mechanics study of the catalytic cycle of water splitting in photosystem II. *J Am Chem Soc* 130, 3428-3442 (2008)

233. E. M. Sproviero, J. A. Gascón, J. P. McEvoy, G. W. Brudvig and V. S. Batista: A model of the oxygen-evolving center of photosystem II predicted by structural refinement based on EXAFS simulations. *J Am Chem Soc* 130, 6728-6730 (2008)

234. E. M. Sproviero, M. B. Newcomer, J. A. Gascón, E. R. Batista, G. W. Brudvig and V. S. Batista: The MoD-QM/MM methodology for structural refinement of

photosystem II and other biological macromolecules. *Photosynth Res* 102, 455-470 (2009)

235. M. Orio, D. A. Pantazis and F. Neese: Density functional theory. *Photosynth Res* 102, 443-453 (2009)

236. H. M. Senn and W. Thiel: QM/MM Methods for Biomolecular Systems. *Angew Chem Int Ed* 48, 1198-1229 (2009)

237. P. Ädelroth, K. Lindberg and L. E. Andréasson: Studies of Ca^{2+} Binding in Spinach Photosystem II Using $^{45}Ca^{2+}$. *Biochemistry* 34, 9021-9027 (1995)

238. G. M. Ananyev, L. Zaltsman, C. Vasko and G. C. Dismukes: The inorganic biochemistry of photosynthetic oxygen evolution/water oxidation. *Biochim Biophys Acta* 1503, 52-68 (2001)

239. R. L. Burnap: D1 protein processing and Mn cluster assembly in light of the emerging Photosystem II structure. *Phys Chem Chem Phys* 6, 4803-4809 (2004)

240. G. C. Dismukes and G. M. Ananyev: Photo-Assembly of the Catalytic Manganese Cluster. In: *Photosystem II: The Light-Driven Water:Plastoquinone Oxidoreductase*. Ed T. Wydrzynski and K. Satoh. Springer, Dordrecht, 609-626 (2005)

241. J. Dasgupta, G. M. Ananyev and G. C. Dismukes: Photoassembly of the Water-Oxidizing Complex in Photosystem II. *Coord Chem Rev* 252, 347-360 (2008)

242. R. Mei and C. F. Yocum: Calcium Retards NH_2OH Inhibition of O_2 Evolution Activity by Stabilization of Mn^{2+} Binding to Photosystem II. *Biochemistry* 30, 7836-7842 (1991)

243. R. Mei and C. Yocum: Characterization of Inhibitory Effects of NH_2OH and Its N-Methyl Derivatives on the O_2-Evolving Complex of Photosystem II. *Photosynth Res* 38, 449-453 (1993)

244. T. Kuntzleman, M. McCarrick, J. Penner-Hahn and C. Yocum: Probing reactive sites within the Photosystem II manganese cluster: Evidence for separate populations of manganese that differ in redox potential. *Phys Chem Chem Phys* 6, 4897-4904 (2004)

245. R. M. Cinco, K. L. M. Holman, J. H. Robblee, J. Yano, S. A. Pizarro, E. Bellacchio, K. Sauer and V. K. Yachandra: Calcium EXAFS establishes the Mn-Ca cluster in the oxygen-evolving complex of photosystem II. *Biochemistry* 41, 12928-12933 (2002)

246. D. F. Ghanotakis, G. T. Babcock and C. F. Yocum: Calcium Reconstitutes High-Rates of Oxygen Evolution in Polypeptide Depleted Photosystem II Preparations. *FEBS Lett* 167, 127-130 (1984)

247. K. L. Westphal, N. Lydakis-Simantiris, R. I. Cukier and G. T. Babcock: Effects of Sr^{2+}-substitution on the reduction rates of $Y_Z^{\cdot}$ in PSII membranes – Evidence for concerted hydrogen-atom transfer in oxygen evolution. *Biochemistry* 39, 16220-16229 (2000)

248. R. M. Cinco, J. H. Robblee, A. Rompel, C. Fernandez, V. K. Yachandra, K. Sauer and M. P. Klein: Strontium EXAFS reveals the proximity of calcium to the manganese cluster of oxygen-evolving photosystem II. *J Phys Chem B* 102, 8248-8256 (1998)

249. R. M. Cinco, J. H. Robblee, J. Messinger, C. Fernandez, K. L. M. Holman, K. Sauer and V. K. Yachandra: Orientation of calcium in the Mn_4Ca cluster of the oxygen-evolving complex determined using polarized strontium EXAFS of photosystem II membranes. *Biochemistry* 43, 13271-13282 (2004)

250. S. H. Kim, W. Gregor, J. M. Peloquin, M. Brynda and R. D. Britt: Investigation of the calcium-binding site of the oxygen evolving complex of photosystem II using ^{87}Sr ESEEM spectroscopy. *J Am Chem Soc* 126, 7228-7237 (2004)

251. A. Boussac, F. Rappaport, P. Carrier, J. M. Verbavatz, R. Gobin, D. Kirilovsky, A. W. Rutherford and M. Sugiura: Biosynthetic Ca^{2+}/Sr^{2+} exchange in the photosystem II oxygen-evolving enzyme of *Thermosynechococcus elongatus*. *J Biol Chem* 279, 22809-22819 (2004)

252. J. Kargul, K. Maghlaoul, J. W. Murray, Z. Deak, A. Boussac, A. W. Rutherford, I. Vass and J. Barber: Purification, crystallization and X-ray diffraction analyses of the *T. elongatus* PSII core dimer with strontium replacing calcium in the oxygen-evolving complex. *Biochim Biophys Acta* 1767, 404-413 (2007)

253. Y. Pushkar, J. Yano, K. Sauer, A. Boussac and V. K. Yachandra: Structural changes in the Mn_4Ca cluster and the mechanism of photosynthetic water splitting. *Proc Natl Acad Sci U S A* 105, 1879-1884 (2008)

254. E. M. Siegbahn: A Structure-Consistent Mechanism for Dioxygen Formation in Photosystem II. *Chem Eur J* 14, 8290-8302 (2008)

255. P. E. M. Siegbahn: Theoretical studies of O-O bond formation in photosystem II. *Inorg Chem* 47, 1779-1786 (2008)

256. P. E. Siegbahn: Water oxidation in photosystem II: oxygen release, proton release and the effect of chloride. *Dalton Trans* 10063-10068 (2009)

257. P. J. Nixon and B. A. Diner: Aspartate 170 of the photosystem II reaction center polypeptide D1 is involved in the assembly of the oxygen-evolving manganese cluster. *Biochemistry* 31, 942-948 (1992)

258. H. A. Chu, A. P. Nguyen and R. J. Debus: Site-Directed Photosystem II Mutants with Perturbed Oxygen-Evolving Properties. 1. Instability or Inefficient Assembly of the Manganese Cluster *in vivo*. *Biochemistry* 33, 6137-6149 (1994)

259. H. A. Chu, A. P. Nguyen and R. J. Debus: Amino-Acid-Residues That Influence the Binding of Manganese or Calcium to Photosystem II. 1. The Lumenal Interhelical Domains of the D1 Polypeptide. *Biochemistry* 34, 5839-5858 (1995)

260. B. A. Diner and P. J. Nixon: The Rate of Reduction of Oxidized Redox-Active Tyrosine, Z^+, by Exogenous Mn^{2+} Is Slowed in a Site-Directed Mutant, at Aspartate 170 of Polypeptide D1 of Photosystem II, Inactive for Photosynthetic Oxygen Evolution. *Biochim Biophys Acta* 1101, 134-138 (1992)

261. J. P. Whitelegge, D. Koo, B. A. Diner, I. Domian and J. M. Erickson: Assembly of the Photosystem II oxygen-evolving complex is inhibited in psbA site-directed mutants of *Chlamydomonas reinhardtii*. Aspartate 170 of the D1 polypeptide. *J Biol Chem* 270, 225-35 (1995)

262. R. J. Debus: Protein ligation of the photosynthetic oxygen-evolving center. *Coord Chem Rev* 252, 244-258 (2008)

263. R. J. Debus, C. Aznar, K. A. Campbell, W. Gregor, B. A. Diner and R. D. Britt: Does aspartate 170 of the D1 polypeptide ligate the manganese cluster in photosystem II? An EPR and ESEEM Study. *Biochemistry* 42, 10600-10608 (2003)

264. T. Noguchi: Light-induced FTIR difference spectroscopy as a powerful tool toward understanding the molecular mechanism of photosynthetic oxygen evolution. *Photosynth Res* 91, 59-69 (2007)

265. T. Noguchi: Fourier transform infrared analysis of the photosynthetic oxygen-evolving center. *Coord Chem Rev* 252, 336-346 (2008)

266. H. A. Chu, R. J. Debus and G. T. Babcock: D1-Asp170 is structurally coupled to the oxygen evolving complex in photosystem II as revealed by light-induced Fourier transform infrared difference spectroscopy. *Biochemistry* 40, 2312-2316 (2001)

267. R. J. Debus, M. A. Strickler, L. M. Walker and W. Hillier: No evidence from FTIR difference spectroscopy that aspartate-170 of the D1 polypeptide ligates a manganese ion that undergoes oxidation during the S_0 to S_1, S_1 to S_2, or S_2 to S_3 transitions in photosystem II. *Biochemistry* 44, 1367-1374 (2005)

268. R. J. Debus, K. A. Campbell, D. P. Pham, A. M. A. Hays and R. D. Britt: Glutamate 189 of the D1 polypeptide modulates the magnetic and redox properties of the manganese cluster and tyrosine Y_Z in photosystem II. *Biochemistry* 39, 6275-6287 (2000)

269. J. Clausen, S. Winkler, A. M. Hays, M. Hundelt, R. J. Debus and W. Junge: Photosynthetic water oxidation in *Synechocystis* sp. PCC6803: mutations D1-E189K, R and Q are without influence on electron transfer at the donor side of photosystem II. *Biochim Biophys Acta* 1506, 224-235 (2001)

270. Y. Kimura, N. Mizusawa, A. Ishii, S. Nakazawa and T. A. Ono: Changes in structural and functional properties of oxygen-evolving complex induced by replacement of D1-glutamate 189 with glutamine in photosystem II: ligation of glutamate 189 carboxylate to the manganese cluster. *J Biol Chem* 280, 37895-37900 (2005)

271. M. A. Strickler, W. Hillier and R. J. Debus: No evidence from FTIR difference spectroscopy that glutamate-189 of the D1 polypeptide ligates a Mn ion that undergoes oxidation during the S_0 to S_1, S_1 to S_2, or S_2 to S_3 transitions in photosystem II. *Biochemistry* 45, 8801-8811 (2006)

272. X. S. Tang, B. A. Diner, B. S. Larsen, M. L. Gilchrist, G. A. Lorigan and R. D. Britt: Identification of Histidine at the Catalytic Site of the Photosynthetic Oxygen-Evolving Complex. *Proc Natl Acad Sci U S A* 91, 704-708 (1994)

273. H. A. Chu, A. P. Nguyen and R. J. Debus: Amino-Acid-Residues That Influence the Binding of Manganese or Calcium to Photosystem II. 2. The Carboxy-Terminal Domain of the D1 Polypeptide. *Biochemistry* 34, 5859-5882 (1995)

274. R. J. Debus, K. A. Campbell, W. Gregor, Z. L. Li, R. L. Burnap and R. D. Britt: Does histidine 332 of the D1 polypeptide ligate the manganese cluster in photosystem II? An electron spin echo envelope modulation study. *Biochemistry* 40, 3690-3699 (2001)

275. T. Noguchi, Y. Inoue and X. S. Tang: Structure of a histidine ligand in the photosynthetic oxygen-evolving complex as studied by light-induced Fourier transform infrared difference spectroscopy. *Biochemistry* 38, 10187-10195 (1999)

276. Y. Kimura, N. Mizusawa, A. Ishii and T. Ono: FTIR detection of structural changes in a histidine ligand during S-state cycling of photosynthetic oxygen-evolving complex. *Biochemistry* 44, 16072-16078 (2005)

277. M. Sugiura, F. Rappaport, K. Brettel, T. Noguchi, A. W. Rutherford and A. Boussac: Site-directed mutagenesis of the *Thermosynechococcus elongatus* photosystem II: The O_2-evolving enzyme lacking the redox-active tyrosine D. *Biochemistry* 43, 13549-13563 (2004)

278. M. Sugiura, A. Boussac, T. Noguchi and F. Rappaport: Influence of Histidine-198 of the D1 subunit on the properties of the primary electron donor, P_{680}, of photosystem II in *Thermosynechococcus elongatus*. *Biochim Biophys Acta* 1777, 331-342 (2008)

279. M. Sugiura, F. Rappaport, W. Hillier, P. Dorlet, Y. Ohno, H. Hayashi and A. Boussac: Evidence that D1-His332 in Photosystem II from *Thermosynechococcus elongatus* Interacts with the S_3-State and not with the S_2-State. *Biochemistry* 48, 7856-7866 (2009)

280. R. O. Cohen, P. J. Nixon and B. A. Diner: Participation of the C-terminal region of the D1-

polypeptide in the first steps in the assembly of the Mn_4Ca cluster of photosystem II. *J Biol Chem* 282, 7209-7218 (2007)

281. M. A. Strickler, L. M. Walker, W. Hillier, R. D. Britt and R. J. Debus: No evidence from FTIR difference spectroscopy that aspartate-342 of the D1 polypeptide ligates a Mn ion that undergoes oxidation during the S_0 to S_1, S_1 to S_2, or S_2 to S_3 transitions in photosystem II. *Biochemistry* 46, 3151-3160 (2007)

282. P. J. Nixon, J. T. Trost and B. A. Diner: Role of the carboxy terminus of polypeptide D1 in the assembly of a functional water-oxidizing manganese cluster in photosystem II of the cyanobacterium *Synechocystis* sp. PCC 6803: assembly requires a free carboxyl group at C-terminal position 344. *Biochemistry* 31, 10859-10871 (1992)

283. P. R. Anbudurai, T. S. Mor, I. Ohad, S. V. Shestakov and H. B. Pakrasi: The *ctpA* Gene Encodes the C-Terminal Processing Protease for the D1 Protein of the Photosystem II Reaction Center Complex. *Proc Natl Acad Sci U S A* 91, 8082-8086 (1994)

284. P. J. Nixon, F. Michoux, J. F. Yu, M. Boehm and J. Komenda: Recent advances in understanding the assembly and repair of photosystem II. *Ann Bot* 106, 1-16 (2010)

285. H. A. Chu, W. Hillier and R. J. Debus: Evidence that the C-terminus of the D1 polypeptide of photosystem II is ligated to the manganese ion that undergoes oxidation during the S_1 to S_2 transition: An isotope-edited FTIR study. *Biochemistry* 43, 3152-3166 (2004)

286. Y. Kimura, N. Mizusawa, T. Yamanari, A. Ishii and T. Ono: Structural changes of D1 C-terminal alpha-carboxylate during S-state cycling in photosynthetic oxygen evolution. *J Biol Chem* 280, 2078-2083 (2005)

287. M. A. Strickler, L. M. Walker, W. Hillier and R. J. Debus: Evidence from biosynthetically incorporated strontium and FTIR difference spectroscopy that the C-terminus of the D1 polypeptide of photosystem II does not ligate calcium. *Biochemistry* 44, 8571-8577 (2005)

288. J. A. Stull, T. A. Stich, R. J. Service, R. J. Debus, S. K. Mandal, W. H. Armstrong and R. D. Britt: ^{13}C ENDOR reveals that the D1 polypeptide C-terminus is directly bound to Mn in the photosystem II oxygen evolving complex. *J Am Chem Soc* 132, 446-447 (2010)

289. C. Rosenberg, J. Christian, T. M. Bricker and C. Putnam-Evans: Site-directed mutagenesis of glutamate residues in the large extrinsic loop of the photosystem II protein CP 43 affects oxygen-evolving activity and PS II assembly. *Biochemistry* 38, 15994-6000 (1999)

290. M. A. Strickler, H. J. Hwang, R. L. Burnap, J. Yano, L. M. Walker, R. J. Service, R. D. Britt, W. Hillier and R. J. Debus: Glutamate-354 of the CP43 polypeptide interacts with the oxygen-evolving Mn_4Ca cluster of photosystem II: a preliminary characterization of the Glu354Gln mutant. *Phil Trans R Soc B* 363, 1179-1187 (2008)

291. Y. Shimada, H. Suzuki, T. Tsuchiya, T. Tomo, T. Noguchi and M. Mimuro: Effect of a Single-Amino Acid Substitution of the 43 kDa Chlorophyll Protein on the Oxygen-Evolving Reaction of the Cyanobacterium *Synechocystis* sp. PCC 6803: Analysis of the Glu354Gln Mutation. *Biochemistry* 48, 6095-6103 (2009)

292. F. Ho: Uncovering channels in photosystem II by computer modelling: current progress, future prospects, and lessons from analogous systems. *Photosynth Res* 98, 503-522 (2008)

293. W. P. Schröder and H. E. Akerlund: H_2O_2 Accessibility to the Photosystem II Donor Side in Protein-Depleted inside-out Thylakoids Measured as Flash-Induced Oxygen Production. *Biochim Biophys Acta* 848, 359-363 (1986)

294. P. L. Fine and W. D. Frasch: The Oxygen-Evolving Complex Requires Chloride to Prevent Hydrogen-Peroxide Formation. *Biochemistry* 31, 12204-12210 (1992)

295. A. Arató, N. Bondarava and A. Krieger-Liszkay: Production of reactive oxygen species in chloride- and calcium-depleted photosystem II and their involvement in photoinhibition. *Biochim Biophys Acta* 1608, 171-180 (2004)

296. R. L. Bradley, K. M. Long and W. D. Frasch: The Involvement of Photosystem II-Generated H_2O_2 in Photoinhibition. *FEBS Lett* 286, 209-213 (1991)

297. A. Krieger-Liszkay, C. Fufezan and A. Trebst: Singlet oxygen production in photosystem II and related protection mechanism. *Photosynth Res* 98, 551-564 (2008)

298. P. Pospísil: Production of reactive oxygen species by photosystem II. *Biochim Biophys Acta* 1787, 1151-1160 (2009)

299. N. Adir, H. Zer, S. Shochat and I. Ohad: Photoinhibition - a historical perspective. *Photosynth Res* 76, 343-370 (2003)

300. E. Tyystjärvi: Photoinhibition of Photosystem II and photodamage of the oxygen evolving manganese cluster. *Coord Chem Rev* 252, 361-376 (2008)

301. Y. Yamamoto, R. Aminaka, M. Yoshioka, M. Khatoon, K. Komayama, D. Takenaka, A. Yamashita, N. Nijo, K. Inagawa, N. Morita, T. Sasaki and Y. Yamamoto: Quality control of photosystem II: impact of light and heat stresses. *Photosynth Res* 98, 589-608 (2008)

302. I. Vass and E. Aro: Photoinhibition of Photosynthetic Electron Transport. In: *Primary Processes of Photosynthesis, Principles and Apparatus*. Ed G. Renger. RSC Publishing, Cambridge, U. K., 1, 393-425 (2008)

303. T. Wydrzynski, W. Hillier and J. Messinger: On the functional significance of substrate accessibility in the photosynthetic water oxidation mechanism. *Physiol Plant* 96, 342-350 (1996)

304. R. Radmer and O. Ollinger: Topography of the O_2-Evolving Site Determined with Water Analogs. *FEBS Lett* 152, 39-43 (1983)

305. W. F. Beck and G. W. Brudvig: Resolution of the Paradox of Ammonia and Hydroxylamine as Substrate-Analogs for the Water-Oxidation Reaction Catalyzed by Photosystem II. *J Am Chem Soc* 110, 1517-1523 (1988)

306. D. A. Force, D. W. Randall, G. A. Lorigan, K. L. Clemens and R. D. Britt: ESEEM studies of alcohol binding to the manganese cluster of the oxygen evolving complex of Photosystem II. *J Am Chem Soc* 120, 13321-13333 (1998)

307. J. M. Anderson: Does functional photosystem II complex have an oxygen channel? *FEBS Lett* 488, 1-4 (2001)

308. J. M. Anderson and W. S. Chow: Structural and functional dynamics of plant photosystem II. *Phil Trans R Soc Lond B* 357, 1421-1430 (2002)

309. F. van Mieghem, K. Brettel, B. Hillmann, A. Kamlowski, A. W. Rutherford and E. Schlodder: Charge Recombination Reactions in Photosystem II. 1. Yields, Recombination Pathways, and Kinetics of the Primary Pair. *Biochemistry* 34, 4798-4813 (1995)

310. T. Noguchi: Dual role of triplet localization on the accessory chlorophyll in the photosystem II reaction center: Photoprotection and photodamage of the D1 protein. *Plant Cell Physiol* 43, 1112-1116 (2002)

311. C. Schweitzer and R. Schmidt: Physical mechanisms of generation and deactivation of singlet oxygen. *Chem Rev* 103, 1685-1757 (2003)

312. J. Clausen and W. Junge: Detection of an intermediate of photosynthetic water oxidation. *Nature* 430, 480-483 (2004)

313. J. Clausen, W. Junge, H. Dau and M. Haumann: Photosynthetic water oxidation at high O_2 backpressure monitored by delayed chlorophyll fluorescence. *Biochemistry* 44, 12775-12779 (2005)

314. W. Junge and J. Clausen: Photosynthetic oxygen production. *Science* 312, 1470 (2006)

315. J. E. Penner-Hahn and C. F. Yocum: Photosynthetic oxygen production - Response. *Science* 312, 1470-1471 (2006)

316. H. Dau and M. Haumann: Photosynthetic oxygen production - Response. *Science* 312, 1471-1472 (2006)

317. D. R. J. Kolling, T. S. Brown, G. Ananyev and G. C. Dismukes: Photosynthetic Oxygen Evolution Is Not Reversed at High Oxygen Pressures: Mechanistic Consequences for the Water-Oxidizing Complex. *Biochemistry* 48, 1381-1389 (2009)

318. M. Haumann, A. Grundmeier, I. Zaharieva and H. Dau: Photosynthetic water oxidation at elevated dioxygen partial pressure monitored by time-resolved X-ray absorption measurements. *Proc Natl Acad Sci U S A* 105, 17384-17389 (2008)

319. C. J. T. de Grotthuss: Memoir on the decomposition of water and of the bodies that it holds in solution by means of galvanic electricity. *Biochim. Biophys Acta* 1757, 871-875 (2006)

320. S. Cukierman: Et tu, Grotthuss! and other unfinished stories. *Biochim Biophys Acta* 1757, 876-885 (2006)

321. P. Brzezinski and P. Adelroth: Design principles of proton-pumping haem-copper oxidases. *Curr Opin Struct Biol* 16, 465-472 (2006)

322. C. A. Wraight: Chance and design - Proton transfer in water, channels and bioenergetic proteins. *Biochim Biophys Acta* 1757, 886-912 (2006)

323. C. A. Wraight: Intraprotein Proton Transfer - Concepts and Realities from the Bacterial Photosynthetic Reaction Center. In: *Biophysical and Structural Aspects of Bioenergetics*. Ed M. Wikstrom. RSC Publishing, Cambridge, UK, 273-312 (2005)

324. H. Ishikita, W. Saenger, B. Loll, J. Biesiadka and E. W. Knapp: Energetics of a possible proton exit pathway for water oxidation in photosystem II. *Biochemistry* 45, 2063-2071 (2006)

325. J. W. Murray and J. Barber: Structural characteristics of channels and pathways in photosystem II including the identification of an oxygen channel. *J Struct Biol* 159, 228-237 (2007)

326. F. M. Ho and S. Styring: Access channels and methanol binding site to the $CaMn_4$ cluster in Photosystem II based on solvent accessibility simulations, with implications for substrate water access. *Biochim Biophys Acta* 1777, 140-153 (2008)

327. S. Vassiliev, P. Comte, A. Mahboob and D. Bruce: Tracking the Flow of Water through Photosystem II Using Molecular Dynamics and Streamline Tracing. *Biochemistry* 49, 1873-1881 (2010)

328. M. Petrek, M. Otyepka, P. Banás, P. Kosinová, J. Koca and J. Damborský: CAVER: a new tool to explore routes from protein clefts, pockets and cavities. *BMC Bioinformatics* 7, 316-324 (2006)

329. E. M. Sproviero, J. A. Gascon, J. P. McEvoy, G. W. Brudvig and V. S. Batista: Quantum mechanics/molecular mechanics structural models of the oxygen-evolving complex of photosystem II. *Curr Opin Struct Biol* 17, 173-180 (2007)

330. P. J. Basser and D. K. Jones: Diffusion-tensor MRI: theory, experimental design and data analysis - a technical review. *NMR Biomed* 15, 456-467 (2002)

331. J. W. Murray, K. Maghlaoui, J. Kargul, M. Sugiura and J. Barber: Analysis of xenon binding to photosystem II by X-ray crystallography. *Photosynth Res* 98, 523-527 (2008)

332. T. Prangé, M. Schiltz, L. Pernot, N. Colloc'h, S. Longhi, W. Bourguet and R. Fourme: Exploring hydrophobic sites in proteins with xenon or krypton. *Proteins* 30, 61-73 (1998)

333. M. L. Quillin, W. A. Breyer, I. J. Griswold and B. W. Matthews: Size versus polarizability in protein-ligand interactions: Binding of noble gases within engineered cavities in phage T4 lysozyme. *J Mol Biol* 302, 955-977 (2000)

334. A. P. Duff, D. M. Trambaiolo, A. E. Cohen, P. J. Ellis, G. A. Juda, E. M. Shepard, D. B. Langley, D. M. Dooley, H. C. Freeman and J. M. Guss: Using xenon as a probe for dioxygen-binding sites in copper amine oxidases. *J Mol Biol* 344, 599-607 (2004)

335. V. M. Luna, Y. Chen, J. A. Fee and C. D. Stout: Crystallographic studies of Xe and Kr binding within the large internal cavity of cytochrome ba_3 from *Thermus thermophilus*: Structural analysis and role of oxygen transport channels in the heme-Cu oxidases. *Biochemistry* 47, 4657-4665 (2008)

336. A. Bondi: van der Waals Volumes and Radii. *J Phys Chem* 68, 441-451 (1964)

337. A. Dalgarno and A. E. Kingston: The Refractive Indices and Verdet Constants of the Inert Gases. *Proc R Soc A* 259, 424-431 (1960)

338. A. C. Newell and R. C. Baird: Absolute Determination of Refractive Indices of Gases at 47.7 Gigahertz. *J Appl Phys* 36, 3751-3759 (1965)

339. N. Colloc'h, L. Gabison, G. Monard, M. Altarsha, M. Chiadmi, G. Marassio, J. S. D. O. Santos, M. El Hajji, B. Castro, J. H. Abraini and T. Prangé: Oxygen pressurized X-ray crystallography: Probing the dioxygen binding site in cofactorless urate oxidase and implications for its catalytic mechanism. *Biophys J* 95, 2415-2422 (2008)

340. W. J. Coleman: Chloride Binding Proteins: Mechanistic Implications for the Oxygen-Evolving Complex of Photosystem II. *Photosynth Res* 23, 1-27 (1990)

341. C. Critchley and A. M. Sargeson: A Manganese-Chloride Cluster as the Functional Center of the O_2 Evolving Enzyme in Photosynthetic Systems. *FEBS Lett* 177, 2-5 (1984)

342. P. O. Sandusky and C. F. Yocum: The Chloride Requirement for Photosynthetic Oxygen Evolution - Analysis of the Effects of Chloride and Other Anions on Amine Inhibition of the Oxygen-Evolving Complex. *Biochim Biophys Acta* 766, 603-611 (1984)

343. R. Damoder, V. V. Klimov and G. C. Dismukes: The effect of Cl^- depletion and X^- reconstitution on the oxygen-evolution rate, the yield of the multiline manganese EPR signal and EPR signal II in the isolated Photosystem-II complex. *Biochim Biophys Acta* 848, 378-391 (1986)

344. S. Zein, L. V. Kulik, J. Yano, J. Kern, Y. Pushkar, A. Zouni, V. K. Yachandra, W. Lubitz, F. Neese and J. Messinger: Focusing the view on nature's water-splitting catalyst. *Philos Trans R Soc B* 363, 1167-1177 (2008)

345. Y. A. Ren, C. X. Zhang and J. Q. Zhao: Substitution of chloride by bromide modifies the low-temperature tyrosine Z oxidation in active photosystem II. *Biochim Biophys Acta* 1797, 1421-1427 (2010)

346. J. W. Murray, K. Maghlaoui, J. Kargul, N. Ishida, T. L. Lai, A. W. Rutherford, M. Sugiura, A. Boussac and J. Barber: X-ray crystallography identifies two chloride binding sites in the oxygen evolving centre of Photosystem II. *Energy Environ Sci* 1, 161-166 (2008)

347. K. Kawakami, Y. Umena, N. Kamiya and J. R. Shen: Location of chloride and its possible functions in oxygen-evolving photosystem II revealed by X-ray crystallography. *Proc Natl Acad Sci U S A* 106, 8567-8572 (2009)

348. P. H. Homann: The Association of Functional Anions with the Oxygen-Evolving Center of Chloroplasts. *Biochim Biophys Acta* 809, 311-319 (1985)

349. W. J. Coleman and Govindjee: A Model for the Mechanism of Chloride Activation of Oxygen Evolution in Photosystem II. *Photosynth Res* 13, 199-223 (1987)

350. K. Olesen and L. E. Andréasson: The function of the chloride ion in photosynthetic oxygen evolution. *Biochemistry* 42, 2025-2035 (2003)

351. T. Wydrzynski, F. Baumgart, F. Macmillan and G. Renger: Is There a Direct Chloride Cofactor Requirement in the Oxygen-Evolving Reactions of Photosystem II. *Photosynth Res* 25, 59-72 (1990)

352. K. Lindberg, T. Wydrzynski, T. Vanngard and L. E. Andréasson: Slow Release of Chloride from ^{36}Cl Labeled Photosystem II Membranes. *FEBS Lett* 264, 153-155 (1990)

353. K. Lindberg, T. Vanngard and L. E. Andréasson: Studies of the Slowly Exchanging Chloride in Photosystem II of Higher Plants. *Photosynth Res* 38, 401-408 (1993)

354. K. Lindberg and L. E. Andréasson: A one-site, two-state model for the binding of anions in photosystem II. *Biochemistry* 35, 14259-14267 (1996)

355. P. van Vliet and A. W. Rutherford: Properties of the chloride-depleted oxygen-evolving complex of photosystem II studied by electron paramagnetic resonance. *Biochemistry* 35, 1829-1839 (1996)

356. V. K. Yachandra, R. D. Guiles, K. Sauer and M. P. Klein: The State of Manganese in the Photosynthetic Apparatus. 5. The Chloride Effect in Photosynthetic Oxygen Evolution. Is Halide Coordinated to the EPR-Active Manganese in the O_2-Evolving Complex? Studies of the Substructure of the Low-Temperature Multiline EPR Signal. *Biochim Biophys Acta* 850, 333-342 (1986)

357. J. A. Laszlo, G. M. Baker and R. A. Dilley: Nonequilibration of Membrane-Associated Protons with the Internal Aqueous Space in Dark-Maintained Chloroplast Thylakoids. *J Bioenerg Biomembr* 16, 37-51 (1984)

358. J. A. Laszlo, G. M. Baker and R. A. Dilley: Chloroplast Thylakoid Membrane Proteins Having Buried Amine Buffering Groups. *Biochim Biophys Acta* 764, 160-169 (1984)

359. F. C. T. Allnutt, E. Atta-Asafo-Adjei and R. A. Dilley: Chloroplast Thylakoid Proteins Associated with Sequestered Proton-Buffering Domains. Plastocyanin Contributes Buffering Groups to Localized Proton Domains. *J Bioenerg Biomembr* 21, 535-551 (1989)

360. N. Ishida, M. Sugiura, F. Rappaport, T. L. Lai, A. W. Rutherford and A. Boussac: Biosynthetic exchange of bromide for chloride and strontium for calcium in the photosystem II oxygen-evolving enzymes. *J Biol Chem* 283, 13330-13340 (2008)

361. M. Haumann, M. Barra, P. Loja, S. Löscher, R. Krivanek, A. Grundmeier, L. E. Andréasson and H. Dau: Bromide does not bind to the Mn_4Ca complex in its S_1 state in Cl^--depleted and Br^--reconstituted oxygen-evolving photosystem II: Evidence from X-ray absorption spectroscopy at the Br K-edge. *Biochemistry* 45, 13101-13107 (2006)

362. G. T. Babcock and K. Sauer: The rapid component of electron paramagnetic resonance signal II: a candidate for the physiological donor to photosystem II in spinach chloroplasts. *Biochim Biophys Acta* 376, 329-44 (1975)

363. B. A. Diner and R. D. Britt: The Redox-Active Tyrosines Y_Z and Y_D. In: *Photosystem II: The Light-Driven Water:Plastoquinone Oxidoreductase*. Ed T. Wydrzynski and K. Satoh. Springer, Dordrecht, 207-233 (2005)

364. R. J. Debus, B. A. Barry, I. Sithole, G. T. Babcock and L. McIntosh: Directed mutagenesis indicates that the donor to P^+_{680} in photosystem II is tyrosine-161 of the D1 polypeptide. *Biochemistry* 27, 9071-9074 (1988)

365. J. G. Metz, P. J. Nixon, M. Rögner, G. W. Brudvig and B. A. Diner: Directed alteration of the D1 polypeptide of photosystem II: evidence that tyrosine-161 is the redox component, Z, connecting the oxygen-evolving complex to the primary electron donor, P680. *Biochemistry* 28, 6960-9 (1989)

366. R. J. Debus, B. A. Barry, G. T. Babcock and L. McIntosh: Site-directed mutagenesis identifies a tyrosine radical involved in the photosynthetic oxygen-evolving system. *Proc Natl Acad Sci U S A* 85, 427-430 (1988)

367. C. W. Hoganson and G. T. Babcock: A metalloradical mechanism for the generation of oxygen from water in photosynthesis. *Science* 277, 1953-1956 (1997)

368. R. Ahlbrink, M. Haumann, D. Cherepanov, O. Bögershausen, A. Mulkidjanian and W. Junge: Function of tyrosine Z in water oxidation by photosystem II: electrostatical promotor instead of hydrogen abstractor. *Biochemistry* 37, 1131-1142 (1998)

369. M. Haumann and W. Junge: Evidence for impaired hydrogen-bonding of tyrosine Y_Z in calcium-depleted photosystem II. *Biochim Biophys Acta* 1411, 121-133 (1999)

370. C. Tommos and G. T. Babcock: Proton and hydrogen currents in photosynthetic water oxidation. *Biochim Biophys Acta* 1458, 199-219 (2000)

371. F. Rappaport and J. Lavergne: Coupling of electron and proton transfer in the photosynthetic water oxidase. *Biochim Biophys Acta* 1503, 246-259 (2001)

372. S. I. Bailey, I. M. Ritchie and F. R. Hewgill: The Construction and Use of Potential-pH Diagrams in Organic Oxidation-Reduction Reactions. *J Chem Soc Perkin Trans 2* 645-652 (1983)

373. C. Tommos, J. J. Skalicky, D. L. Pilloud, A. J. Wand and P. L. Dutton: De novo proteins as models of radical enzymes. *Biochemistry* 38, 9495-9507 (1999)

374. W. T. Dixon and D. Murphy: Determination of Acidity Constants of Some Phenol Radical Cations by Means of Electron Spin Resonance. *J Chem Soc Faraday Trans II* 72, 1221-1230 (1976)

375. C. Berthomieu and R. Hienerwadel: Vibrational spectroscopy to study the properties of redox-active tyrosines in photosystem II and other proteins. *Biochim Biophys Acta* 1707, 51-66 (2005)

376. F. Rappaport, A. Boussac, D. A. Force, J. Peloquin, M. Brynda, M. Sugiura, S. Un, R. D. Britt and B. A. Diner: Probing the coupling between proton and electron transfer in photosystem II core complexes containing a 3-fluorotyrosine. *J Am Chem Soc* 131, 4425-4433 (2009)

377. M. R. Seyedsayamdost, S. Y. Reece, D. G. Nocera and J. Stubbe: Mono-, di-, tri-, and tetra-substituted fluorotyrosines: New probes for enzymes that use tyrosyl radicals in catalysis. *J Am Chem Soc* 128, 1569-1579 (2006)

378. H. Ishikita and E. W. Knapp: Function of redox-active tyrosine in photosystem II. *Biophys J* 90, 3886-3896 (2006)

379. I. Vass and S. Styring: pH-Dependent Charge Equilibria between Tyrosine-D and the S-States in Photosystem II. Estimation of Relative Midpoint Redox Potentials. *Biochemistry* 30, 830-839 (1991)

380. G. Renger: Oxidative photosynthetic water splitting: energetics, kinetics and mechanism. *Photosynth Res* 92, 407-425 (2007)

381. G. Renger and P. Kühn: Reaction pattern and mechanism of light induced oxidative water splitting in photosynthesis. *Biochim Biophys Acta* 1767, 458-471 (2007)

382. H. J. Eckert and G. Renger: Temperature-Dependence of $P680^+$ Reduction in O_2-Evolving PS II Membrane Fragments at Different Redox States S_i of the Water Oxidizing System. *FEBS Lett* 236, 425-431 (1988)

383. M. J. Schilstra, F. Rappaport, J. H. A. Nugent, C. J. Barnett and D. R. Klug: Proton/hydrogen transfer affects the S-state-dependent microsecond phases of $P680^+$ reduction during water splitting. *Biochemistry* 37, 3974-3981 (1998)

384. A. M. A. Hays, I. R. Vassiliev, J. H. Golbeck and R. J. Debus: Role of D1-His190 in proton-coupled electron transfer reactions in photosystem II: A chemical complementation study. *Biochemistry* 37, 11352-11365 (1998)

385. A. M. A. Hays, I. R. Vassiliev, J. H. Golbeck and R. J. Debus: Role of D1-His190 in the proton-coupled oxidation of tyrosine Y_Z in manganese-depleted photosystem II. *Biochemistry* 38, 11851-11865 (1999)

386. P. Kühn, H. Eckert, H. J. Eichler and G. Renger: Analysis of the $P680^{+\cdot}$ reduction pattern and its temperature dependence in oxygen-evolving PSII core complexes from a thermophilic cyanobacteria and higher plants. *Phys Chem Chem Phys* 6, 4838-4843 (2004)

387. M. Karge, K. D. Irrgang, S. Sellin, R. Feinäugle, B. Liu, H. J. Eckert, H. J. Eichler and G. Renger: Effects of hydrogen/deuterium exchange on photosynthetic water cleavage in PS II core complexes from spinach. *FEBS Lett* 378, 140-144 (1996)

388. M. Haumann, O. Bögershausen, D. Cherepanov, R. Ahlbrink and W. Junge: Photosynthetic oxygen evolution: H/D isotope effects and the coupling between electron and proton transfer during the redox reactions at the oxidizing side of Photosystem II. *Photosynth Res* 51, 193-208 (1997)

389. G. Christen and G. Renger: The role of hydrogen bonds for the multiphasic $P680^{+\cdot}$ reduction by Y_Z in photosystem II with intact oxygen evolution capacity. Analysis of kinetic H/D isotope exchange effects. *Biochemistry* 38, 2068-2077 (1999)

390. B. Meyer, E. Schlodder, J. P. Dekker and H. T. Witt: O_2 Evolution and Chl a_{II}^+ ($P\text{-}680^+$) Nanosecond Reduction Kinetics in Single Flashes as a Function of pH. *Biochim Biophys Acta* 974, 36-43 (1989)

391. G. Christen, A. Seeliger and G. Renger: $P680^{+\cdot}$ reduction kinetics and redox transition probability of the water oxidizing complex as a function of pH and H/D isotope exchange in spinach thylakoids. *Biochemistry* 38, 6082-6092 (1999)

392. P. Kühn, J. Pieper, O. Kaminskaya, H. J. Eckert, R. E. Lechner, V. Shuvalov and G. Renger: Reaction pattern of photosystem II: oxidative water cleavage and protein flexibility. *Photosynth Res* 84, 317-323 (2005)

393. V. Petrouleas, D. Koulougliotis and N. Ioannidis: Trapping of metalloradical intermediates of the S-states at liquid helium temperatures. Overview of the phenomenology and mechanistic implications. *Biochemistry* 44, 6723-6728 (2005)

394. K. G. V. Havelius, J. Sjöholm, F. M. Ho, F. Mamedov and S. Styring: Metalloradical EPR Signals from the $Y_{Z^{\cdot}}$ S-State Intermediates in Photosystem II. *Appl Magn Reson* 37, 151-176 (2010)

395. S. Styring and A. W. Rutherford: Deactivation Kinetics and Temperature-Dependence of the S-State Transitions in the Oxygen-Evolving System of Photosystem II Measured by EPR Spectroscopy. *Biochim Biophys Acta* 933, 378-387 (1988)

396. C. X. Zhang, A. Boussac and A. W. Rutherford: Low-temperature electron transfer in photosystem II: A tyrosyl radical and semiquinone charge pair. *Biochemistry* 43, 13787-13795 (2004)

397. N. Ioannidis, G. Zahariou and V. Petrouleas: Trapping of the S_2 to S_3 state intermediate of the oxygen-evolving complex of photosystem II. *Biochemistry* 45, 6252-6259 (2006)

398. A. Boussac, J. J. Girerd and A. W. Rutherford: Conversion of the spin state of the manganese complex in photosystem II induced by near-infrared light. *Biochemistry* 35, 6984-6989 (1996)

399. A. Boussac, S. Un, O. Horner and A. W. Rutherford: High-spin states ($S > {}^5/_2$) of the photosystem II manganese complex. *Biochemistry* 37, 4001-4007 (1998)

400. A. Boussac, H. Kuhl, S. Un, M. Rögner and A. W. Rutherford: Effect of near-infrared light on the S_2-state of the manganese complex of photosystem II from *Synechococcus elongatus*. *Biochemistry* 37, 8995-9000 (1998)

401. A. Boussac, M. Sugiura, D. Kirilovsky and A. W. Rutherford: Near-infrared-induced transitions in the manganese cluster of photosystem II: Action spectra for the

S_2 and S_3 redox states. *Plant Cell Physiol* 46, 837-842 (2005)

402. D. Koulougliotis, J. R. Shen, N. Ioannidis and V. Petrouleas: Near-IR irradiation of the S_2 state of the water oxidizing complex of photosystem II at liquid helium temperatures produces the metalloradical intermediate attributed to $S_1Y_Z^{\cdot}$ *Biochemistry* 42, 3045-3053 (2003)

403. A. Boussac, M. Sugiura, Y. Inoue and A. W. Rutherford: EPR study of the oxygen evolving complex in His-tagged photosystem II from the cyanobacterium *Synechococcus elongatus*. *Biochemistry* 39, 13788-13799 (2000)

404. Y. Sanakis, N. Ioannidis, G. Sioros and V. Petrouleas: A novel $S = {}^{7}/_{2}$ configuration of the Mn cluster of photosystem II. *J Am Chem Soc* 123, 10766-10767 (2001)

405. N. Ioannidis and V. Petrouleas: Decay products of the S_3 state of the oxygen-evolving complex of photosystem II at cryogenic temperatures. Pathways to the formation of the $S = {}^{7}/_{2}$ S_2 state configuration. *Biochemistry* 41, 9580-9588 (2002)

406. N. Ioannidis, J. H. A. Nugent and V. Petrouleas: Intermediates of the S_3 state of the oxygen-evolving complex of photosystem II. *Biochemistry* 41, 9589-9600 (2002)

407. J. Sjöholm, K. G. V. Havelius, F. Mamedov and S. Styring: The S_0 State of the Water Oxidizing Complex in Photosystem II: pH Dependence of the EPR Split Signal Induction and Mechanistic Implications. *Biochemistry* 48, 9393-9404 (2009)

408. K. G. V. Havelius and S. Styring: pH dependent competition between Y_Z and Y_D in photosystem II probed by illumination at 5 K. *Biochemistry* 46, 7865-7874 (2007)

409. H. Suzuki, M. Sugiura and T. Noguchi: pH dependence of the flash-induced S-state transitions in the oxygen-evolving center of photosystem II from *Thermosynechoccocus elongatus* as revealed by Fourier transform infrared spectroscopy. *Biochemistry* 44, 1708-1718 (2005)

410. A. W. Rutherford, A. Boussac and P. Faller: The stable tyrosyl radical in Photosystem II: why D? *Biochim Biophys Acta* 1655, 222-230 (2004)

411. W. F. J. Vermaas, A. W. Rutherford and Ö. Hansson: Site-Directed Mutagenesis in Photosystem II of the Cyanobacterium *Synechocystis* sp. PCC 6803 - Donor D Is a Tyrosine Residue in the D2 Protein. *Proc Natl Acad Sci U S A* 85, 8477-8481 (1988)

412. G. M. Ananyev, I. Sakiyan, B. A. Diner and G. C. Dismukes: A functional role for tyrosine-D in assembly of the inorganic core of the water oxidase complex of photosystem II and the kinetics of water oxidation. *Biochemistry* 41, 974-980 (2002)

413. C. A. Buser, L. K. Thompson, B. A. Diner and G. W. Brudvig: Electron-transfer reactions in manganese-depleted photosystem II. *Biochemistry* 29, 8977-8985 (1990)

414. P. Faller, R. J. Debus, K. Brettel, M. Sugiura, A. W. Rutherford and A. Boussac: Rapid formation of the stable tyrosyl radical in photosystem II. *Proc Natl Acad Sci U S A* 98, 14368-14373 (2001)

415. P. Faller, A. W. Rutherford and R. J. Debus: Tyrosine D oxidation at cryogenic temperature in photosystem II. *Biochemistry* 41, 12914-12920 (2002)

416. S. Styring and A. W. Rutherford: In the Oxygen-Evolving Complex of Photosystem II the S_0 State Is Oxidized to the S_1 State by D^+ (Signal II_{slow}). *Biochemistry* 26, 2401-2405 (1987)

417. S. Isgandarova, G. Renger and J. Messinger: Functional differences of photosystem II from *Synechococcus elongatus* and spinach characterized by flash induced oxygen evolution patterns. *Biochemistry* 42, 8929-8938 (2003)

418. D. Shevela, B. Nöring, H. J. Eckert, J. Messinger and G. Renger: Characterization of the water oxidizing complex of photosystem II of the Chl *d*-containing cyanobacterium *Acaryochloris marina* via its reactivity towards endogenous electron donors and acceptors. *Phys Chem Chem Phys* 8, 3460-3466 (2006)

419. G. T. Babcock and K. Sauer: Electron-Paramagnetic Resonance Signal II in Spinach Chloroplasts. I. Kinetic-Analysis for Untreated Chloroplasts. *Biochim Biophys Acta* 325, 483-503 (1973)

420. A. Boussac and A. L. Etienne: Midpoint Potential of Signal II (Slow) in Tris-Washed Photosystem-II Particles. *Biochim Biophys Acta* 766, 576-581 (1984)

421. G. T. Babcock, B. A. Barry, R. J. Debus, C. W. Hoganson, M. Atamian, L. McIntosh, I. Sithole and C. F. Yocum: Water oxidation in photosystem II: from radical chemistry to multielectron chemistry. *Biochemistry* 28, 9557-9565 (1989)

422. C. Tommos, L. Davidsson, B. Svensson, C. Madsen, W. Vermaas and S. Styring: Modified EPR-Spectra of the $Tyrosine_D$ Radical in Photosystem II in Site-Directed Mutants of *Synechocystis* sp. PCC 6803: Identification of Side Chains in the Immediate Vicinity of $Tyrosine_D$ on the D2 Protein. *Biochemistry* 32, 5436-5441 (1993)

423. X. S. Tang, D. A. Chisholm, G. C. Dismukes, G. W. Brudvig and B. A. Diner: Spectroscopic evidence from site-directed mutants of *Synechocystis* PCC6803 in favor of a close interaction between histidine 189 and redox-active tyrosine 160, both of polypeptide D2 of the photosystem II reaction center. *Biochemistry* 32, 13742-13748 (1993)

424. S. Un, X. S. Tang and B. A. Diner: 245 GHz high-field EPR study of tyrosine-D^o and tyrosine-Z^o in mutants of photosystem II. *Biochemistry* 35, 679-684 (1996)

425. D. A. Force, D. W. Randall, R. D. Britt, X. S. Tang and B. A. Diner: ^{2}H ESE-ENDOR study of hydrogen bonding to the tyrosine radicals $Y_{D^\cdot}$ and $Y_{Z^\cdot}$ of photosystem II. *J Am Chem Soc* 117, 12643-12644 (1995)

426. K. A. Campbell, J. M. Peloquin, B. A. Diner, X. S. Tang, D. A. Chisholm and R. D. Britt: The τ-nitrogen of D2 histidine 189 is the hydrogen bond donor to the tyrosine radical $Y_{D^\cdot}$ of photosystem II. *J Am Chem Soc* 119, 4787-4788 (1997)

427. R. Hienerwadel, B. A. Diner and C. Berthomieu: Molecular origin of the pH dependence of tyrosine D oxidation kinetics and radical stability in photosystem II. *Biochim Biophys Acta* 1777, 525-531 (2008)

428. R. Hart and P. J. O'Malley: A quantum mechanics/molecular mechanics study of the tyrosine residue, Tyr_D, of Photosystem II. *Biochim Biophys Acta* 1797, 250-254 (2010)

429. J. Lavergne and W. Junge: Proton Release during the Redox Cycle of the Water Oxidase. *Photosynth Res* 38, 279-296 (1993)

430. W. Junge, M. Haumann, R. Ahlbrink, A. Mulkidjanian and J. Clausen: Electrostatics and proton transfer in photosynthetic water oxidation. *Philos Trans R Soc Lond B* 357, 1407-1418 (2002)

431. H. Suzuki, M. Sugiura and T. Noguchi: Monitoring Proton Release during Photosynthetic Water Oxidation in Photosystem II by Means of Isotope-Edited Infrared Spectroscopy. *J Am Chem Soc* 131, 7849-7857 (2009)

432. C. F. Fowler: Proton Evolution from Photosystem II Stoichiometry and Mechanistic Considerations. *Biochim Biophys Acta* 462, 414-421 (1977)

433. S. Saphon and A. R. Crofts: Protolytic Reactions in Photosystem II: A New Model for Release of Protons Accompanying Photooxidation of Water. *Z Naturforsch C* 32, 617-626 (1977)

434. J. M. Bowes and A. R. Crofts: The Role of pH and Membrane Potential in the Reactions of Photosystem II as Measured by Effects on Delayed Fluorescence. *Biochim Biophys Acta* 637, 464-472 (1981)

435. B. Wille and J. Lavergne: Measurement of Proton Translocation in Thylakoids under Flashing Light Using a Spin-Labeled Amine. *Photobiochem Photobiophys* 4, 131-144 (1982)

436. V. Förster and W. Junge: Stoichiometry and Kinetics of Proton Release Upon Photosynthetic Water Oxidation. *Photochem Photobiol* 41, 183-190 (1985)

437. F. Rappaport and J. Lavergne: Proton Release during Successive Oxidation Steps of the Photosynthetic Water Oxidation Process - Stoichiometries and pH Dependence. *Biochemistry* 30, 10004-10012 (1991)

438. E. Schlodder and H. T. Witt: Stoichiometry of proton release from the catalytic center in photosynthetic water oxidation - Reexamination by a glass electrode study at pH 5.5-7.2. *J Biol Chem* 274, 30387-30392 (1999)

439. A. B. Hope and A. Morland: Proton Translocations in Isolated Spinach Chloroplasts after Single-Turnover Actinic Flashes. *Aust J Plant Physiol* 6, 289-304 (1979)

440. P. Jahns and W. Junge: Proton release during the four steps of photosynthetic water oxidation: induction of 1:1:1:1 pattern due to lack of chlorophyll *a*/*b* binding proteins. *Biochemistry* 31, 7398-7403 (1992)

441. K. Lübbers, M. Haumann and W. Junge: Photosynthetic Water Oxidation under Flashing Light. Oxygen Release, Proton Release and Absorption Transients in the near Ultraviolet - a Comparison between Thylakoids and a Reaction-Centre Core Preparation. *Biochim Biophys Acta* 1183, 210-214 (1993)

442. U. Wacker, E. Haag and G. Renger: Investigation of pH-change-patterns of photosystem-II membrane fragments from spinach. In: *Current Research in Photosynthesis*. Ed M. Baltscheffsky. Kluwer, Dordrecht, 1, 869-872 (1990)

443. J. P. McEvoy and G. W. Brudvig: Structure-based mechanism of photosynthetic water oxidation. *Phys Chem Chem Phys* 6, 4754-4763 (2004)

444. N. Knoepfle, T. M. Bricker and C. Putnam-Evans: Site-directed mutagenesis of basic arginine residues 305 and 342 in the CP 43 protein of photosystem II affects oxygen-evolving activity in *Synechocystis* 6803. *Biochemistry* 38, 1582-1588 (1999)

445. G. Ananyev, T. Nguyen, C. Putnam-Evans and G. C. Dismukes: Mutagenesis of CP43-arginine-357 to serine reveals new evidence for (bi)carbonate functioning in the water oxidizing complex of Photosystem II. *Photochem Photobiol Sci* 4, 991-998 (2005)

446. H. J. Hwang, P. Dilbeck, R. J. Debus and R. L. Burnap: Mutation of arginine 357 of the CP43 protein of photosystem II severely impairs the catalytic S-state cycle of the H_2O oxidation complex. *Biochemistry* 46, 11987-11997 (2007)

447. J. Barber, K. Ferreira, K. Maghlaoui and S. Iwata: Structural model of the oxygen-evolving centre of photosystem II with mechanistic implications. *Phys Chem Chem Phys* 6, 4737-4742 (2004)

448. J. De Las Rivas and J. Barber: Analysis of the structure of the PsbO protein and its implications. *Photosynth Res* 81, 329-343 (2004)

449. T. Shutova, V. V. Klimov, B. Andersson and G. Samuelsson: A cluster of carboxylic groups in PsbO protein is involved in proton transfer from the water oxidizing complex of Photosystem II. *Biochim Biophys Acta* 1767, 434-440 (2007)

450. R. J. Service, W. Hillier and R. J. Debus: Evidence from FTIR Difference Spectroscopy of an Extensive Network of Hydrogen Bonds near the Oxygen-Evolving Mn_4Ca Cluster of Photosystem II Involving D1-Glu65, D2-Glu312, and D1-Glu329. *Biochemistry* 49, 6655-6669 (2010)

451. W. Hillier and T. Wydrzynski: ^{18}O-Water exchange in photosystem II: Substrate binding and intermediates of the water splitting cycle. *Coord Chem Rev* 252, 306-317 (2008)

452. T. Noguchi: FTIR detection of water reactions in the oxygen-evolving centre of photosystem II. *Phil Trans R Soc B* 363, 1189-1195 (2008)

453. T. Wydrzynski, N. Zumbulyadis, P. G. Schmidt, H. S. Gutowsky and Govindjee: Proton Relaxation and Charge Accumulation during Oxygen Evolution in Photosynthesis. *Proc Natl Acad Sci U S A* 73, 1196-1198 (1976)

454. O. Hansson, L. E. Andréasson and T. Vänngard: Oxygen from Water Is Coordinated to Manganese in the S_2 State of Photosystem II. *FEBS Lett* 195, 151-154 (1986)

455. M. C. W. Evans, J. H. A. Nugent, R. J. Ball, I. Muhiuddin and R. J. Pace: Evidence for a direct manganese-oxygen ligand in water binding to the S_2 state of the photosynthetic water oxidation complex. *Biochemistry* 43, 989-994 (2004)

456. J. H. Su, W. Lubitz and J. Messinger: Probing mode and site of substrate water binding to the oxygen-evolving complex in the S_2 state of photosystem II by ^{17}O-HYSCORE Spectroscopy. *J Am Chem Soc* 130, 786-787 (2008)

457. K. A. Ahrling, M. C. W. Evans, J. H. A. Nugent, R. J. Ball and R. J. Pace: ESEEM studies of substrate water and small alcohol binding to the oxygen-evolving complex of photosystem II during functional turnover. *Biochemistry* 45, 7069-7082 (2006)

458. H. Yamada, H. Mino and S. Itoh: Protons bound to the Mn cluster in photosystem II oxygen evolving complex detected by proton matrix ENDOR. *Biochim Biophys Acta* 1767, 197-203 (2007)

459. J. Messinger, M. Badger and T. Wydrzynski: Detection of *One* Slowly Exchanging Substrate Water Molecule in the S_3 State of Photosystem II. *Proc Natl Acad Sci U S A* 92, 3209-3213 (1995)

460. W. Hillier, J. Messinger and T. Wydrzynski: Kinetic determination of the fast exchanging substrate water molecule in the S_3 state of photosystem II. *Biochemistry* 37, 16908-16914 (1998)

461. W. Hillier and T. Wydrzynski: The affinities for the two substrate water binding sites in the O_2 evolving complex of photosystem II vary independently during S-state turnover. *Biochemistry* 39, 4399-4405 (2000)

462. R. Tagore, H. Y. Chen, R. H. Crabtree and G. W. Brudvig: Determination of μ-oxo exchange rates in di-μ-oxo dimanganese complexes by electrospray ionization mass spectrometry. *J Am Chem Soc* 128, 9457-9465 (2006)

463. R. Tagore, R. H. Crabtree and G. W. Brudvig: Distinct mechanisms of bridging-oxo exchange in di-μ-O dimanganese complexes with and without water-binding sites: implications for water binding in the O_2-evolving complex of photosystem II. *Inorg Chem* 46, 2193-2203 (2007)

464. G. Hendry and T. Wydrzynski: ^{18}O isotope exchange measurements reveal that calcium is involved in the binding of one substrate-water molecule to the oxygen-evolving complex in photosystem II. *Biochemistry* 42, 6209-6217 (2003)

465. S. Singh, R. J. Debus, T. Wydrzynski and W. Hillier: Investigation of substrate water interactions at the high-affinity Mn site in the photosystem II oxygen-evolving complex. *Phil Trans R Soc B* 363, 1229-1235 (2008)

466. T. Noguchi and M. Sugiura: Structure of an active water molecule in the water-oxidizing complex of photosystem II as studied by FTIR spectroscopy. *Biochemistry* 39, 10943-10949 (2000)

467. T. Noguchi and M. Sugiura: Analysis of flash-induced FTIR difference spectra of the S-state cycle in the photosynthetic water-oxidizing complex by uniform ^{15}N and ^{13}C isotope labeling. *Biochemistry* 42, 6035-6042 (2003)

468. T. Noguchi and M. Sugiura: FTIR detection of water reactions during the flash-induced S-state cycle of the photosynthetic water-oxidizing complex. *Biochemistry* 41, 15706-15712 (2002)

469. T. Noguchi and M. Sugiura: Flash-induced FTIR difference spectra of the water oxidizing complex in moderately hydrated photosystem II core films: Effect of hydration extent on S-state transitions. *Biochemistry* 41, 2322-2330 (2002)

470. G. Hendry and T. Wydrzynski: The two substrate-water molecules are already bound to the oxygen-evolving complex in the S_2 state of photosystem II. *Biochemistry* 41, 13328-13334 (2002)

471. S. Y. Venyaminov and F. G. Prendergast: Water (H_2O and D_2O) molar absorptivity in the 1000–4000 cm^{-1} range and quantitative infrared spectroscopy of aqueous solutions. *Anal Biochem* 248, 234-245 (1997)

472. H. Suzuki, M. Sugiura and T. Noguchi: Monitoring water reactions during the S-state cycle of the

photosynthetic water-oxidizing center: Detection of the DOD bending vibrations by means of Fourier transform infrared spectroscopy. *Biochemistry* 47, 11024-11030 (2008)

473. V. K. Yachandra: The Catalytic Manganese Cluster: Organization of the Metal Ions. In: *Photosystem II: The Light-Driven Water:Plastoquinone Oxidoreductase*. Ed T. Wydrzynski and K. Satoh. Springer, Dordrecht, 235-260 (2005)

474. J. Messinger: Evaluation of different mechanistic proposals for water oxidation in photosynthesis on the basis of Mn_4O_xCa structures for the catalytic site and spectroscopic data. *Phys Chem Chem Phys* 6, 4764-4771 (2004)

475. P. E. M. Siegbahn: Structures and Energetics for O_2 Formation in Photosystem II. *Acc Chem Res* 42, 1871-1880 (2009)

476. J. B. Vincent and G. Christou: A Molecular ´Double-Pivot´ Mechanism for Water Oxidation. *Inorg Chim Acta* 136, L41-L43 (1987)

477. W. Ruettinger, M. Yagi, K. Wolf, S. Bernasek and G. C. Dismukes: O_2 evolution from the manganese-oxo cubane core $Mn_4O_4^{6+}$: A molecular mimic of the photosynthetic water oxidation enzyme? *J Am Chem Soc* 122, 10353-10357 (2000)

478. A. E. Kuznetsov, Y. V. Geletii, C. L. Hill and D. G. Musaev: Insights into the Mechanism of O_2 Formation and Release from the $Mn_4O_4L_6$ "Cubane" Cluster. *J Phys Chem A* 114, 11417-11424 (2010)

479. V. L. Pecoraro, M. J. Baldwin, M. T. Caudle, W. Y. Hsieh and N. A. Law: A proposal for water oxidation in photosystem II. *Pure Appl Chem* 70, 925-929 (1998)

480. J. S. Vrettos, J. Limburg and G. W. Brudvig: Mechanism of photosynthetic water oxidation: combining biophysical studies of photosystem II with inorganic model chemistry. *Biochim Biophys Acta* 1503, 229-245 (2001)

481. J. Limburg, V. A. Szalai and G. W. Brudvig: A mechanistic and structural model for the formation and reactivity of a Mn^V=O species in photosynthetic water oxidation. *J Chem Soc, Dalton Trans* 1353-1361 (1999)

482. H. Koike, B. Hanssum, Y. Inoue and G. Renger: Temperature-Dependence of S-State Transition in a Thermophilic Cyanobacterium, *Synechococcus vulcanus* Copeland Measured by Absorption Changes in the Ultraviolet Region. *Biochim Biophys Acta* 893, 524-533 (1987)

483. G. Renger and B. Hanssum: Studies on the reaction coordinates of the water oxidase in PS II membrane fragments from spinach. *FEBS Lett* 299, 28-32 (1992)

484. M. Karge, K. D. Irrgang and G. Renger: Analysis of the reaction coordinate of photosynthetic water oxidation by kinetic measurements of 355 nm absorption changes at different temperatures in photosystem II preparations suspended in either H_2O or D_2O. *Biochemistry* 36, 8904-8913 (1997)

485. J. Clausen, R. J. Debus and W. Junge: Time-resolved oxygen production by PSII: chasing chemical intermediates. *Biochim Biophys Acta* 1655, 184-194 (2004)

486. F. Rappaport, M. Blanchard-Desce and J. Lavergne: Kinetics of Electron-Transfer and Electrochromic Change during the Redox Transitions of the Photosynthetic Oxygen-Evolving Complex. *Biochim Biophys Acta* 1184, 178-192 (1994)

487. G. Renger and W. Weiss: Studies on the Nature of the Water-Oxidizing Enzyme. 3. Spectral Characterization of the Intermediary Redox States in the Water-Oxidizing Enzyme System Y. *Biochim Biophys Acta* 850, 184-196 (1986)

488. J. P. Dekker, J. J. Plijter, L. Ouwehand and H. J. Van Gorkom: Kinetics of Manganese Redox Transitions in the Oxygen-Evolving Apparatus of Photosynthesis. *Biochim Biophys Acta* 767, 176-179 (1984)

489. M. R. Razeghifard and R. J. Pace: EPR kinetic studies of oxygen release in thylakoids and PSII membranes: A kinetic intermediate in the S_3 to S_0 transition. *Biochemistry* 38, 1252-1257 (1999)

490. J. Clausen and W. Junge: Search for intermediates of photosynthetic water oxidation. *Photosynth Res* 84, 339-345 (2005)

491. J. R. Shen, Y. Umena, K. Kawakami and N. Kamiya: Crystal structure of oxygen evolving photosystem II at an atomic resolution. In: *15th International Congress of Photosynthesis*. Beijing, China (2010)

492. W. Humphrey, A. Dalke and K. Schulten: VMD: Visual molecular dynamics. *J. Mol. Graphics* 14, 33-38 (1996)

493. The PyMOL Molecular Graphics System, Schrödinger, LLC

Key Words: Electron transfer, EPR, ENDOR, FTIR, proton transfer, X-ray crystallography, X-ray spectroscopy, Review

Send correspondence to: Athina Zouni, Max-Volmer-Laboratorium für Biophysikalische Chemie, Technische Universität Berlin, Strasse des 17. Juni 135, D-10623 Berlin, Germany, Tel: 493031425650, Fax: 493031421122, E-mail: athina.zouni@tu-berlin.de

http://www.bioscience.org/current/vol16.htm